ATMIRE

Title	Geology and mineralization of the Pajarita mountain layered peralkaline syenitic pluton-hosted REE-Zr prospect, Mescalero Apache Reservation, New Mexico
Item Type	Text
Authors	Berger, Michael Lee
Publisher	Colorado School of Mines. Arthur Lakes Library
Rights	Copyright of the original work is retained by the author.
Download date	2026-11-28 07:42:05
Link to Item	https://hdl.handle.net/11124/172145

GEOLOGY AND MINERALIZATION OF THE PAJARITA MOUNTAIN LAYERED PERALKALINE SYENITIC PLUTON-HOSTED REE-ZR PROSPECT, MESCALERO APACHE RESERVATION, NEW MEXICO

by

Michael Berger

A thesis submitted to the Faculty and the Board of Trustees of the Colorado School of Mines in partial fulfillment of the requirements for the degree of Master of Science (Geology).

Golden, Colorado

Date _____

Signed: _____
Michael Lee Berger

Signed: _____
Dr. Richard Wendlandt
Thesis Advisor

Signed: _____
Dr. Alexander Gysi
Thesis Advisor

Golden, Colorado

Date _____

Signed: _____
Dr. M. Stephen Enders
Professor and Department Head
of Geology and Geological
Engineering

ABSTRACT

Peralkaline plutons represent some of the best known future sources of rare earth elements (REE), and, specifically, the more valuable heavy (H)REE. These plutons are diverse in size, morphology and enrichment, and understanding the factors that control the distribution of REE and other desirable elements is critical to efficient exploration for potential resources. The Pajarita Mountain peralkaline syenitic pluton, located on the Mescalero Apache Reservation in southern New Mexico, is prospective for REE, including yttrium (Y), and zirconium (Zr), but has not previously been extensively studied.

This study investigates the REE-Zr mineralization and the igneous processes involved in the genesis of the pluton through field mapping, logging of 762 m of new drilled core, whole-rock geochemistry, and detailed petrographic description of the principle lithologies predominantly via optical microscopy and FE-SEM mineral chemistry. Evidence is presented indicating that the Pajarita Mountain pluton is a layered intrusion that is composed of peralkaline syenitic cumulate rocks. REE-Zr mineralization dominantly occurs in the form of magmatic eudialyte group minerals, which are partly replaced by secondary minerals formed during late stage alteration. Layering is defined by phase, texture, and/or mode, and contacts between layers may be abrupt or gradational. Specific layered sequences are locally repeated within the studied sections, and their descriptions may have significance for REE and Zr exploration at Pajarita Mountain and in other similar peralkaline plutons.

Based on detailed petrographic observations, field relations, whole-rock geochemistry, and interpretation of layered sequences, this study recognizes several processes in the genesis of the Pajarita Mountain pluton. These include emplacement of at least three major peralkaline

magma pulses, crystal separation and accumulation, and interaction of the cumulus pile with evolving melts. The latter may involve magma mixing related to magma recharge. Each of these processes appears to have played a role in the genesis of the pluton and to have had an impact on the distribution of REE and Zr mineralization.

The three major peralkaline magmatic episodes are represented by peralkaline syenitic rocks of Types I-III; minor pegmatites were also emplaced (Type IV). Cross-cutting relationships suggest that Type III rocks formed first, followed by Type II, then Type I cumulates, with Type IV forming last. Correlation of sections from two study areas enables division of the pluton into three layered zones, the Lower Layered, Central Mixed, and Upper Layered Zones. The Lower Layered Zone consists predominantly of layered Type I cumulates, while the Central Mixed Zone features rocks of all four types, including bands of Type I cumulates, and the Upper Layered Zone consists of a basal Type I layered sequence overlain by Type II rocks. Type I cumulates display the best developed cumulus textures and commonly show layering by mode, texture and/or phase. They contain the most abundant eudialyte and greatest REE-Zr concentrations, typically at the base of layered successions.

TABLE OF CONTENTS

ABSTRACT..... iii

LIST OF FIGURES..... vii

LIST OF TABLES..... ix

CHAPTER 1 INTRODUCTION..... 1

CHAPTER 2 GEOLOGIC SETTING..... 6

Regional geology and previous work..... 6

General geology of the study area..... 10

CHAPTER 3 METHODS..... 13

CHAPTER 4 RESULTS..... 16

4.1 Mineralogy of the Pajarita Mountain peralkaline cumulate suite..... 16

Alkali feldspar..... 18

Na-Fe amphibole..... 21

Quartz..... 23

Eudialyte..... 25

Fluorite..... 27

Aenigmatite..... 28

4.2 Replacement textures..... 29

Pseudomorphs after eudialyte..... 29

Aegirine pseudomorphs after amphibole..... 31

Reaction textures in igneous minerals..... 32

4.3 Rock classification of the Pajarita Mountain layered cumulate suite..... 34

4.3.1 Type I peralkaline syenitic cumulates..... 38

Quartz megacrystic eudialyte-amphibole syenite cumulate (QM EASC)……. 38

Eudialyte-amphibole syenite cumulate (EASC)……. 40

Eudialyte syenite cumulate (ESC)……..…… 42

4.3.2 Type II peralkaline syenitic cumulates …….. 44

Porphyritic eudialyte-amphibole syenite cumulate (PEAS)……... 46

Porphyritic eudialyte amphibole syenite cumulate with quartz megacrysts (PEASQ)…….. 47

4.3.3 Type III peralkaline syenitic cumulates: Porphyritic aenigmatite-amphibole syenite cumulate (PAAS)…….. 49

4.3.4 Type IV peralkaline rocks: peralkaline pegmatites (PP)…… 50

4.3.5 Fine-grained mafic intrusions (FGI)……... 52

4.3.6 Basement xenoliths (BX) ……... 52

4.3.7 Permian sedimentary rocks (PS) …… 53

4.4 Whole-rock geochemistry……... 58

CHAPTER 5 INTERPRETATION OF LAYERED SEQUENCES……. 62

5.1. Layered sequences and correlation of North and South Area …… 62

5.2 Igneous processes…… 69

CHAPTER 6 CONCLUSIONS…….…… 74

REFERENCES……... 77

APPENDIX A…… 81

LIST OF FIGURES

Figure 2.1. Map of generalized geologic provinces of southern New Mexico (from Moore et al., 1988)…….. 7

Figure 2.2. Geologic map of Pajarita Mountain pluton, modified from Jacobson (1986).... 11

Figure 4.1. Photomicrographs of alkali feldspar……... 19

Figure 4.2. Photomicrographs of Na-Fe amphibole……. 23

Figure 4.3. Photomicrographs of quartz…… 25

Figure 4.4. Photomicrographs of eudialyte…….…….. 26

Figure 4.5. Photomicrographs of fluorite…….…… 28

Figure 4.6. Photomicrograph of aenigmatite…….……... 29

Figure 4.7. Photomicrographs of pseudomorphs after eudialyte……... 30

Figure 4.8. Images of aegirine pseudomorphs after amphibole…… 32

Figure 4.9. Photomicrographs of quartz replacement textures…….. 33

Figure 4.10. Photomicrographs of amphibole replacement textures……... 33

Figure 4.11. Maps and cross-sections of North and South study areas……... 35

Figure 4.12. Images of QM EASC…….. 40

Figure 4.13. Images of EASC……. 41

Figure 4.14. Images of ESC…… 43

Figure 4.15. Images of PEAS…….. 45

Figure 4.16. Images of PEASQ……... 48

Figure 4.17. Images of PAAS……. 50

Figure 4.18. Images of fine-grained mafic intrusions (FGI)……... 54

Figure 4.19. Images of basement xenoliths (BX)…… 56

Figure 4.20. Images of Permian sedimentary rocks (PS)…… 58

Figure 5.1. Schematic diagram of QM Member mineralogy and mineralization grades….. 63

Figure 5.2. Schematic diagram of correlation of sections from North and South Areas…... 66

Figure 5.3. Stratigraphic column of Lower Layered Zone lithologies, members, and mineralization grades…….. 69

Figure A.1. Backscatter electron images of alkali feldspar grains sampled by EDS spot analyses……... 82

Figure A.2. Backscatter electron image of cumulus amphibole grain with adcumulus overgrowth. Same grain shown in Fig. 4.2A……. 83

Figure A.3. Backscatter electron image of aenigmatite from unit PAAS…….. 84

LIST OF TABLES

Table 2.1. Radiometric dates from previous literature on Pajarita Mountain..……. 6

Table 4.1. Table of mineral abbreviations…….……..……. 17

Table 4.2. Summary of mineralogy and distinguishing features of lithologies……... 37

Table 4.3. Representative whole-rock major and trace element analyses of Pajarita Mountain peralkaline lithologies and estimated modal mineralogy of samples.. 60

Table 5.1. Summary of characteristics of mixed units……. 65

Table A.1. Data from energy-dispersive X-ray spectroscopy (EDS) spot analyses on alkali feldspar (Afs A) grain shown in Figs. A.1B and 4.1B.....…… 82

Table A.2. Data from EDS spot analyses on alkali feldspar (Afs B) grain shown in Figs. A.1C and 4.1C…… 83

Table A.3. Data from EDS spot analyses on amphibole grains shown in Figs. A.3 and 4.2A……. 84

CHAPTER 1

INTRODUCTION

The rare earth elements (REE), including the lanthanides, yttrium and scandium, are relatively abundant in the crust, despite the nomenclature. Economically extractable REE deposits, on the other hand, in which processing-amenable mineralogy meets sufficient concentration, are truly rare. Due to the growing role these elements play in electronics, alternative energy and other high-technology applications, exploration for potential REE resources continues, albeit with a shift in focus (Chakhmouradian and Wall, 2012). Development of new applications for the heavy (H)REE (Tb-Lu+Y), increasing global demand, and a limited number of REE producers have led to renewed interest in understanding the processes that enrich REE in the crust, and particularly the rarer HREE.

Peralkaline (molar ([Na+K)/Al] > 1) syenitic and granitic rocks are enriched to potentially economic grades in the full spectrum of light (L)REE and HREE. These occurrences are also enriched in other high field strength elements (HFSE), including Zr, Hf, Nb, Ta and Ti. Rare earth elements occurrences hosted in peralkaline rocks are of great economic interest due to their favorable concentrations of HREE and their large sizes. Examples of potential REE deposits hosted in peralkaline plutons include the Strange Lake peralkaline granitic pluton in Quebec (Gysi et al., 2016) and the Nechalacho syenitic layered intrusive in Northwest Territories (Möller et al., 2016), Canada.

Peralkaline rocks have been hypothesized to reach their characteristic enrichment in HFSE through a low degree of partial melting of metasomatized mantle and high degrees of fractionation. Previous metasomatism of this mantle material by an alkali-rich fluid is invoked

to explain the excess of alkalis present in peralkaline rocks (Martin and De Vito, 2005). This alkali metasomatism increases alkali content in the mantle material in question, possibly producing Na amphibole and Na pyroxene. A low degree of partial melting of this alkali-enriched material is theorized to produce a strongly sodic transitional or alkali basaltic melt. Such a melt undergoing protracted fractionation may produce a peralkaline, silica-undersaturated melt. Abundant alkali elements and volatile elements (e.g., F, B, P, and Cl) modify the solidus temperatures and viscosities of these melts, enabling them to build exceptional HFSE enrichment during fractionation (Dostal, 2016). Highly-evolved melts produced in this way are believed to represent the origin of agpaitic rocks (feldspathoid-bearing peralkaline rocks containing complex zirconosilicate minerals such as eudialyte), which form in plutons that are generally silica-undersaturated. Examples of these mostly syenitic layered complexes include Nechalacho in Canada, Ilímaussaq in Greenland, and Norra Kärr in southern Sweden. More evolved silica-oversaturated peralkaline plutons, such as Strange Lake in Quebec, also contain complex zirconosilicates and are enriched in the REE, but are less common. While there is debate as to whether the formation of silica-oversaturated peralkaline melts requires a higher degree of crustal assimilation (McDonald, 2012), there is agreement that these melts share a similarly complex history involving metasomatism and fractionation (Martin and De Vito, 2005).

Many peralkaline intrusions consist of layered cumulate bodies, with the REE and other HFSE commonly concentrated beyond the abundances present in the melt via fractional crystallization (Sheard et al., 2012). Whole-rock grades of total rare earth oxides (TREO), including all REE as oxides (REE_2O_3 plus Y_2O_3), plus zirconium oxide (ZrO_2), are commonly several weight percent. Layering produced by fractional crystallization includes textural and mineralogical variations that control the spatial distribution of HFSE-bearing minerals and

concentrates these elements into high-grade intervals (Dostal, 2016). In many cases, the dominant magmatic minerals hosting REE and other HFSE in these peralkaline rocks are complex zirconosilicates of the eudialyte group (referred to henceforth as "eudialyte"), which has the general formula $Na_{15}Ca_6(Fe^{2+}Mn^{2+})_3Zr_3(Si_{25}O_{73})(O,OH,H_2O)_3(OH,Cl)_2$. Many other HFSE-bearing phases have been identified in these intrusions, including zirconosilicates (e.g. zircon, gittinsite, catapleiite, aenigmatite), silicates (e.g. allanite- and cerite-(Ce)), phosphates (e.g. xenotime-(Y) and monazite-(Ce)), and fluorocarbonates (e.g. bastnäsite- and parisite-(Ce)). However, the variability of post-cumulus processes and the near ubiquity of subsolidus alteration often make discrimination of igneous vs. hydrothermal phases troublesome.

In several peralkaline intrusions, hydrothermal and magmatic processes have been found to significantly affect the mineralogical and spatial distribution of the REE and other HFSE, such as in the Strange Lake pluton in Quebec (Gysi et al., 2016; Gysi and Williams-Jones, 2013) and the Nechalacho syenitic layered intrusive in the Northwest Territories, Canada (Sheard et al., 2012; Möller et al., 2016). In these potentially economic REE deposits, the original HFSE enrichment is believed to have been localized by fractional crystallization. The Nechalacho prospect shows evidence that eudialyte was the original magmatic host to HFSE and formed distinct cumulate layering (Möller et al., 2016); the Strange Lake prospect displays pegmatite-rich zones where the highest metal concentrations have been found such as the B zone (Gysi et al., 2016).

The Mesoproterozoic Pajarita Mountain pluton is a silica-oversaturated, layered syenitic body host to potentially economic REE-Zr mineralization in primary eudialyte. Pajarita Mountain was explored by Molycorp, Inc. from the mid-1980s to the early 1990s as a potential source of yttrium and zirconium. This work included geologic mapping, petrography, twenty

drill holes drilled to a maximum depth of 61 meters, and preliminary metallurgical testing. From this work, Molycorp delineated a "recoverable resource" of 2.7 million short tons grading 0.18 wt.% Y_2O_3 and 1.20 wt.% ZrO_2 extractable by open pit mining (Sherer, 1990). Because whole-rock REE and other HFSE concentrations at Pajarita Mountain appear to correspond well to estimates of the original modal eudialyte content, this occurrence represents a suitable locality for an investigation into the magmatic processes involved in the genesis of the intrusion and the roles magmatic processes play in concentrating REE-Zr in silica-saturated peralkaline systems.

The purpose of this study was to assess the role and types of magmatic processes that led to REE enrichment in the Pajarita Mountain pluton, and the petrographic and geochemical signatures that can be used to recognize these processes in other similar potential deposits. This study draws upon new data collected from 2013 to 2015 by staff from the Division of Energy & Mineral Development, Office of the Assistant Secretary for Indian Affairs, United States Department of the Interior (DEMD). Conducted on behalf of the Mescalero Apache Tribe, the DEMD project was aimed at confirming and expanding upon Molycorp's data so as to give a preliminary sense of the prospect's potential as a future REE-Zr resource.

This work combines field observations, including geologic mapping and detailed logging of 762 m of newly drilled core, data from previous mapping, core logging, and whole-rock geochemistry data, and a comprehensive petrographic study at the hand sample and thin section scales with new whole-rock geochemical data to develop a detailed lithologic description of the pluton. Additional data were collected on mineral chemistry and microtextural relationships using backscatter electron (BSE) imaging, energy-dispersive X-ray spectroscopy (EDS), a proprietary automated mineralogy system, and cathodoluminescence. These observations were

combined to interpret the igneous mechanisms at work in the pluton and their implications for exploration for REE-Zr resources in similar peralkaline systems.

CHAPTER 2

GEOLOGIC SETTING

Regional geology and previous work

Pajarita Mountain is a mid-Proterozoic (1100-1225 Ma; Table 2.1) peralkaline pluton located in the northeastern corner of the Mescalero Apache Reservation in central southern New Mexico. The project area is located roughly 190 km northeast of El Paso, TX and 25 km southeast of Ruidoso, NM, within the eastern Rio Grande Rift province, between the Great Plains province to the east and the Basin and Range province to the west (Fig. 2.1). The Pajarita Mountain pluton lies within the southern end of a belt of Mesoproterozoic A-type plutons associated with the Grenville orogeny (McLemore, 2010). The nearest occurrence of Precambrian rocks to Pajarita Mountain is at Bent Dome, 40 kilometers to the west-southwest, and immediately west of the Mescalero Reservation (Moore et al, 1988).

Table 2.1. Radiometric dates from previous literature on Pajarita Mountain

Age as given	Lithologic unit	Method	Mineral	Source
1170 ± 24 Ma	"Riebeckite granite"	K-Ar	Riebeckite	Kelley, 1968
1155 ± 25 Ma	"Riebeckite 'granite'"	Rb-Sr	Feldspar	Kelley, 1968
1190 ± 25 Ma	"Syenite pegmatite"	K-Ar	Hornblende	Kelley, 1968
1150 ± 40 Ma	"Quartz syenite-alkali granite"	K-Ar	Amphibole	Moore et al., 1988
1175 ± 15 Ma	"Riebeckite granite"	Rb-Sr	Feldspar	Bauer & Pollock, 1993
1180 ± 25 Ma	"Riebeckite granite"	K-Ar	Riebeckite	Bauer & Pollock, 1993
1200 ± 25 Ma	"Pegmatite/syenite"	K-Ar	Hornblende	Bauer & Pollock, 1993

Precambrian rocks across central and southern New Mexico are interpreted to be the remnants of the Permian Pedernal uplift (Kottlowski, 1985). The Precambrian east-west trend including diorite-monzodiorite at Bent and syenite-quartz syenite at Pajarita Mountain is believed to be a relic of varying degrees of uplift during this time. Cambrian, Ordovician,

Silurian, Devonian, and Carboniferous sedimentary rocks are well exposed along the Sacramento Mountain escarpment south of the Mescalero Reservation and at Bent, but progressively pinch out against the rising topography of this east-west-trending highland. Only Permian rocks are exposed on the flanks of Pajarita Mountain, suggesting that it was a topographic high through most of the Paleozoic. Regionally distributed Mesozoic strata are absent across most of the surrounding area, having been eroded during late Cretaceous to early Tertiary Laramide uplift (Moore et al, 1988).

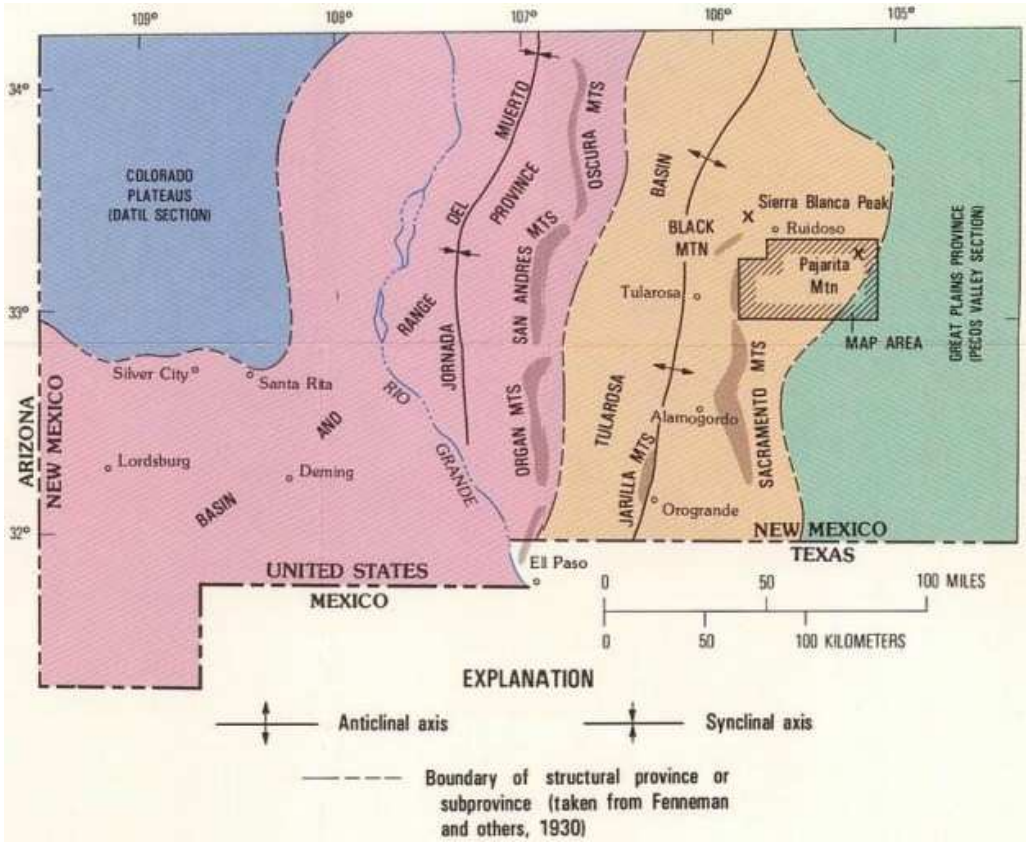


Figure 2.1. Location map including generalized geologic provinces of southern New Mexico, from Moore et al., 1988. The area highlighted as "Map Area" is an incomplete border of the Mescalero Apache Reservation; it includes the southern and eastern portions of the reservation, which were mapped in that study; the Northwestern portion of the reservation, mapped in a later study, is not outlined here.

Cambrian to Lower Tertiary sedimentary rocks and Tertiary to Quaternary volcanic and intrusive rocks cover most of southern New Mexico (Moore et al., 1985). Structural and erosional patterns in these rocks record Permian uplift as well as tectonism and magmatism of Laramide through Rio Grande Rift ages (Moore et al., 1988). Roughly 5 km^2 of the Pajarita Mountain pluton are exposed through an erosional window in this sequence on the northern, eastern and southern flanks of Pajarita Mountain (Fig. 2.2). Though the full size and morphology of the Pajarita Mountain peralkaline pluton are unknown, aeromagnetic surveys of the Mescalero Apache Reservation suggest that it is substantially larger than the exposed area. Interpretation of aeromagnetic data indicates a circular body roughly 8 km in diameter (Jacobson, 1986, vol. II). This body consists of a large magnetic low caused by the non-magnetic peralkaline rocks surrounding a magnetic high attributed to the moderate to strong magnetic signature of the cross-cutting mafic bodies (Tabet, 1991). Kelley (1968) interpreted Bouguer gravity data to suggest that the Pajarita Mountain crystalline rocks are part of a much larger arcuate complex extending tens of kilometers to the northwest and southeast beneath the exposed Paleozoic strata.

The summit of Pajarita Mountain rises roughly 350 meters above the surrounding plain and is composed of both peralkaline intrusive rocks and Permian sedimentary rocks that unconformably overlie them. This sedimentary succession consists of cherty, fossiliferous limestone, with minor dolostone, gypsum and clastic rocks, belonging to the Lower Permian Yeso and San Andres formations (Kelley, 1968). These regionally prevalent units wholly surround and thin near their contacts to the Pajarita Mountain crystalline rocks, dipping shallowly away from the summit of the mountain on all sides (Kelley, 1968). The rocks into which the peralkaline pluton was intruded are not exposed at the surface and have not been

intersected in drill core. Strongly altered gabbroic xenoliths within the pluton provide the only possible evidence of its host.

The Laramide Orogeny produced extensive normal faulting and horst-graben architecture within Paleozoic and Mesozoic rocks in the Northern Sacramento Mountains (Moore et al., 1988) that appears to have affected Pajarita Mountain. Early Laramide structures in the area comprise anastomosing northeast-trending normal faults. These faults are believed to have served as conduits for significant Tertiary igneous activity that began at roughly 39 Ma (Moore et al., 1991). To the north and west of the Mescalero Apache Reservation, this igneous activity is represented by the Black Mountain stock and swarms of alkali gabbro and monzogabbro dikes. The widespread Sierra Blanca volcanic pile was erupted and intruded by later feeder plugs, including the Capitan Mountain complex and numerous smaller intrusions during the following twelve million years (Moore et al., 1988, 1991). Stocks, plugs, dike swarms and flows of the Black Mountain-Sierra Blanca complex dominate the landscape just kilometers north and northwest of Pajarita Mountain. Controlled by a predominantly north-northeast-trending normal fault zone believed to be a shallow manifestation of reactivated Precambrian basement faults (Moore et al., 1991), these Tertiary bodies intruded into and through the regionally pervasive Permian to Tertiary sedimentary succession. Dikes and sills theorized to be related to this period of magmatism emplaced within San Andres carbonate rocks are visible in road cuts within several kilometers of their contact to the Pajarita Mountain crystalline rocks (Sherer, 1990). A north-northeast-trending fault, which parallels the regional trend of Tertiary extension, cuts the North study area and locally features fine-grained, tabular, meters-thick mafic dikes. While these bodies were not studied in detail, dike-filled faults of this orientation are characteristic features of Tertiary extension across the Tularosa Basin (Moore et al., 1988).

Numerous late (post-peralkaline) mafic bodies, some approaching half a square kilometer in estimated area (mapped by surface magnetic highs), are present within the Pajarita Mountain complex (Jacobson, 1986). While the North Area fault's initial movement and some of the mafic rocks may be Precambrian, as reported by previous authors, it can reasonably be postulated that at least some of the mafic rocks (and associated alteration) that cross-cut the Pajarita Mountain intrusion are related to Tertiary deformation and magmatism.

Tertiary alkalic igneous activity is also regionally associated with epithermal- and porphyry-related base and precious metal mineralization of the Lincoln County Porphyry Belt, a southern portion of an early to mid-Tertiary alkalic province extending from western Texas to central-northern Montana (Woodward, 1991). The north-south-trending structures that accommodated the causative mineralizing intrusions and fluids that created this mineralized zone cross through the western portion of the Mescalero Apache Reservation, and base and precious metal anomalies have been recorded on the reservation (Moore et al., 1985). Millimeter- to centimeter-scale carbonate±quartz±pyrite±galena veinlets observed in both peralkaline and fine-grained mafic rocks at Pajarita Mountain spatially correlate with black to brown pseudomorphic alteration of eudialyte and may represent a distal manifestation of this period of mineralization. Although Pajarita Mountain is situated in the far east of the Rio Grande Rift zone, the expansive Quaternary Valley of Fires lava flow 65 kilometers northwest of Pajarita Mountain leaves open the possibility that the area has been affected by extension and volcanism to the present day.

General geology of the study area

Peralkaline rock units used in maps, cross-sections, and other figures developed for this study are described in detail in Chapters 4 and 5. Based on mapping of two study areas, the North and South Area, many details regarding the peralkaline units differ from those described

by Molycorp. As a result, the map in Figure 2.2 has been generalized to show only the distribution of Proterozoic peralkaline syenites and quartz syenites, younger mafic bodies, Permian sedimentary units, and alluvial cover.

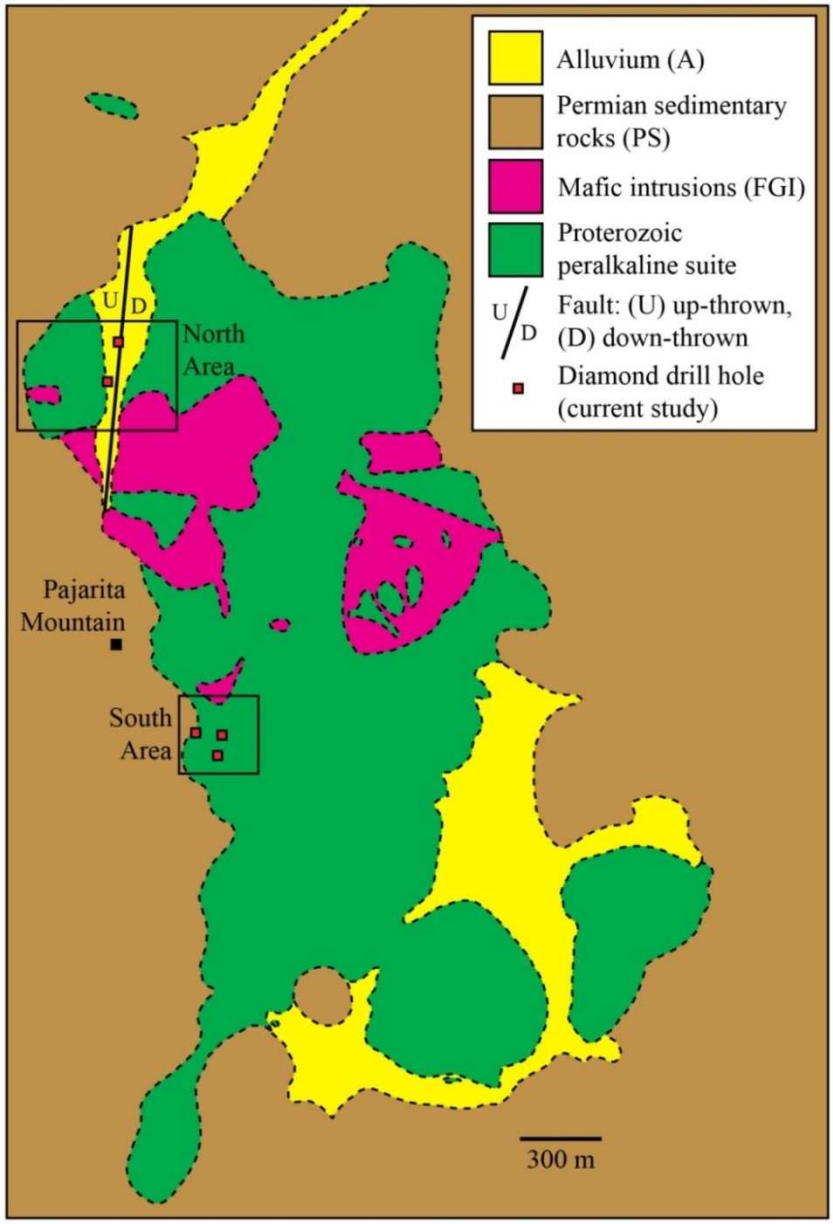


Figure 2.2. Geologic map of the Pajarita Mountain pluton showing the mid-Proterozoic peralkaline rocks, later Permian sedimentary units and mafic intrusions. Map digitized and modified from Molycorp mapping in Jacobson (1986). All data are from Molycorp work with the exception of locations of drilling sites for the current study and the approximate location of the fault in the North Area. North direction corresponds to top. Location of this map corresponds to the "X" in the northeastern corner of the Mescalero Apache Reservation in Fig. 2.1.

The two areas studied in this work were selected because they are the sites of the 2013 drilling by DEMD on behalf of the Mescalero Apache Tribe. DEMD drilled five holes, including two in the North Area and three in the South Area. DEMD twinned one Molycorp hole in the North Area and two in the South Area. All five holes were drilled to 152 meters. Drilling sites were selected based on the aim of twinning at least one Molycorp drill hole in both North and South Areas and their accessibility to a truck-borne drill rig. The original drilling sites were selected by Molycorp on the basis of grid surface sampling of outcrop and contouring of yttrium (Y) and zirconium (Zr) concentrations, following surface mapping of the entire exposure of the Pajarita Mountain pluton. In the present study, the areas surrounding the two clusters of drill holes were mapped to confirm and expand upon Molycorp's geologic mapping. Large parts of the study area consist of multiple peralkaline lithologies occurring together on too small a scale (less than three meters of core or continuous outcrop) to be mapped individually. These areas form more complex mixed units described in chapter 5.

CHAPTER 3

METHODS

Field mapping began in the summer of 2013 and was completed in the summer of 2014. Mapping focused on the Molycorp and DEMD drilling areas and their immediate surroundings (North and South Areas; see previous chapter, Fig. 2.2) and the five new drill cores were logged. Field and core descriptions included general geology, modal mineralogy, structure/layering/ foliation, mineralization, and alteration. Rock units were broken out based loosely on Molycorp's descriptions; however, because more complex rock textures were observed than previously described by Molycorp, new rock units were described to distinguish igneous features present in the different zones of the layered syenitic intrusion. Cross-sections were created by combining surface maps and core logs, including digitization and interpretation of Molycorp core logs, to develop an understanding for the distribution of lithologies and mineralization.

From this geological framework, representative samples were selected from the main lithologic units and their major variants in order to conduct a detailed petrographic study of the layered sequences identified at Pajarita Mountain. Forty-four polished thin sections were created from 9 field and 36 drill core samples. Drill core was favored because eudialyte weathers readily, and some bias was given to strongly mineralized zones due to the economic motivation for the project. Thin sections were prepared and inspected using optical microscopy. Three polished thin sections were inspected using a hot-cathode CL microscope by Lumic Special Microscopes, Germany, operated at 14kV and with a current density of ca. 10 $\mu A\ mm^2$.

For the purpose of investigating economic potential, DEMD had all 762 meters of core sampled for whole rock analysis by Activation Laboratories Ancaster. Sample intervals were

marked on 1.5 m intervals and, where possible, were adjusted to account for geological features such as rock type, textural changes, and alteration zones. All core was sawed in half, and one half of the full length of core in each interval was processed as a single sample. Samples were sawed and bagged by Hazen Laboratories of Golden, Colorado. The remaining half of all core was returned to DEMD for recordkeeping. Each sample was crushed to 80% -10 mesh, riffle split to yield a 250 gram sample, and pulverized to 95% -200 mesh. These pulps were subjected to lithium metaborate/tetraborate fusion and analyzed by inductively-coupled plasma mass spectrometry (ICP-MS) for major oxides (SiO_2, Al_2O_3, Fe_2O_3 as total Fe, MgO, MnO, CaO, TiO_2, Na_2O, K_2O, P_2O_5) and trace elements (ActLabs analytical package 8-REE). An additional analysis for F was conducted via ion selective electrode method (ActLabs analytical package 8-F: Li metaborate/tetraborate fusion, nitric acid digestion, automated fluoride ion activity analyzer). A total of 501 drill core samples were submitted for these analyses, and 96 samples representing major rock types were tested for specific gravity prior to comminution.

A second round of targeted whole rock geochemical sampling was conducted based on petrographic analysis, whole rock geochemistry, and the need for samples of smaller scale to obtain representative analyses of lithologies that occur in narrower bands than were practical to isolate for analysis in the early whole rock survey. This second survey focused on smaller scale variations in geology (modal mineralogy, textural features, alteration) and included measurement of FeO by titration (ActLabs analytical package 4F-FeO). Eighty-three samples were analyzed via the same methods listed above for the same package of major oxides, trace elements, fluorine, and FeO.

Six thin sections representing major lithologies were studied with the TESCAN MIRA3 LMH Schottky field-emission scanning electron microscope (FE-SEM) at the Colorado School

of Mines Department of Geology & Geological Engineering. The working distance used was 10 mm at 25.0 kV acceleration for BSE photomicrographs and EDS analyses, with a measurement time of 30.0 seconds for EDS. Analyses were conducted on amphibole, feldspar, eudialyte, aenigmatite, fluorite and several minerals replacing eudialyte in thin sections representing major rock types from North and South area drill cores. BSE imaging and EDS were used to test whether specific mineral grains displayed significant compositional variations due to zoning. EDS was utilized to investigate the major constituents of eudialyte, amphibole, and feldspars and to determine whether cumulus and intercumulus amphibole could be distinguished compositionally at this resolution. Six polished rock chip samples from one North Area drill core were analyzed using a fully automated QEMSCAN® system. This system combines a Carl Zeiss EVO 50 SEM, four Bruker X275HR EDS detectors and the iDiscover® proprietary software. Using a working distance of 23 mm at 25 kV acceleration voltage, field image scans produced false color mineral distribution maps. Chip samples mapped via QEMSCAN® at an early stage were corroborated by optical inspection of thin sections equivalent to four of these samples.

CHAPTER 4

RESULTS

4.1 Mineralogy of the Pajarita Mountain peralkaline cumulate suite

The major primary minerals that occur in all Pajarita Mountain peralkaline syenitic rocks include alkali feldspar, Na-Fe amphibole (arfvedsonite/riebeckite), quartz, eudialyte, and fluorite. All minerals occur as both cumulus and post-cumulus phases with varying modal abundances and textural relationships, which yield the distinguishing characteristics of the different lithologies described in section 4.3. One subset of the peralkaline rocks contains oikocrystic aenigmatite. Common secondary minerals include aegirine, pseudomorphs after eudialyte, fluorite, molybdenite, sphalerite, and galena. Abbreviations for mineral names are listed in Table 4.1.

Terms describing mineral textures in peralkaline rocks include those applied to layered intrusions, namely those referring to the relationship of grains to cumulus processes. These terms are used after the fashion of Irvine (1982). While Irvine's terminology is both descriptive and interpretive, it is appropriate given that the Pajarita Mountain pluton is being interpreted as a complex, multi-event, layered intrusion. Most of the peralkaline syenitic rocks do not show an archetypal cumulate texture, such as a network of euhedral cumulus grains enveloped by one or several oikocrystic intercumulus minerals, as seen in the well-studied layered mafic intrusions (i.e., Bushveld, Stillwater). Cumulus grains are defined here as those that crystallized, were separated from their parent melt, and concentrated into a framework of grains predominantly in contact with one another. "Post-cumulus" is used to describe any mineral growth following the

original cumulus grains, and includes the more precise terms “adcumulus”, “poikilitic”, “oikocrystic” and “intercumulus”.

Table 4.1. Table of Mineral Abbreviations

Eudialyte	Eud
Na-Fe amphibole	Amph
Quartz	Qtz
Alkali feldspar	Afs
K-feldspar	Kfs*
Albite	Alb*
Fluorite	Fluo
Aenigmatite	Aen
Apatite	Apt
Aegirine	Aeg
Calcite	Cal
Unknown Zr-Ca silicate	ZrS
Unknown REE silicate 1	RS1
Unknown REE silicate 2	RS2
Unknown Fe-Mg-Ca silicate	US
Sphalerite	Sph
Galena	Gn
Molybdenite	Mol
Orthopyroxene	Opx
Clinopyroxene	Cpx
Biotite	Bt
Plagioclase	Plag
Opaque mineral(s), undifferentiated	Opq

*Asterisk indicates abbreviation is used where end-member composition has been determined by EDS.

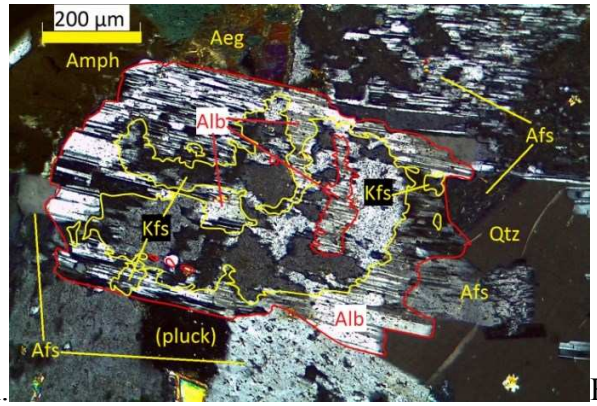
Cumulus grains vary from exquisitely euhedral grains to anhedral grains whose size and textural relationships suggest that they were present during formation of the original cumulus framework but whose growth continued following accumulation. The resultant “accommodative” contacts around other cumulus grains can result in an anhedral final form. Crucial for such anhedral grains to be classified as cumulus is a lack of evidence for a change in

conditions during crystallization, such as a cessation of growth. Many grains show clear zonal boundaries (i.e. variations in birefringence colors, pleochroism, fracturing, mineral and/or fluid inclusion content) between a cumulus grain core and a post-accumulation overgrowth of the same mineral. The core of the grain in such a texture is described as cumulus, while the overgrowth is classified as adcumulus. The hybrid term "cumulus-adcumulus grain" is used in this study to describe grains displaying this type of development. In this section, photomicrographs are used to show typical end-member examples of minerals that display typical cumulus vs. post-cumulus textures characteristic of specific lithologies. Mineral textures are also interpreted in terms of the processes that may have created them.

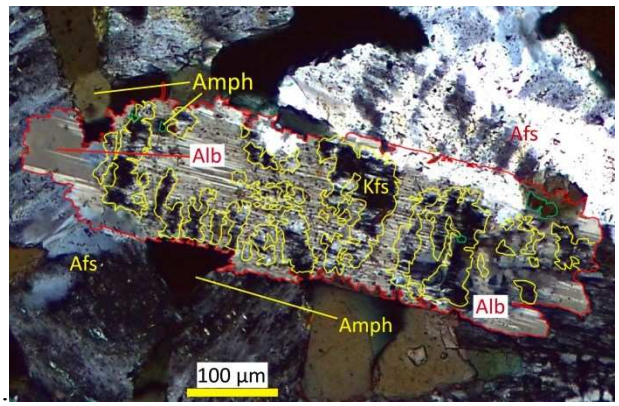
Alkali feldspar

Alkali feldspar occurs in all peralkaline syenitic units at Pajarita Mountain. Four distinct textural varieties were identified. Each major peralkaline syenitic rock type (I-III; see Section 4.3) contains two main textural variants of alkali feldspar as groundmass cumulus grains and one of two coarser-grained textural variants. Groundmass alkali feldspar variants include: Afs A, subhedral to anhedral, mantled, partially resorbed grains with irregularly shaped compositional zones in their cores (Fig. 4.1A-B); and Afs B, anhedral to subhedral grains lacking clear mantles but displaying more consistently sub-parallel, often through-going pseudo-perthitic compositional zones (Fig. 4.1C-D). Groundmass alkali feldspar grains vary in size, habit (may be predominantly blocky or prismatic), and overall shape of compositional zones (from erratic to quite regular in terms of orientation and thickness) with the overall characteristics of different peralkaline lithologies' groundmasses. However, these two textural populations are common to all peralkaline syenitic rocks observed. EDS indicates end-member K-feldspar and albite compositional zones, with albite being dominant in grain mantles.

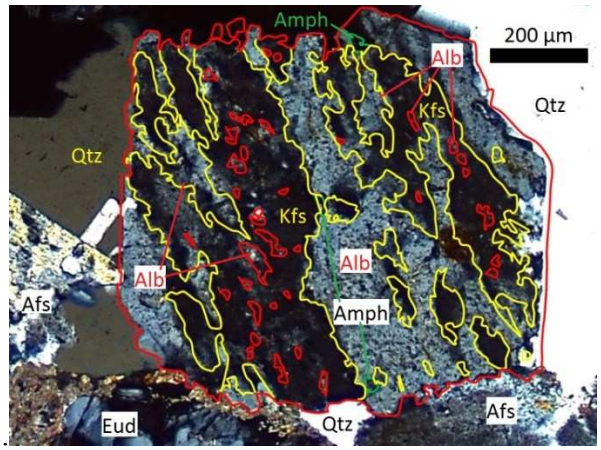
Figure 4.1. Photomicrographs of alkali feldspar grains representing the four principle textural variants, all under cross-polarized light (XPL). Outlined Alb and Kfs compositional zones were determined by BSE and EDS (see Appendix A). A. Afs A. Medium-grained, blocky, subhedral groundmass grain showing subhedral Kfs-dominant core with erratically-oriented Kfs and Alb zones and Alb-dominant mantle. B. Afs A. Finer-grained, prismatic, subhedral groundmass grain with variably developed Alb mantle around core of sub-parallel lensoid Kfs zones enveloped by Alb. Mantle partially envelops adjacent Amph. C. Afs B. Medium-grained, blocky, subhedral groundmass grain with broadly sub-parallel, through-going pseudo-perthitic compositional zones. D. Afs B. Fine-grained, prismatic subhedral grain with through-going compositional zones showing greater consistency in thickness and orientation. E. Afs C. Coarse-grained, prismatic, subhedral alkali feldspar phenocryst with up to four concentric optical zones including partchy Alb mantle. Note the amphibole inclusions, intergrowth with adjacent medium-grained Afs A-B grains, partial envelopment of Eud grain, and Afs C grain's envelopment by optically continuous Qtz. F. Afs C. Concentrically zoned, subhedral Afs phenocryst enveloped by fine-grained groundmass of Afs A-B and anhedral Amph, Eud and Fluo. G. Afs D. Coarse-grained, euhedral phenocryst with sharp contact to obvious anhedral mantle. More classical wispy perthitic texture in core and mantle with coarser lamellae in mantle. Mantle envelops fine-grained groundmass Amph and Afs.


200 µm
Aeg
Amph
Alb
Afs
Kfs
Kfs
Qtz
Afs
Alb
(pluck)
Afs

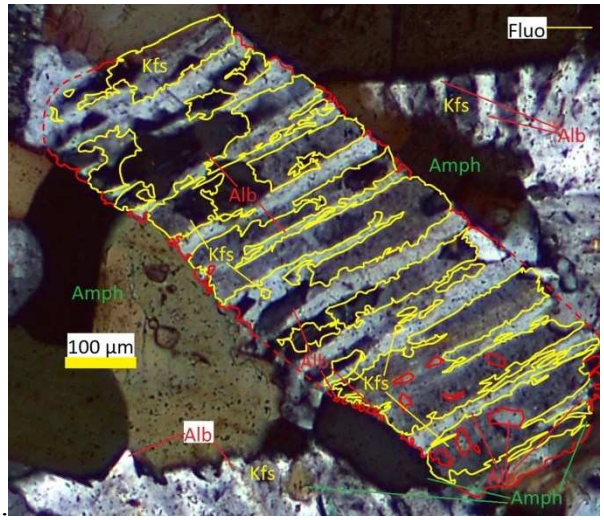
A.


Amph
Alb
Afs
Kfs
Afs
Amph
Alb
100 µm

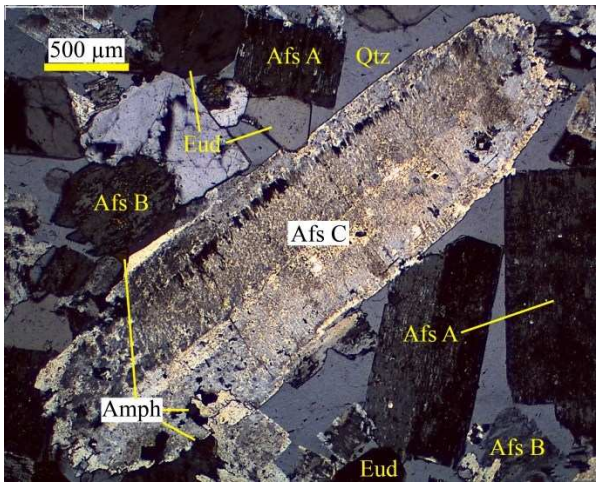
B.


Amph
200 µm
Alb
Qtz
Kfs
Qtz
Kfs
Alb
Alb
Amph
Afs
Eud
Qtz
Afs

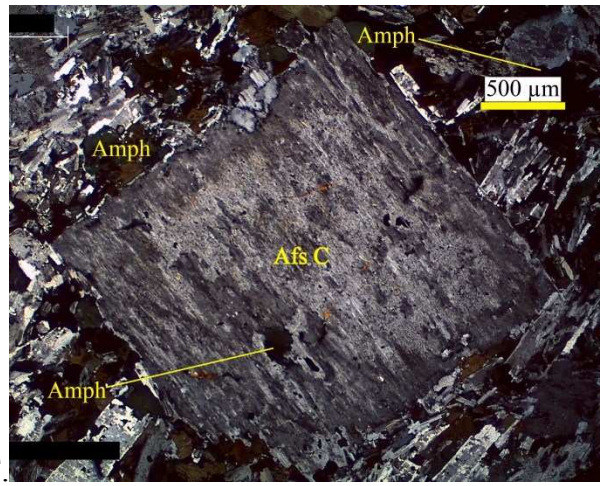
C.


Fluo
Kfs
Kfs
Alb
Amph
Alb
Kfs
Amph
100 µm
Kfs
Alb
Kfs
Amph

D.


500 µm
Afs A
Qtz
Eud
Afs B
Afs C
Afs A
Amph
Afs B
Eud

E.


Amph
500 µm
Amph
Afs C
Amph

F.

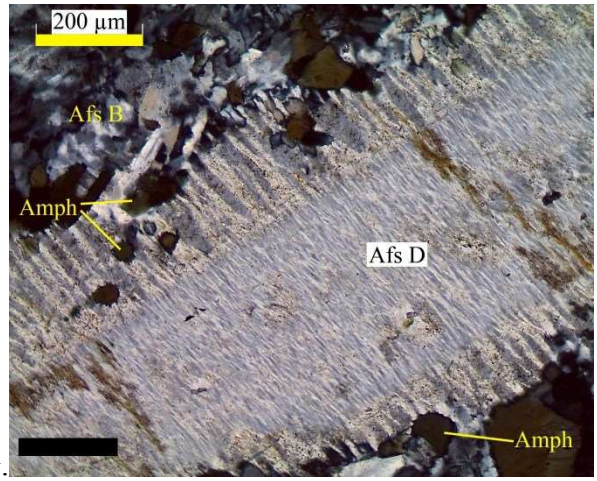
G. 

Figure 4.1. (cont.).

The two coarser-grained alkali feldspar variants comprise typically better-formed, subhedral to euhedral phenocrysts that are several times larger than groundmass grains. The first, Afs C (Fig. 4.1 E-F), displays two or more concentric optical zones and may have a similar core-mantle texture to variant Afs A. The second coarse-grained variant, Afs D (Fig. 4.1G), comprises euhedral phenocrysts with sharp contacts to obvious anhedral or subhedral mantles. Both cores and mantles in Afs D grains display more classical perthitic textures than are observed in Afs B. Alkali feldspar textures are interpreted as evidence of processes involved in the genesis of the pluton (see Chapter 5).

Na-Fe Amphibole (riebeckite/arfvedsonite)

Na-Fe amphibole occurs as both cumulus and intercumulus phases, most commonly as aggregates of cumulus-adcumulus grains (Fig. 4.2A). Cumulus grains may be blocky or prismatic, although no cumulus grain retains more than a subhedral form due to adcumulus overgrowth. Where prismatic amphibole grains comprise greater than 35 vol.%, they typically display moderate to strong parallel orientation. Cumulus and adcumulus amphibole may be discriminated by optical zonation, which may take the form of color variations under crossed

polars (Fig. 4.2A) and/or changes in fluid and mineral inclusion abundance. Cumulus amphibole grain boundaries may also be decipherable from adcumulus overgrowths through their contacts to cumulus grains of other phases. For example, the pseudomorphed cumulus eudialyte grain shown at the bottom right of Fig. 4.2A shares a contact to the cumulus amphibole grain whose outline is visible via color variation. Both cumulus grains are enveloped by adcumulus overgrowth, a relationship which suggests that accumulation of a framework of early grains preceded adcumulus amphibole overgrowth. Cumulus amphibole grains with no adcumulus growth have not been observed. Minor inclusions of fluorite and apatite (Fig. 4.2D) are common.

In rocks with low modal amphibole abundances (15 vol.% or less), amphibole almost exclusively displays an intercumulus texture, occurring as optically continuous, sub-rounded clots or patches up to one centimeter in diameter (Fig. 4.2B-C). This texture typically accompanies high modal amounts of eudialyte (15 vol.% or more). These amphibole clots may contain relatively inclusion free cores that are similar in size to the surrounding cumulus framework grains. This texture may indicate late-crystallizing amphibole replacing early cumulus minerals (possible partial replacement of Eud and Afs in Fig. 4.2B) and continuing to grow into available interstitial space. Alternatively, it may represent early amphibole grains from which adcumulus extensions have grown. Also suggesting late amphibole are adcumulus amphibole apophyses interdigitated into alkali feldspar grains, typically favoring K-feldspar rich zones (Fig. 4.1C-D). Contacts between intercumulus amphibole and intercumulus quartz typically show amphibole partially lining intercumulus spaces filled by quartz, suggesting replacement by quartz or vice versa (outer margins of intercumulus amphibole clots in Fig. 4.2B-

C). Additionally, amphibole commonly shows replacement by aegirine, ranging from distal grain edges only to complete pseudomorphic replacement (Fig. 4.2B-C).

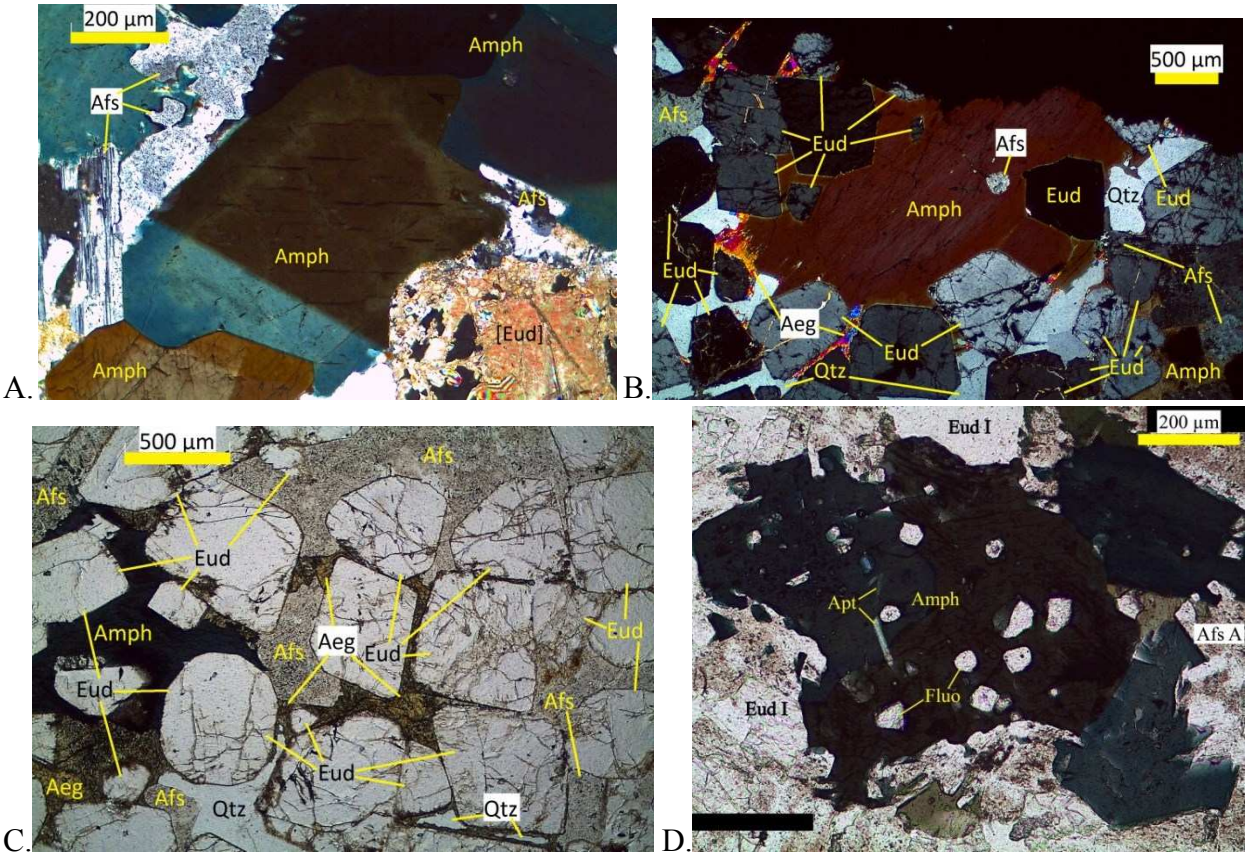


Figure 4.2. Photomicrographs of Na-Fe amphibole. A. Cumulus-adcumulus amphibole aggregate with central weakly resorbed cumulus grain in contact with altered cumulus eudialyte. XPL. B. Intercumulus amphibole clot with large core. XPL. C. Intercumulus amphibole, partially altered to aegirine, sharing intercumulus space with alkali feldspar and quartz. PPL. D. Dominantly intercumulus amphibole grain rich in inclusions of fluorite and apatite. PPL.

Quartz

Quartz appears with cumulus and intercumulus textures, the latter being far more common than the former. Intercumulus quartz occurs in most peralkaline syenitic rocks as oikocrysts up to one centimeter across comprising 5 to 15 vol.% (Fig. 4.3). Where intercumulus

quartz is abundant, post-cumulus amphibole and alkali feldspar overgrowths are less pronounced. Relationships between intercumulus quartz and post-cumulus amphibole and alkali feldspar may be complex, with some textures suggesting replacement of alkali feldspar and amphibole by intercumulus quartz (Fig. 4.3A-B). Replacement varies from minor to significant and, like amphibole, quartz appears to favor contacts between albite and K-feldspar when replacing alkali feldspar. Additionally, quartz is locally observed to contribute to pseudomorphic replacement of eudialyte by several minerals (Fig. 4.7C).

Textural evidence suggests the presence of cumulus quartz grains in a specific subset of the Pajarita Mountain peralkaline rocks (quartz megacrystic eudialyte-amphibole syenite cumulate – see section 4.3). In one sample, cumulus quartz grains wholly rimmed by intercumulus amphibole were observed (Fig. 4.3C). More typically, these quartz megacrysts are made up of cumulus quartz grains overgrown by optically continuous intercumulus quartz (Fig. 4.3D). This texture results in quartz grains significantly larger than those of any other mineral population in the rock (typically 3-8mm in diameter), comprising up to 40 vol.%. These grains may also, like the large amphibole clots, be suggestive of late quartz replacing cumulus grains such as alkali feldspar and amphibole, leaving atypically small inclusions of these minerals (Fig. 4.3D). The relative proportions of cumulus and intercumulus quartz in these megacrystic quartz zones were not confidently determined due to optical continuity. Two samples of this sub-type were analyzed via cathodoluminescence microscopy, including one containing the discrete cumulus quartz grains enveloped by intercumulus amphibole (Fig. 4.3C). These analyses did not provide conclusive evidence for or against the interpretation of these grains as cumulus quartz cores.

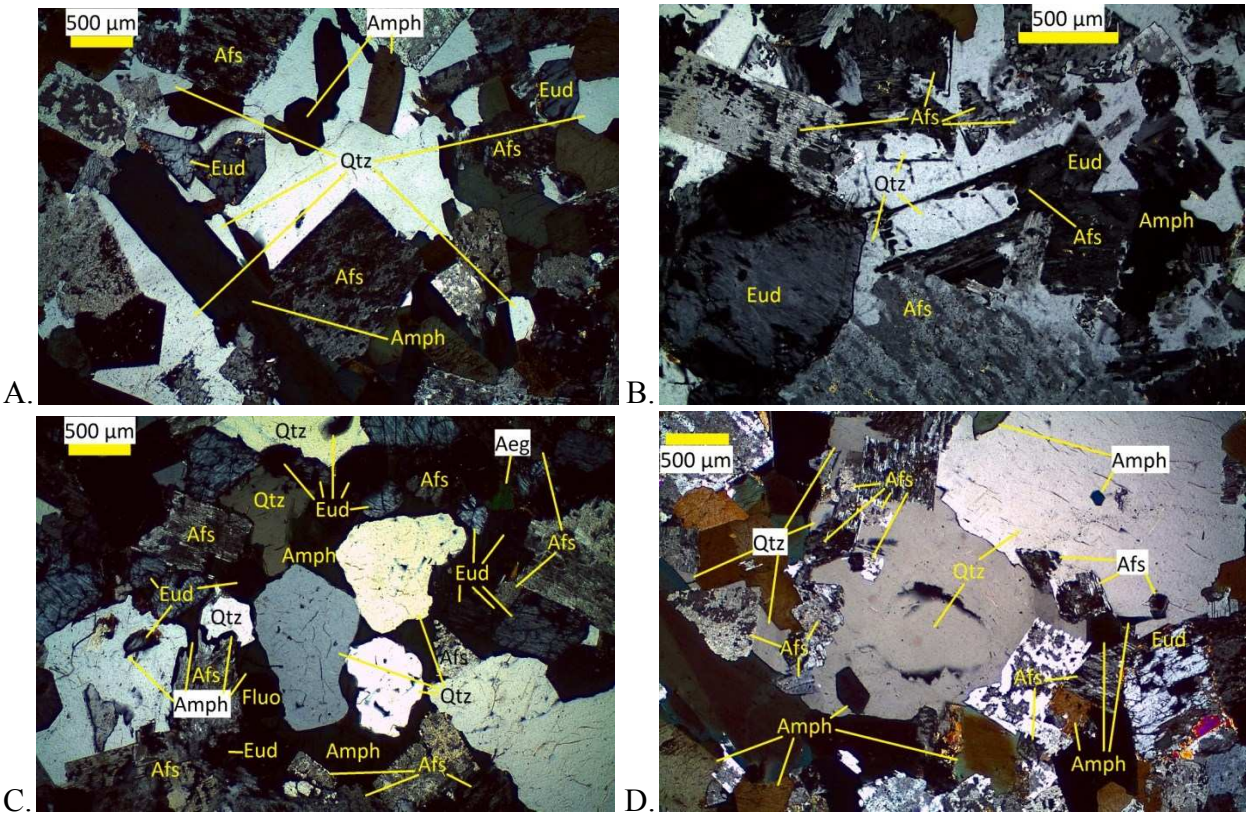


Figure 4.3. Photomicrographs of quartz. All XPL. A. Typical oikocrystic quartz domain in a zone poor in adcumulus amphibole and alkali feldspar. B. Skeletal alkali feldspar grains in-filled by oikocrystic quartz. C. Anhedral cumulus quartz grains fully surrounded by a single amphibole oikocryst. D. Hypothesized cumulus quartz grain (cumulus grain margins suggested by sub-rounded pattern of plucking) within quartz megacryst. Note adjacent second quartz megacryst.

Eudialyte

Eudialyte, the principal mineral of economic interest at Pajarita Mountain, occurs as anhedral to euhedral cumulus grains and oikocrysts. Cumulus grains typically show well-developed crystal faces at contacts with oikocrystic quartz and euhedral morphology where wholly included in quartz (Fig. 4.4A). Cumulus eudialyte is similarly euhedral at contacts with oikocrystic amphibole and with alkali feldspar showing significant adcumulus growth (Fig. 4.2B-C). In samples with high ratios of cumulus to oikocrystic minerals, cumulus eudialyte grains show accommodative contacts around other cumulus grains (Fig. 4.4B) and may wholly envelop grains of alkali feldspar and amphibole. Individual grains may have anhedral contacts

with other cumulus grains but euhedral contacts to intercumulus phases. Where cumulus textures are well developed with euhedral cumulus grains enclosed in oikocrystic post-cumulus minerals, eudialyte is commonly more abundant (Fig. 4.4A; Fig. 4.2B-C).

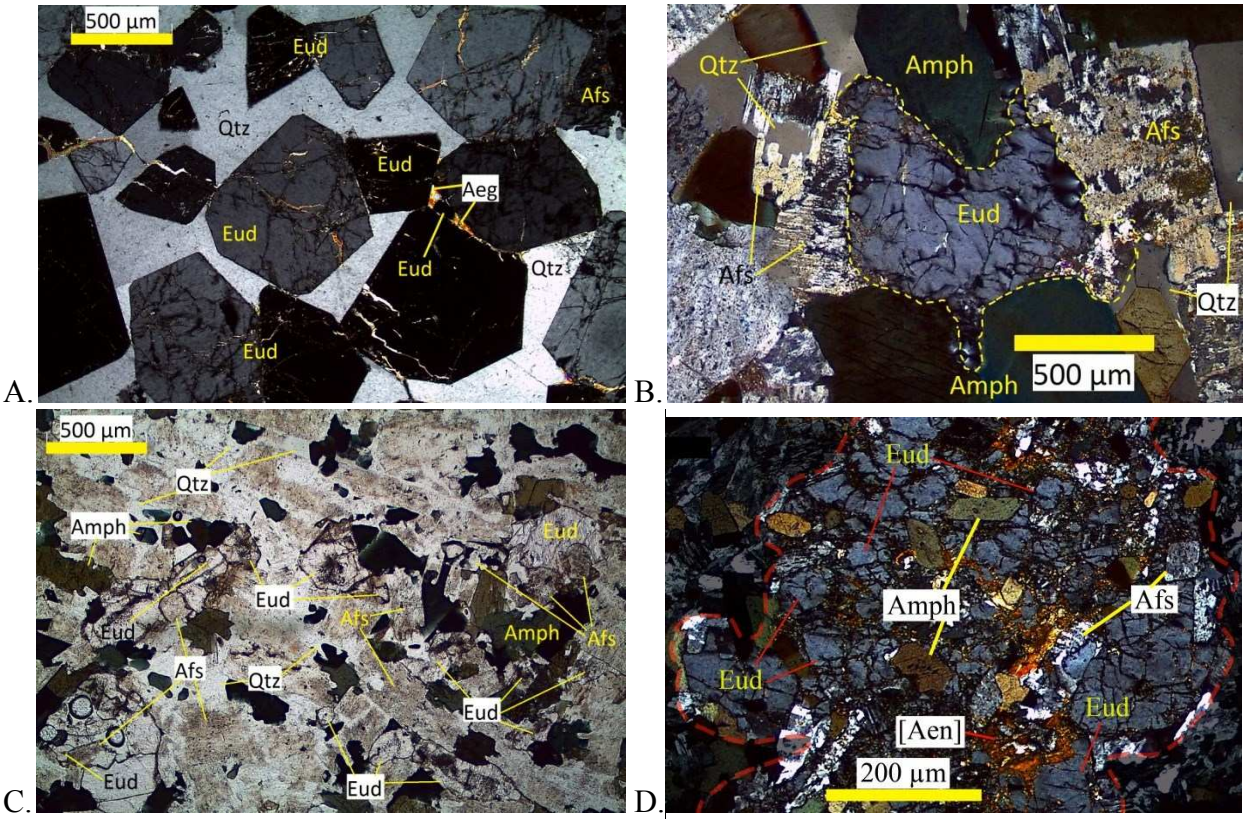


Figure 4.4. Photomicrographs of eudialyte in Pajarita Mountain peralkaline rocks. A. Abundant euhedral cumulus eudialyte, showing characteristic fracturing and high relief, within a single quartz oikocryst. XPL. B. Slightly altered anhedral cumulus eudialyte grain (with some plucking) with accommodative contacts to adjacent cumulus alkali feldspar and amphibole. Possible replacement of Afs core by intercumulus quartz. XPL. C. Fine-grained anhedral to sub-poikilitic cumulus eudialyte accommodating alkali feldspar and amphibole, showing common "dust rim" alteration and plucking. PPL. D. Part of a single large eudialyte oikocryst (within red dashes) enveloping fine-grained cumulus alkali feldspar and amphibole and altered poikilitic aenigmatite ([Aen]). XPL.

Anhedral cumulus eudialyte is observed in some fine-grained peralkaline syenitic rocks with poorly developed cumulus textures (Fig. 4.4C). Though anhedral, these grains are interpreted as cumulus given their occurrence alongside subhedral cumulus alkali feldspar crystals and cumulus-adcumulus amphibole. Eudialyte grains locally appear in direct contact

with cumulus cores of alkali feldspar grains and are accommodated within post-cumulus mantles. This texture suggests eudialyte crystallizing roughly coeval with the other groundmass minerals.

Oikocrystic eudialyte (Fig. 4.4D) occurs primarily in discrete, irregular zones within fine-grained peralkaline syenitic rocks showing more poorly developed cumulus textures. Multiple eudialyte oikocrysts, accompanied by atypically abundant alkali feldspar and quartz, make up these zones. These oikocrysts are generally several millimeters across and envelop all groundmass minerals observed in this rock type (alkali feldspar, amphibole, fluorite, and oikocrystic aenigmatite). This texture suggests largely post-cumulus appearance of eudialyte, whereas the other major texture types are indicative of appearance at the early to main portion of the cumulus crystallization phase. Eudialyte that partially encloses cumulus grains, referred to as sub-poikilitic, appears in medium-grained syenitic cumulates as well, but is not a prevailing texture. Eudialyte also commonly shows alteration that manifests itself as partial to complete replacement by secondary minerals (see section 4.2).

Fluorite

Fluorite is a common accessory mineral. It is often present as minor inclusions in amphibole, locally with apatite (Fig. 4.2D). Where samples are dominated by euhedral cumulus grains and oikocrystic intercumulus minerals, fluorite may be observed as rare subhedral to euhedral cumulus grains (Fig. 4.5A,C). Fluorite is most abundant (up to 4 vol.%) in fine-grained peralkaline rocks with strong adcumulus growth, where it occurs as anhedral groundmass grains and inclusions in amphibole. In these rocks, groundmass fluorite typically shares the same intergranular spaces with post-cumulus amphibole (Fig. 4.5D) and is nearly always in contact

with amphibole. In fine-grained samples containing disseminated eudialyte, fluorite is often in contact with enclosing eudialyte (Fig 4.5C). In aenigmatite-bearing rocks, fluorite inclusions in aenigmatite are common (Fig. 4.5B).

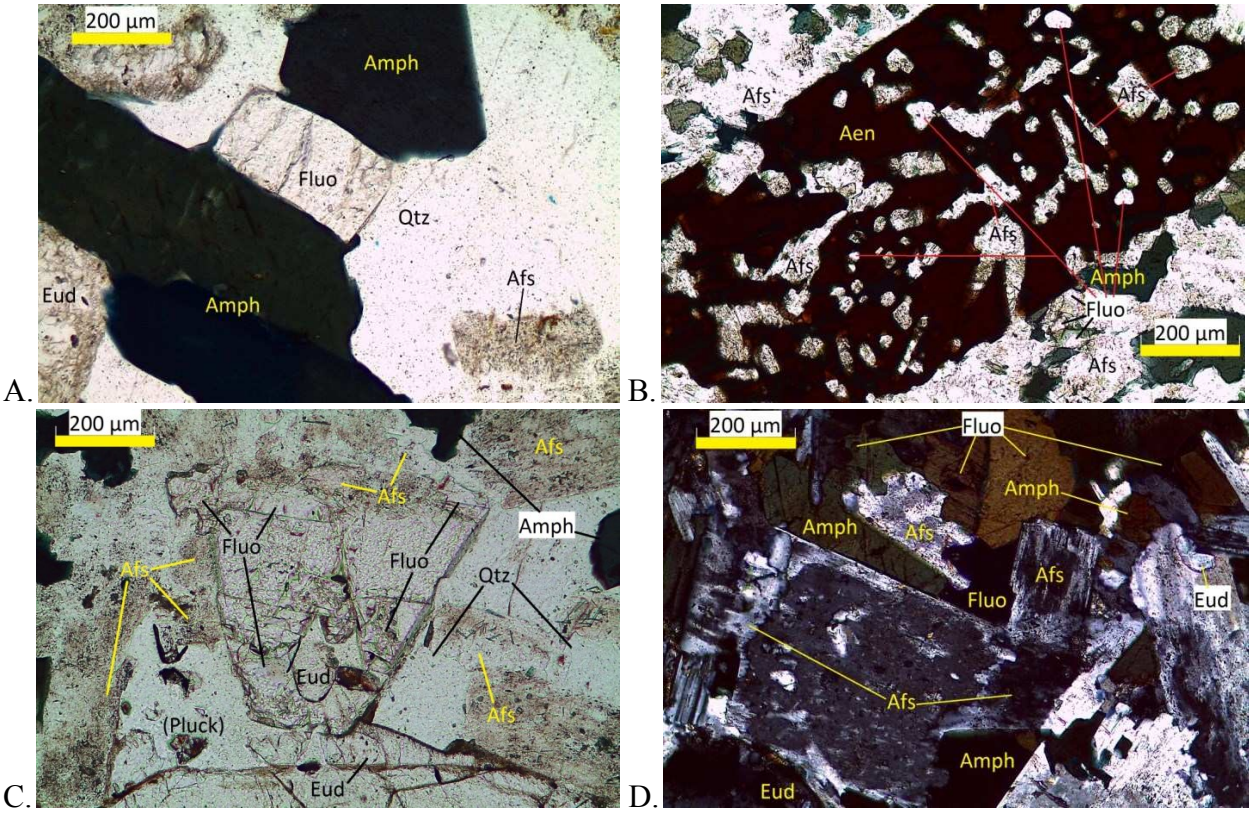


Figure 4.5. Photomicrographs of fluorite in Pajarita Mountain peralkaline rocks. A. Subhedral, possibly cumulus fluorite enclosed within cumulus-adcumulus amphibole and oikocrystic quartz. PPL. B. Anhedral fluorite inclusions in poikilitic aenigmatite and fine-grained groundmass. PPL. C. Subhedral fluorite grain with anhedral overgrowths and eudialyte inclusion. PPL. D. Anhedral fluorite and amphibole sharing intercumulus space. XPL.

Aenigmatite

Poikilitic aenigmatite grains (Fig. 4.5B) enclosing alkali feldspar and fluorite grains comprise roughly 2-15% of a single type of fine-grained peralkaline rocks (porphyritic aenigmatite-amphibole syenite cumulate – see section 4.3). Aenigmatite grains are typically 0.4 mm by 0.8 mm (up to 0.75 mm by 1.4 mm) and may be partially to wholly altered to an orange and/or blue fibrous mineral (Fig. 4.6). Unaltered grains are interpreted to be aenigmatite based

on EDS major element analyses, optical properties, and textural and morphological/textural similarities to aenigmatite from other peralkaline intrusive occurrences.

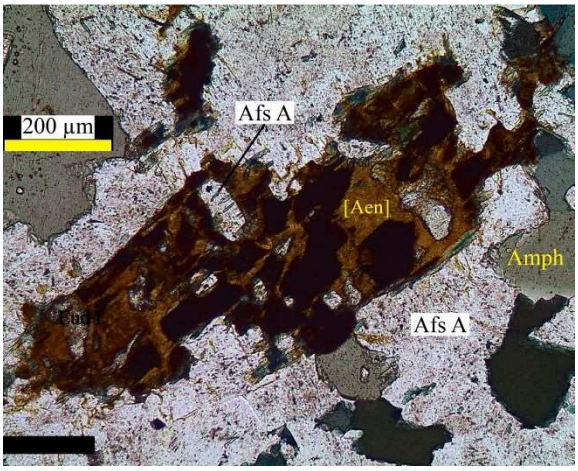


Figure 4.6. Photomicrograph of poikilitic aenigmatite altered to orange and blue fibrous minerals. PPL.

4.2 Replacement textures

Pseudomorphs after eudialyte

Several types of alteration were observed in Pajarita Mountain peralkaline rocks, the most common being pseudomorphs after eudialyte and aegirinization of amphibole. Four types of alteration of eudialyte were observed, each taking the form of partial to complete polymineralic pseudomorphism defined by their color in hand sample. Variations include alteration of eudialyte grains to white, dark brown to black, deep green, and orange minerals. The former three types are interpreted to be products of hypogene alteration, while the latter, observed predominantly near the surface, faults or fractures, appears to be caused by weathering.

In white-altered eudialyte, calcite and quartz, along with several other phases, replace eudialyte. This alteration does not clearly correlate to any other type of alteration (i.e. aegirinization of amphibole). In addition, EDS of selected minerals indicated the presence of

bladed Ca-zirconosilicates (most likely gittinsite), two unknown REE-bearing silicates that may be aluminocerite-(Ce) (RS1) and ferriallanite-(La) (RS2), and an unidentified Fe-Mg-Ca silicate (US). The presence of REE- and Zr-silicates and the lack of an obvious change in bulk REE and Zr grades where this alteration is present suggest that this alteration was not responsible for significant spatial remobilization of these elements.

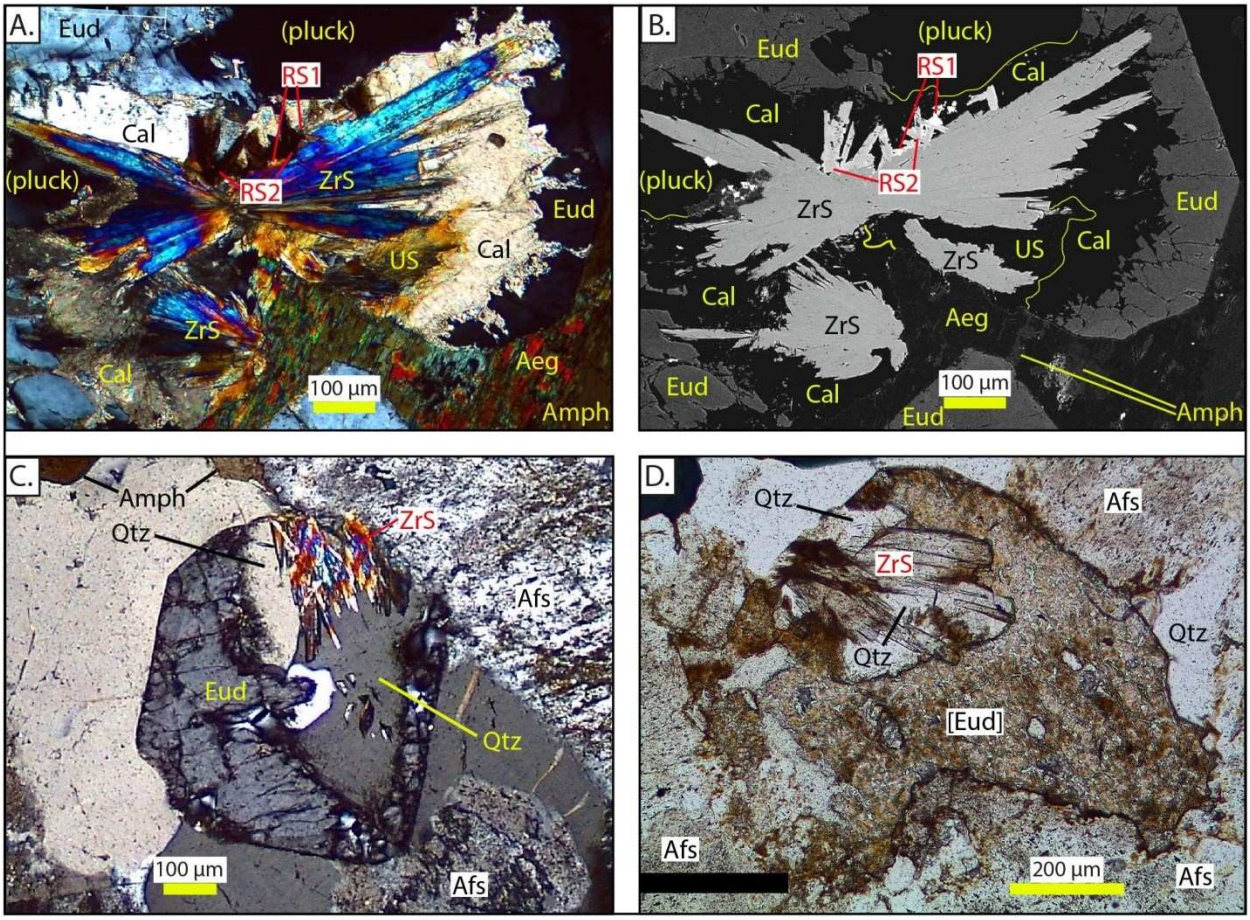


Figure 4.7. Photomicrographs of eudialyte alteration/replacement. A. Intense "white" type hypogene alteration of two eudialyte grains. Alteration minerals include calcite, an unknown Ca-zirconosilicate (ZrS; either gittinsite or armstrongite), at least two REE-bearing silicate phases (RS1, RS2), and an unidentified Fe-Mg-Ca silicate (US). Note aegirine replacement at edges of amphibole grain. XPL. B. BSE image of grain seen in A. C. Partial hypogene white-altered cumulus eudialyte in-filled by two quartz oikocrysts. Adjacent amphibole is unaltered. XPL. D. "Brown" type hypogene alteration of eudialyte overprinted on partial pseudomorphic white alteration. XPL.

Many altered eudialyte grains are partially replaced or in-filled by late quartz (Fig. 4.7C-D). This quartz is almost always in optical continuity with adjacent poikilitic quartz. Fig. 4.7C shows a partially white-altered eudialyte grain that has been partially in-filled by poikilitic quartz from two oikocrysts with distinct optical orientations. This texture suggests that some dissolution and replacement of eudialyte with minerals of the "white" alteration suite preceded precipitation of at least some intercumulus quartz, possibly making this alteration late magmatic in origin.

Macroscopically dark brown eudialyte alteration (Fig. 4.7D) results in a very fine-grained matrix of unknown mineralogy. It was not studied by BSE and EDS. It is considered hypogene because it occurs at significant depth and far from observed structures that might have allowed weathering via surface water infiltration.

Aegirine pseudomorphs after amphibole

All of the peralkaline syenitic rocks display some degree of replacement of amphibole by aegirine. Where replacement is incomplete, it is typically seen only at grain margins (Fig. 4). This alteration varies in abundance from a few grain margins to wholesale pseudomorphism of nearly all amphibole (Fig. 4.8). While pervasive aegirinization locally co-occurs with high-grade mineralization, there is no robust positive correlation between them, and many strongly mineralized zones show only trace aegirine. It is worth noting, however, that the most strongly mineralized core interval observed in this study displays pervasive aegirinization of amphibole (see Fig. 4.8). That this interval also contains abundant pink (largely unaltered) eudialyte points to the lack of a clear correlation between aegirinization and eudialyte alteration. While aegirinization does not correlate strongly with the observed types of eudialyte alteration, there is evidence that sulfides (galena, sphalerite, unknowns) accompanied aegirine in replacing

amphibole (Fig. 4.8). This association is commonly observed in pegmatites, in which amphibole is partially to fully replaced by aegirine, and grains of galena and sphalerite up to 4 mm across have been observed.

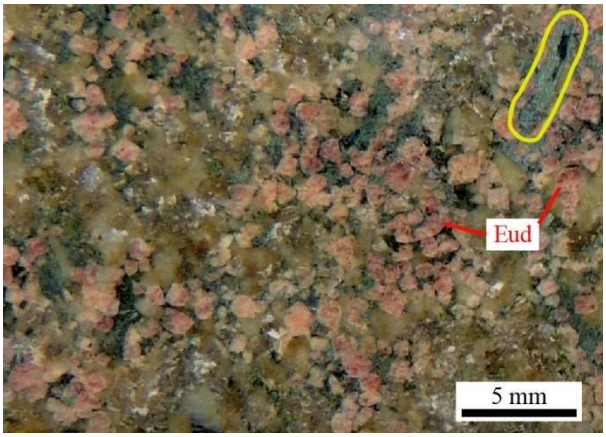


Figure 4.8. Image of pervasive Aeg replacement of dominantly intercumulus Amph with abundant, mostly pink-tan to red, unaltered Eud. White spots may represent very fine-grained Eud with white alteration. Note 75% Aeg replacement of coarse Amph grain (circled).

Reaction textures in igneous minerals

In addition to alteration of magmatic minerals, it also is common for the primary magmatic minerals to show textures suggesting replacement of one another. These textures may comprise pervasive replacement of one intercumulus phase by another or adcumulus growth from one cumulus grain into an adjacent cumulus grain. Several textures mentioned above may be interpreted as indicating strong replacement of early cumulus grains by amphibole or quartz. Replacement of alkali feldspar by quartz locally favors grain cores (Fig. 4.9A), which EDS analyses revealed to be dominantly K-feldspar. Oikocrystic quartz may also fill voids in eudialyte that has undergone partial replacement by secondary quartz and calcite (Fig. 4.7C-D).

Amphibole almost universally shows a degree of replacement of alkali feldspar. This may take the form of interdigitated contacts where amphibole exploits compositional zone

boundaries in adjacent alkali feldspar grains (Fig. 4.10A). Amphibole may also extensively replace alkali feldspar grains to the point of obscuring original grain margins (Fig. 4.10B).

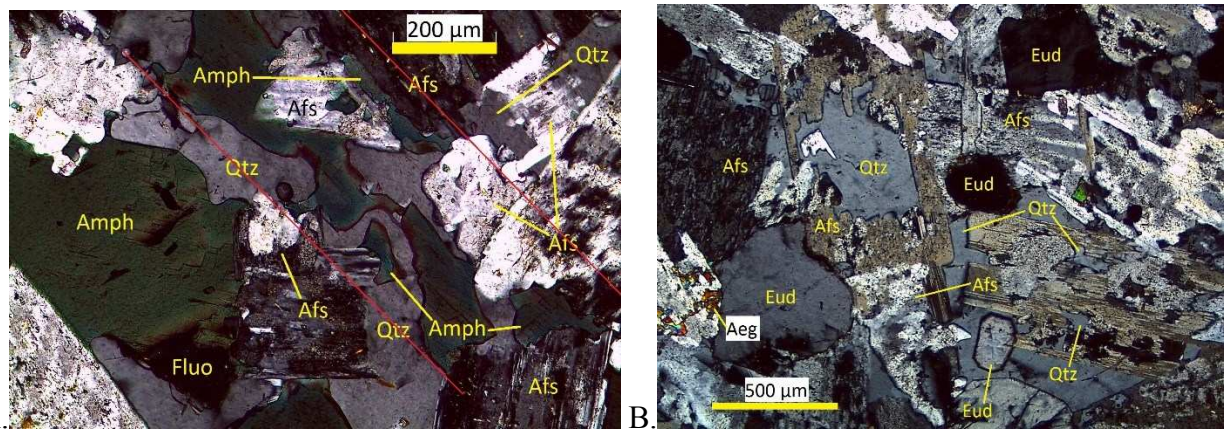


Figure 4.9. Photomicrographs of quartz replacement textures, XPL. A. Oikocrystic quartz replacing amphibole and alkali feldspar. Amphibole between the red lines has a single optical orientation, indicating a single grain irregularly cross-cut by late quartz. Quartz also preferentially replaces the core of Afs grain at upper right, as well as a second amphibole grain at left. Note that both amphibole grains show prior replacement of Afs. B. Quartz preferentially replacing cores of alkali feldspar grains, likely dominantly K-feldspar.

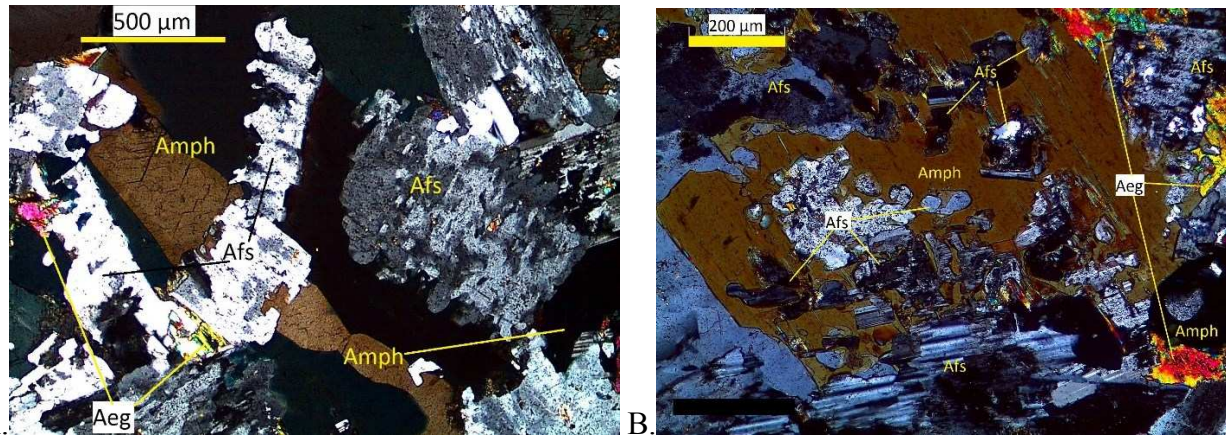


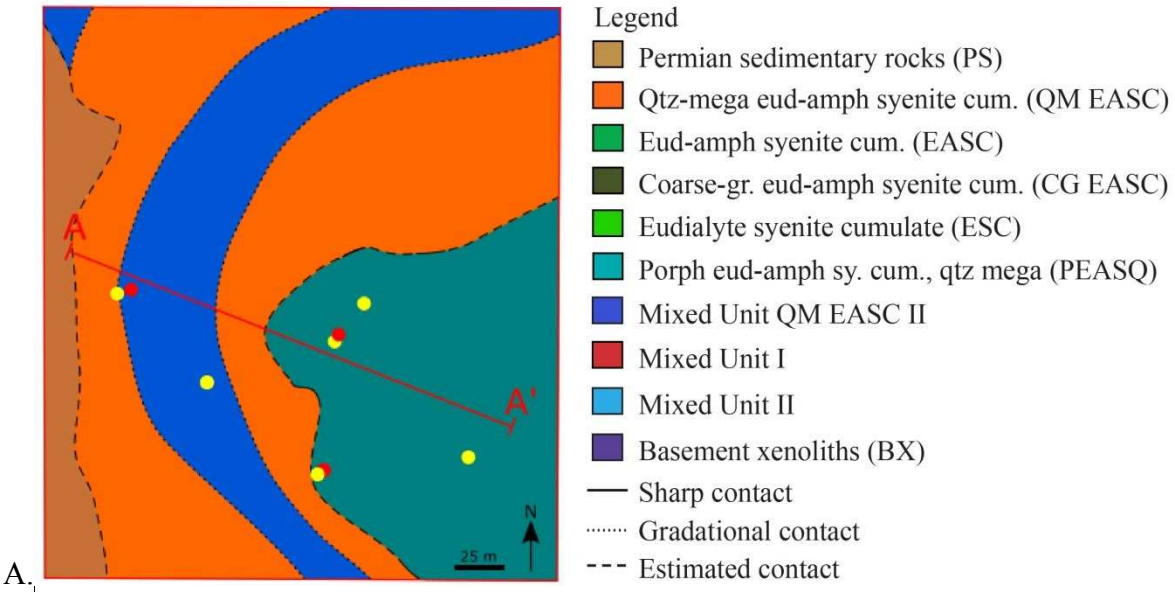
Figure 4.10. Photomicrographs of amphibole replacement textures, XPL. A. Cumulus-adcumulus amphibole with embayed contacts to alkali feldspar suggesting preferential replacement along alkali feldspar compositional zone margins. B. Intercumulus amphibole pervasively replacing multiple alkali feldspar grains.

4.3 Rock classification of the Pajarita Mountain layered cumulate suite

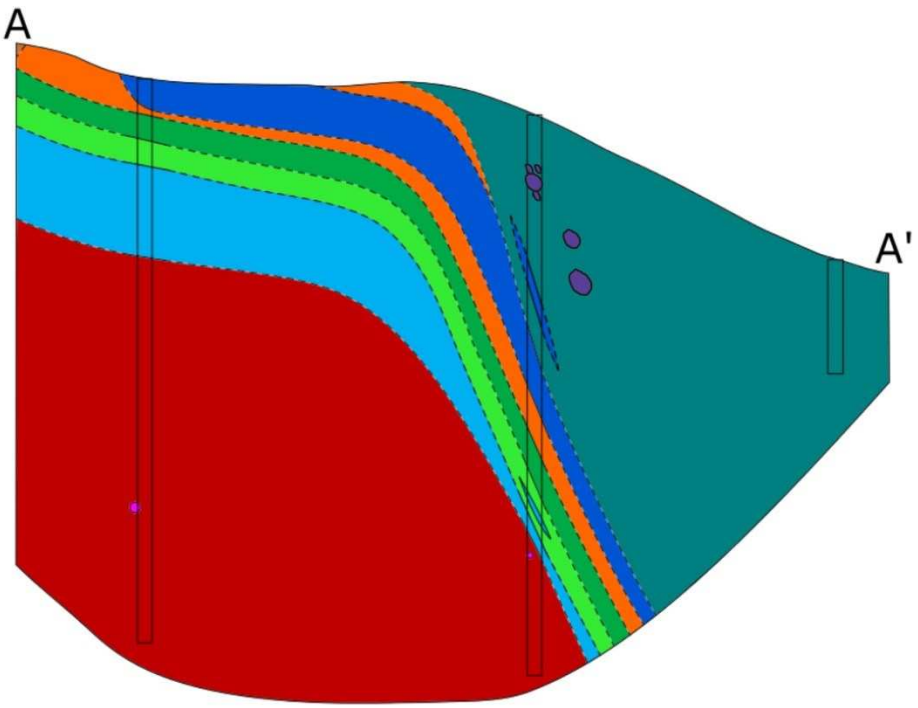
Based on mineralogy, textural relationships, and relative ages, the Pajarita Mountain peralkaline syenitic rocks can be classified into three peralkaline syenitic cumulate types (Types I-III) and peralkaline pegmatites (Type IV). Most rock types display textural and modal mineralogical variations that allow them to be sub-classified into multiple lithologies. Based on cross-cutting relationships, one can distinguish relative timing of each rock type, where rock Type III is the oldest and Type I the youngest. Some lithologies within the same rock type have gradational contacts to one another. Table 4.2 provides a summary of the lithologies described in this study, the rock type to which they belong, their cumulus mineralogy, their distinguishing characteristics, and acronyms used to refer to them. Figure 4.11 shows the distribution of the different lithologies within the studied North and South sections.

There are continuous variations in modal mineralogy and degree of adcumulus growth (and therefore overall texture) within individual cumulate lithologies. This variability necessitates that lithologies are classified primarily by cumulus mineralogy and texture, with less emphasis on modal mineralogy. The terms "syenitic/syenite cumulate" are used loosely, with recognition that "syenite" has a precise definition in the modal mineralogy-based International Union of Geological Science (IUGS) classification system for plutonic rocks that is not fully reflected in the lithologies described in this study. However, all lithologies within the Pajarita Mountain peralkaline suite contain alkali feldspar as their exclusive feldspar species, and this general term, while imperfect, gives a broad sense for their bulk mineralogy. The naming convention adopted here adds specificity by listing cumulus minerals and/or textures that distinguish a given lithology before or after the general term "syenite cumulate". Under the IUGS classification system, by modal mineralogy, the peralkaline lithologies described here

would be classified quartz alkali feldspar syenite, alkali feldspar syenite, and alkali feldspar granite.



A.

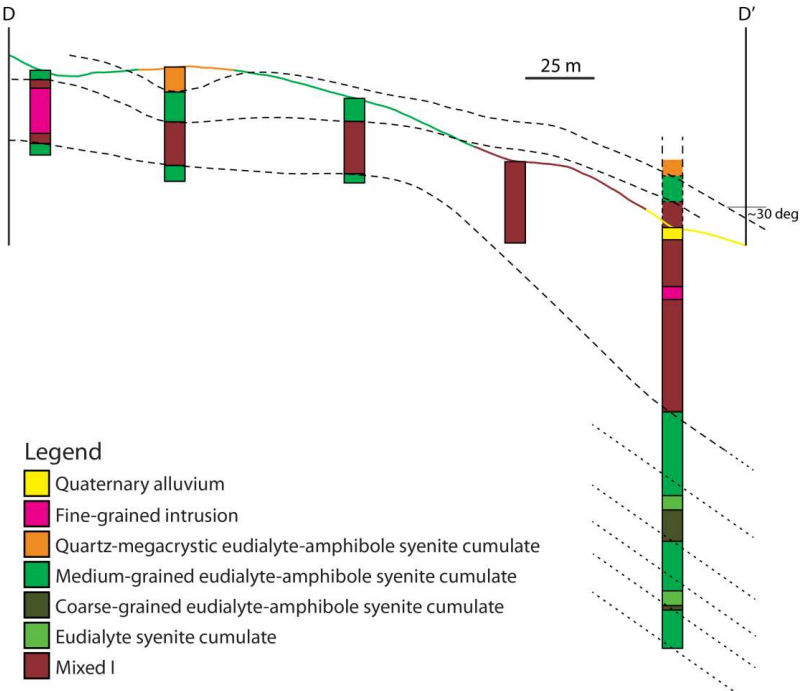


B.

Figure 4.11. Maps and cross-sections of South and North Areas. A. Geologic map of South Area. B. Cross-section through South Area A-A'. C. Geologic map of North Area. D. Cross-section through North Area D-D'. Shallow strip logs are Molycorp holes interpreted into this study's rock units from core logs. Finely dashed lines indicate dip magnitude of structural features including sharp layer contacts and preferentially oriented cumulus amphibole.

C.





D.

Figure 4.11. (cont.).

Table 4.2. Summary of mineralogy and distinguishing features of lithologies

Pajarita Mountain peralkaline cumulate suite				
Peralkaline syenite types	Lithology	Acronym	Cumulus mineralogy*	Distinguishing features
Type I	Quartz-megacrystic eudialyte-amphibole syenite cumulate	QM EASC	**Qtz**-Eud-Afs-Amph±Fl	Macroscopic, sub-rounded Qtz megacrysts 10 – 40%
	Eudialyte-amphibole syenite cumulate	EASC	Eud-Afs-Amph±Fl	Medium or coarse grain size, common cm- to m-scale modal layering, often depleted in Eud
	Eudialyte syenite cumulate	ESC	**Eud**-Afs	Abundant Eud (>15%); minor Amph (<15%), dominantly interstitial
Type II	Porphyritic eudialyte-amphibole syenite cumulate with quartz megacrysts	PEASQ	**Qtz-**Eud-Afs-Amph-Fl	Porphyritic texture, sparse Qtz megacrysts (<10%), fine-grained Eud
	Porphyritic eudialyte-amphibole syenite cumulate	PEAS	Eud-Afs-Amph±Fl	Porphyritic lithic inclusions in Type I rocks; Qtz megacrysts absent
Type III	Porphyritic aenigmatite-amphibole syenite cumulate	PAAS	Afs-Amph-Fl	Very dark grey with subtle black Aen grains; cross-cut/ pockmarked by clots of oikocrystic Eud & abundant Afs
Type IV	Peralkaline pegmatites	PP	±Amph±Afs	Very coarse grain size; intense alteration of Amph & Eud
*Bold type indicates distinguishing cumulus minerals; subsolidus alteration minerals excluded				
Non-peralkaline lithologies				
Relative age	Lithology	Acronym	Composition	Distinguishing features
Post-peralkaline	Permian sedimentary rocks	PS	Cal, dol, Fe oxide, chert, rock frags, fossils, amorphous carbon	Abundant ammonites, petroleum smell upon fracturing; detrital fragments of Pajarita Mountain cumulate suite (i.e. Qtz megacrysts)
	Fine-grained mafic intrusion	FGI	Plag, Bt, Opq, Opx, Fl	Medium grey, weakly to moderately magnetic, aphanitic; common xenoliths of Pajarita Mountain peralkaline suite
Pre-peralkaline	Basement xenoliths	BX	Plag, Opx, Cpx, Opq	Dark grey; hairline veinlets and intense, patchy alteration common; baked contacts; non-magnetic

4.3.1 Type I peralkaline syenitic cumulates

Type I rocks comprise a suite of medium- to coarse-grained cumulate rocks with cumulus mineralogy always including alkali feldspar, amphibole and eudialyte, with occurrences of cumulus quartz and fluorite. Adcumulus textures are characteristic, although the degree of grain overgrowth is highly variable. The highest grade mineralization and the layered segments of the intrusion occur in Type I rocks (see Section 5.1). Surface samples of Type I rocks were found to contain the greatest concentrations of Y and Zr based on grid sampling by Molycorp, who tested accessible areas with high-grade surface contours by core drilling. As the drill cores upon which the current study is based are from the same areas, Type I rocks are the main focus of this work.

Quartz megacrystic eudialyte-amphibole syenite cumulate (QM EASC)

This lithology is typically composed of cumulus and adcumulus alkali feldspar (Afs A-C; 40-65%), cumulus and adcumulus amphibole (20-35%), quartz as megacrysts and oikocrystic in-fill (10-40%), and cumulus eudialyte (10-20%). This rock type occurs in several textural varieties (Fig. 4.12), which are described below. QM EASC is observed at surface and in core in both North and South Areas (Fig. 4.11), with the most closely studied occurrences situated at the same stratigraphic interval in both study areas. In these occurrences, it commonly displays gradational contacts to underlying eudialyte-amphibole syenite cumulate (EASC) defined by a decrease in the size and abundance of quartz megacrysts. In some occurrences, this contact is abrupt. Where gradational contacts are present, the lower contact is marked on cross-sections where cumulus quartz is no longer macroscopically visible. QM EASC that occurs in this sequence is labeled QM EASC I on maps and cross-sections. It appears to be roughly 3-12 m thick.

QM EASC also occurs as bands within an exceptionally heterogeneous mixed unit, QM EASC II (Fig. 4.12B), which is observed mostly in the South Area. In addition to QM EASC, this unit consists of bands or inclusions of EASC, eudialyte-syenite cumulate (Type I, ESC), peralkaline pegmatite (Type IV, PP), Type II porphyritic eudialyte-amphibole syenite cumulate with quartz megacrysts (PEASQ) and without (PEAS), and porphyritic aenigmatite-amphibole syenite cumulate (Type III, PAAS). This mixed unit occurs at the upper contact of QM EASC and as bands cross-cutting other Type I and Type II rocks in both study areas (Fig. 4.11). Inclusions of PEAS are always present, while roughly half of the observed QM EASC II zones contain inclusions of PAAS. Within QM EASC II mixed zones, bands of PEASQ may be up to 4 meters thick, while bands of QM EASC may be up to 1 meter thick and bands of EASC may reach 2 meters thick; pegmatitic zones do not exceed 30 cm in thickness. QM EASC bands in these zones may appear layered, with sub-parallel-oriented zones that alternate in amphibole content from enriched (<45 vol.%) to typical (20-30 vol.%) on a scale of several centimeters (Fig. 4.12C), with the abundance of quartz megacrysts decreasing in amphibole-rich layers. Contacts between QM EASC II and other units are typically sharp, marked by an inclusion or an abrupt contact to another lithology.

An eudialyte-rich variety of this unit (QM EASC III – Fig. 4.12D) with finer-grained quartz megacrysts is found in the North Area as a roughly one meter-thick layer. This unit displays characteristics typically found in eudialyte syenite cumulate (see ESC below), namely minor, dominantly intercumulus amphibole (5-10 vol.% as clots) and a greater abundance of eudialyte (22-25%) than observed in any other occurrence of QM EASC. Like QM EASC, however, it contains cumulus quartz grains (Fig. 4.3C), albeit in a finer size distribution (0.75-1.5

mm rather than the typical 3-7 mm). This occurrence contains the amphibole-rimmed cumulus quartz grains described in section 4.1 (Fig. 4.3C).

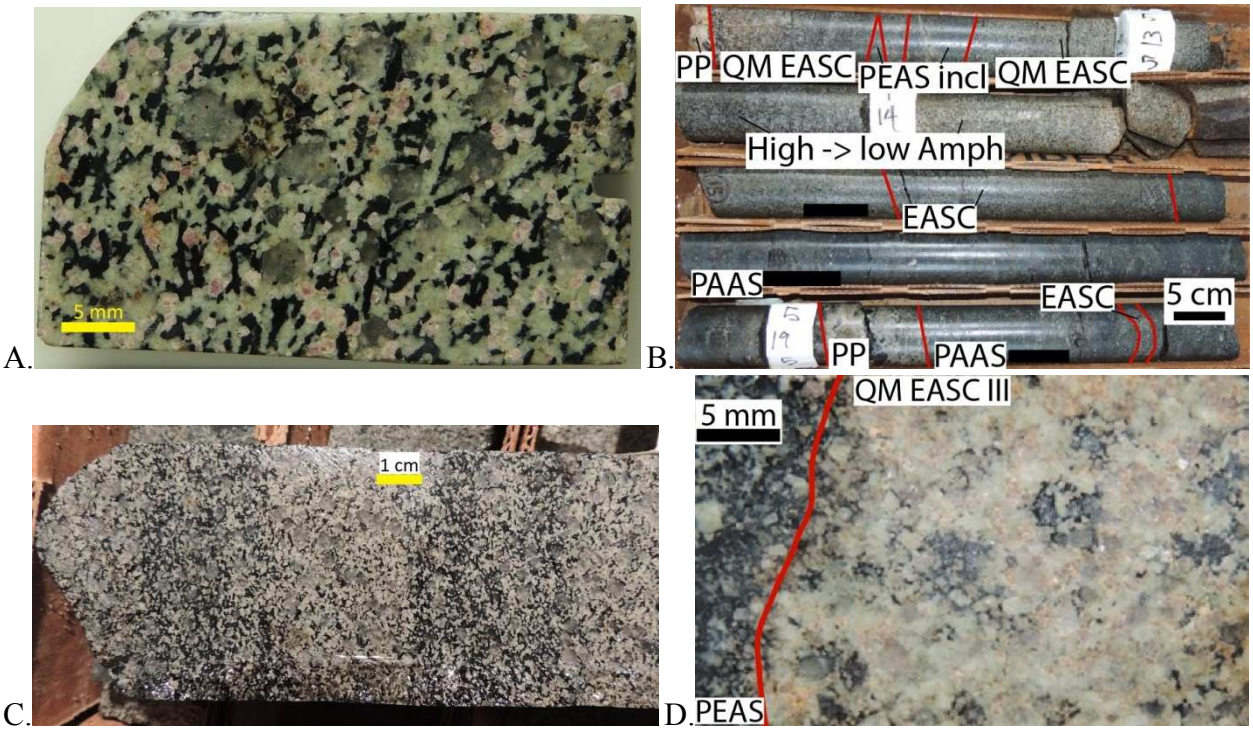


Figure 4.12. Textural variations of quartz megacrystic eudialyte-amphibole syenite cumulate. A. Typical QM EASC. Billet from QM EASC I in the South Area. B. Mixed unit QM EASC II. This ~3 meter interval contains rocks of Types I-IV. Contacts are abrupt except gradational change from high to low Amph QM EASC. C. QM EASC band within QM EASC II zone in the South Area. Amphibole content defines layers at cm scale. D. QM EASC III from North Area with contact to PEAS inclusion. The Fig. 4.3C photomicrograph showing distinct amphibole-rimmed cumulus quartz was cut from this billet.

Eudialyte-amphibole syenite cumulate (EASC)

Eudialyte-amphibole syenite cumulates are medium- to coarse-grained rocks with 15-50% Na-Fe amphibole with predominantly cumulus-adcumulus textures (Fig. 4.13) and cumulus alkali feldspar, eudialyte and, rarely, fluorite. Amphibole and alkali feldspar abundances are roughly inversely proportional to one another, with higher modal alkali feldspar correlating with higher eudialyte content. Amphibole crystals in EASC containing high modal amphibole (>35 vol.%) commonly display preferred orientation. These amphibole-rich EASC occurrences also

commonly feature scarcer and finer-grained eudialyte, with a lower ratio of cumulus to adcumulus growth, than is typical for EASC. EASC with lower modal amphibole (<25%) are characterized by amphibole crystals showing a lower ratio of cumulus to adcumulus growth. This results in a somewhat patchy texture with dominantly interstitial amphibole and abundant eudialyte.

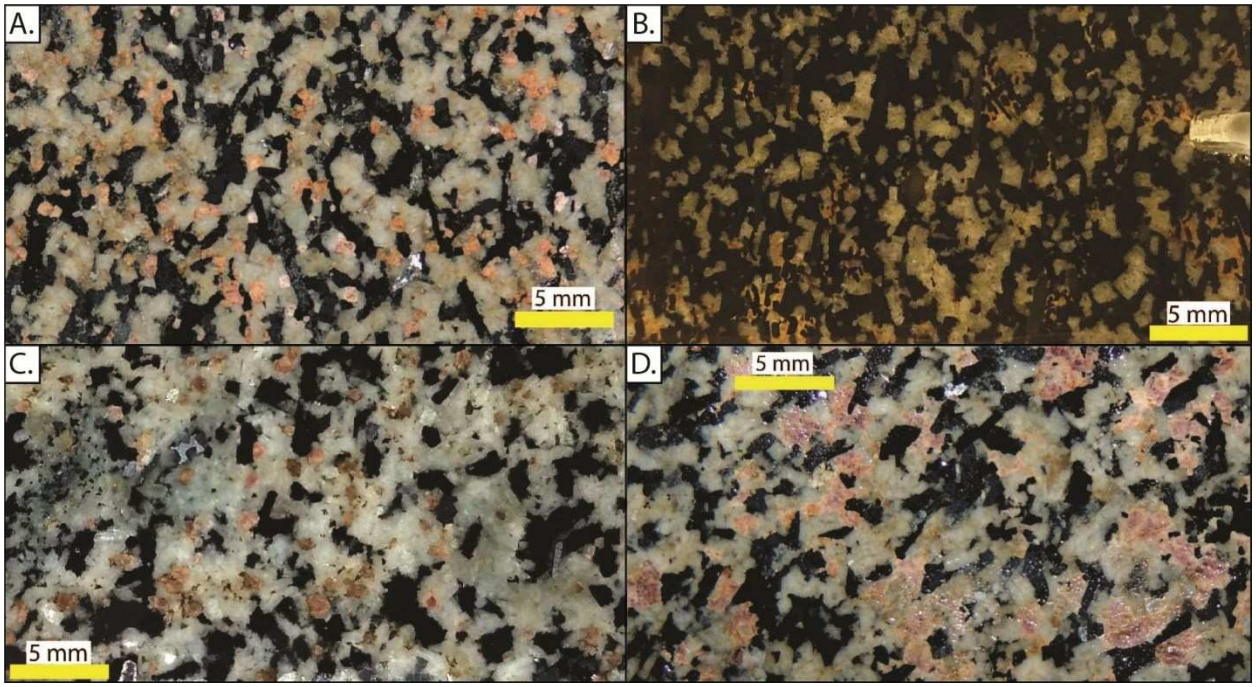


Figure 4.13. Cut hand samples of eudialyte-amphibole syenite cumulate. A. Typical EASC I (South Area) with moderate amphibole. B. EASC with high modal amphibole and fine-grained, dominantly intercumulus eudialyte (orange), North Area. C. EASC with low modal amphibole, North Area. D. EASC with high modal eudialyte, North Area. Note atypically coarse eudialyte grains, some partly enveloping alkali feldspar and amphibole grains.

EASC occurs as the middle lithology of the layered quartz megacryst-bearing cumulate sequence mentioned above (EASC I – Fig. 4.11B, Fig. 4.13A) with gradational contacts to QM EASC I/II above and ESC I below. These occurrences may feature lenses oscillating between high and low modal amphibole on a scale of several centimeters (Fig. 4.13B-C). EASC I constitutes the most eudialyte-poor interval in this layered cumulate sequence, typically containing 5-8% modal eudialyte. Many other variants of EASC were observed, varying in core

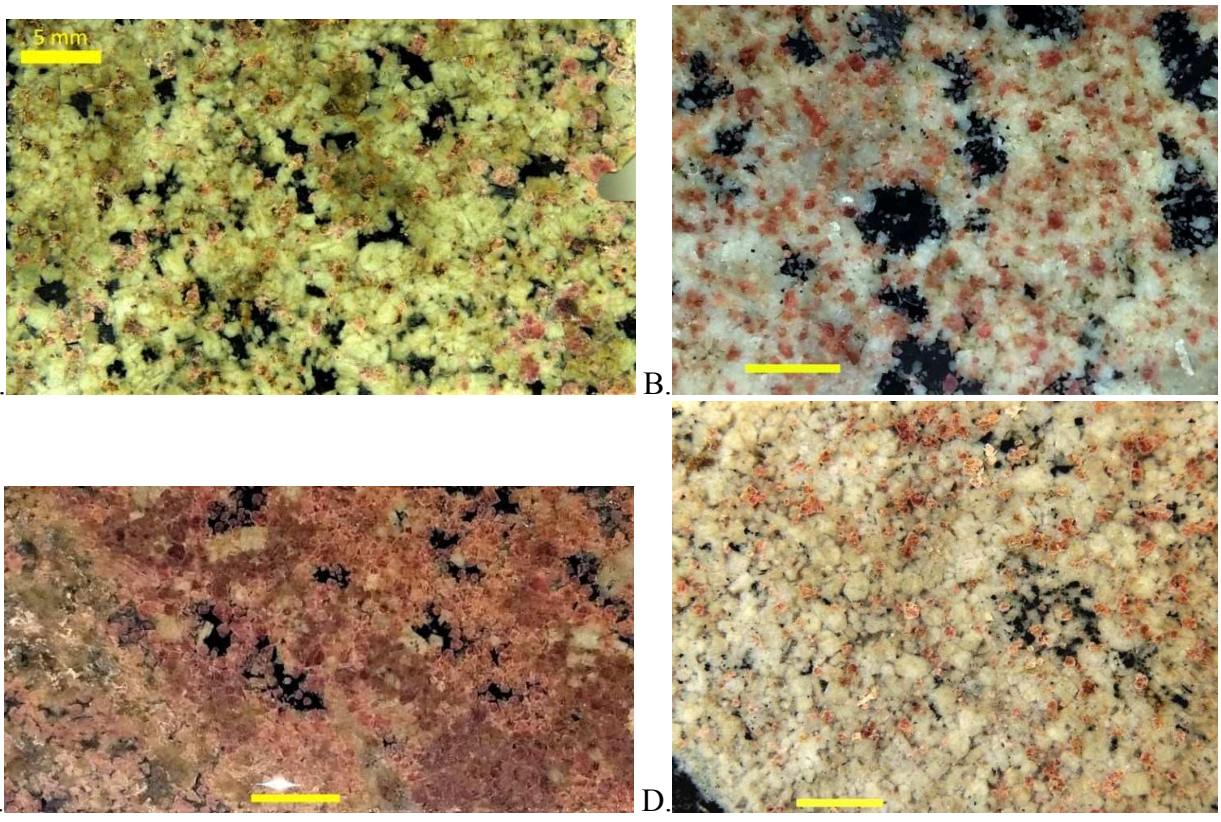
thickness size from several centimeters to several meters. One notable variant is medium- to coarse-grained (2-3 mm) and eudialyte-rich (CG EASC – Fig. 4.13D) that occurs beneath both high-grade ESC lenses in the North Area section. The coarser-grained appearance comes from atypically large prismatic cumulus-adcumulus amphibole (up to 8 mm in length) and/or medium- to coarse-grained eudialyte grains (up to 1 cm) that are rich in amphibole and alkali feldspar inclusions. These locally poikilitic eudialyte clots were observed in several other minor varieties of EASC. CG EASC intervals are relatively well mineralized; eudialyte in CQ EASC is typically 12-15 vol. % but may reach 25%.

Eudialyte syenite cumulate (ESC)

ESC represents many of the most strongly mineralized parts of the Pajarita Mountain pluton as it contains the highest concentrations of eudialyte (Fig. 4.14). This unit can easily be distinguished from EASC by the presence of minor amphibole (<15%), almost exclusively in sub-rounded clots or patches with intercumulus texture as seen in Fig. 4.2B-C. In addition, this rock type is composed of abundant cumulus eudialyte (15-50%) and alkali feldspar (50-55%) with intercumulus quartz. Amphibole patches up to 1 cm in diameter led previous workers to label occurrences of this rock unit as “spotted dikes”. Quartz is intercumulus, constituting up to 30% as oikocrysts 3-15 mm across. These grains may wholly include cumulus eudialyte and/or alkali feldspar and give a matrix-supported appearance (Fig. 4.4A).

ESC occurs at the base of several layered sequences. In the quartz megacryst-bearing layered cumulate sequence mentioned above, ESC I (Fig. 4.14A) occurs below unit EASC I where amphibole gradationally decreases down-section below roughly 15 vol.%. This change is

accompanied by increasing eudialyte and amphibole content. A similar occurrence of rocks with the same cumulus mineralogy, designated ESC II (Fig. 4.14B), occurs at the base of layered cumulus sequences in the North Area (see section 5.1) with a gradational upper contact to EASC with low modal amphibole. In these sequences, cumulus eudialyte and alkali feldspar dominate the lower part of the unit. As modal amphibole decreases, the number of intercumulus amphibole clots decreases and the size of their inclusion-poor cores tends to increase, giving amphibole in ESC II a coarser appearance than is seen in ESC I.



A. B. C. D.

Figure 4.14. Images of eudialyte syenite cumulate. Scale bars are all 5 mm. A. ESC I near base of quartz megacryst-bearing layered cumulate sequence. B. ESC II near base of major North Area layered sequence. C. ESC III, North Area. The photomicrograph showing euhedral Eud in oikocrystic Qtz in Fig. 4.4A was cut from this billet. D. ESC band from unit Mixed I (see section 5.1), North Area. Eudialyte content and grain size increase with distance from the PEAS inclusion in the bottom left corner.

ESC III is unique in its spectacular grade with the highest REE-Zr concentrations reported from Pajarita Mountain to date. The ESC III sample in Fig. 4.14C grades 3.795 wt.% TREO and 7.47 wt.% ZrO_2. This ESC variant consists of a single occurrence that is part of a more complex layered sequence than those hosting ESC I and II, and its cumulus mineralogy is almost exclusively alkali feldspar and eudialyte (up to 50 vol.%). It occurs at the base of a cyclic unit similar in many ways to those hosting ESC II.

ESC IV (Fig. 4.14D) consists of irregular bands of eudialyte-alkali feldspar cumulate up to 20 cm thick that comprise roughly 15% of map unit Mixed I in both North and South Areas. This unit can be quite heterogeneous in modal mineralogy both within and between bands, due at least in part to these bands' modest volume and variable degree of interaction with the surrounding rock. The remainder of the unit consists of Type II peralkaline lithic inclusions that will be discussed in section 4.3.2.

4.3.2 Type II peralkaline syenitic cumulates

Peralkaline rocks of Type II are fine-grained porphyritic cumulates. However, these rocks show less distinct cumulus textures than Type I due to finer grain size and a greater degree of adcumulus growth. This rock type largely consists of the same cumulus and post-cumulus assemblage as Type I rocks with the addition of a second, coarser-grained population of alkali feldspar phenocrysts (Afs C – see Fig. 4.1D). One variant of Type II rocks occurs throughout both study areas as lithic inclusions in Type I bodies, comprising trace to 90 vol.%. A second subset of Type II rocks occurs as a thick (>60 meters) body overlying the quartz megacryst-bearing layered sequence in the South Area. Cross-cutting relationships indicate that both varieties of Type II rocks were emplaced before Type I rocks.

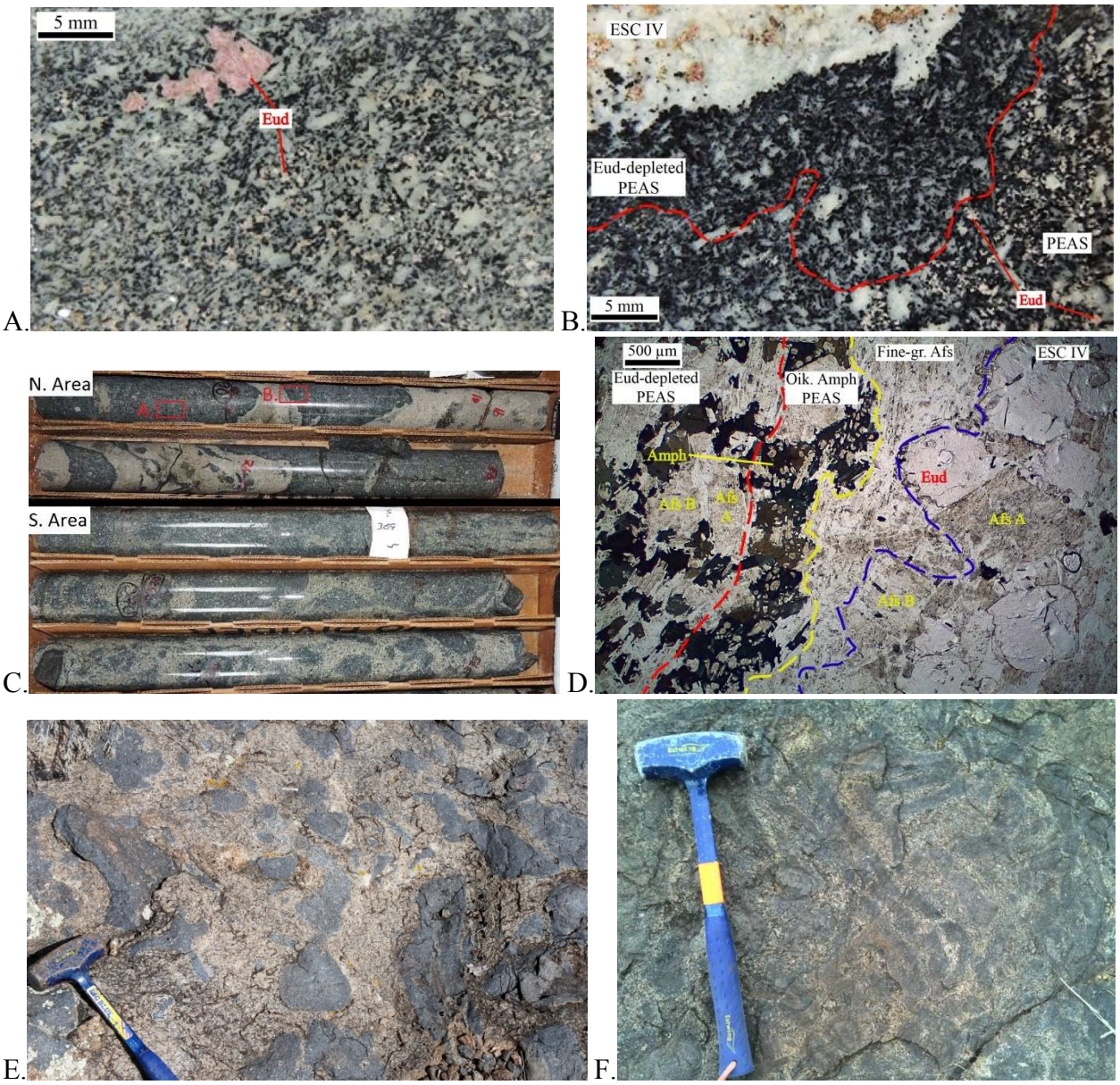


Figure 4.15. Field and core sample photos of PEAS. A. Billet from the center of a typical PEAS inclusion. Minor discontinuous lens of medium- to coarse-gr. sub-poikilitic Eud (± oikocrystic Qtz) is characteristic. B. PEAS inclusion in contact with band of host ESC. Red dashes outline eudialyte-depleted zone adjacent to contact. C. Drill core from North and South Areas showing PEAS inclusions hosted by ESC (core box is 0.61 m long). N. Area core shows sharp contacts and cm-scale inclusions in ESC. S. Area core shows subtler contacts. Locations outlined in red are equivalent to those of the billets shown in A. and B. D. Photomicrograph of PEAS-ESC contact. From left side of image to red line is eudialyte-depleted PEAS. Between red and yellow lines is contact zone rich in oikocrystic amphibole. Between yellow and blue lines is fine-gr., preferentially aligned Afs. From blue line to right side of image is ESC IV with a more typical texture and Eud enrichment. PPL. E. PEAS inclusions with sub-rounded edges, erratic orientations and irregular shapes, hosted in amphibole-poor QM EASC, South Area. F. PEAS inclusions hosted in QM EASC, showing localized preferential orientation of sub-rounded elongate inclusions, South Area.

Porphyritic eudialyte-amphibole syenite (PEAS)

This lithology (Fig. 4.15; p. 45) is a fine-grained, feldspar-phyric, eudialyte-bearing cumulate characterized by sub-poikilitic amphibole (20-35%) and an overall melanocratic appearance. In addition, its mineralogy includes cumulus and adcumulus alkali feldspar (dominantly Afs A-B; 0.3-1.0mm; 40-45%), cumulus-adcumulus subhedral to sub-poikilitic eudialyte (10-12%), a second population of coarser-grained subhedral alkali feldspar phenocrysts (Afs C; 1.5-3.0mm; 10-15%), anhedral fluorite (1-3%), and oikocrystic quartz (0-8%). Amphibole generally forms aggregates with adcumulus overgrowths that give them an overall anhedral sub-poikilitic appearance. Eudialyte is poorly formed relative to eudialyte in Type I cumulate rocks, but it spans from relatively early subhedral cumulus grains showing both pre- and post-accumulation/compaction growth to relatively late sub-poikilitic grains showing dominantly adcumulus growth.

The petrographic samples studied represent PEAS inclusions hosted by ESC IV from the North Area. In this occurrence, these inclusions typically make up greater than 75% of the rock by volume and are separated from one another by ESC IV bands (Fig. 4.15C, N. Area). PEAS inclusions occur within nearly every other rock unit identified in this study, in abundances varying from less than 1 vol.% within tens of square meters of outcrop to over 80 vol.% through multiple meters of drill core. Individual inclusions vary in size from a few millimeters to 1.2 meters in apparent thickness and typically display rounded margins. Where whole inclusions are visible, they often show sub-parallel-oriented elongate morphologies (Fig. 4.14G). Angular contacts and erratic shapes and orientations are also locally present (Fig. 4.15E). As shown in Fig. 4.15C, contacts between PEAS inclusions and the host lithology vary from sharp to almost gradational, the latter indicating partial incorporation of PEAS inclusions into the later Type I

melt. Reaction between inclusion and host is also suggested by envelopes of white fine-grained alkali feldspar up to ~1 cm thick surrounding inclusions (Fig. 4.15E); Afs grains in these envelopes may display moderate preferential alignment parallel to contacts (Fig. 4.15D). A subtler envelope, up to several cm thick and defined by strong depletion or absence of eudialyte, is typically present within PEAS inclusions adjacent to their contacts to the host rock (Fig. 4.15B). The photomicrograph in Fig. 4.15D shows (moving from left to right) this eudialyte depletion zone; a thinner zone of oikocrystic amphibole characteristic of the contact to ESC; the zone of preferentially aligned fine-grained alkali feldspar in ESC; and a more typical ESC IV texture.

Porphyritic eudialyte-amphibole syenite with quartz megacrysts (PEASQ)

This lithology is similar to PEAS but is characterized by the presence of up to 10 vol.% quartz megacrysts (Fig. 4.16). These megacrysts are typically finer grained than the megacrysts seen in QM EASC. PEASQ is a porphyritic cumulate with a fine-grained groundmass mineralogy consisting of subhedral cumulus alkali feldspar (Afs A-B; 32%), amphibole ranging from cumulus-adcumulus to poikilitic (~20%), subhedral to sub-poikilitic cumulus eudialyte (~10%), anhedral fluorite (~1%), and oikocrystic and megacrystic quartz (<10%). The coarser-grained population of alkali feldspar (Afs C) comprises roughly 15%.

Macroscopically, PEASQ shows considerable textural variability. Eudialyte may appear in sub-rounded patches roughly 1 cm in diameter (Fig. 4.16B), and the rock shows a sub-orbicular texture suggesting the presence of intensely reacted lithic inclusions of similar mineralogy but overall lighter color. Rare lithic inclusions of PEAS were observed (Fig. 4.16B).

PEASQ contains pegmatites up to 30 cm thick, as well as irregularly-oriented, medium- to coarse-grained bands up to 3 cm thick of predominantly amphibole and eudialyte, and basement xenoliths.

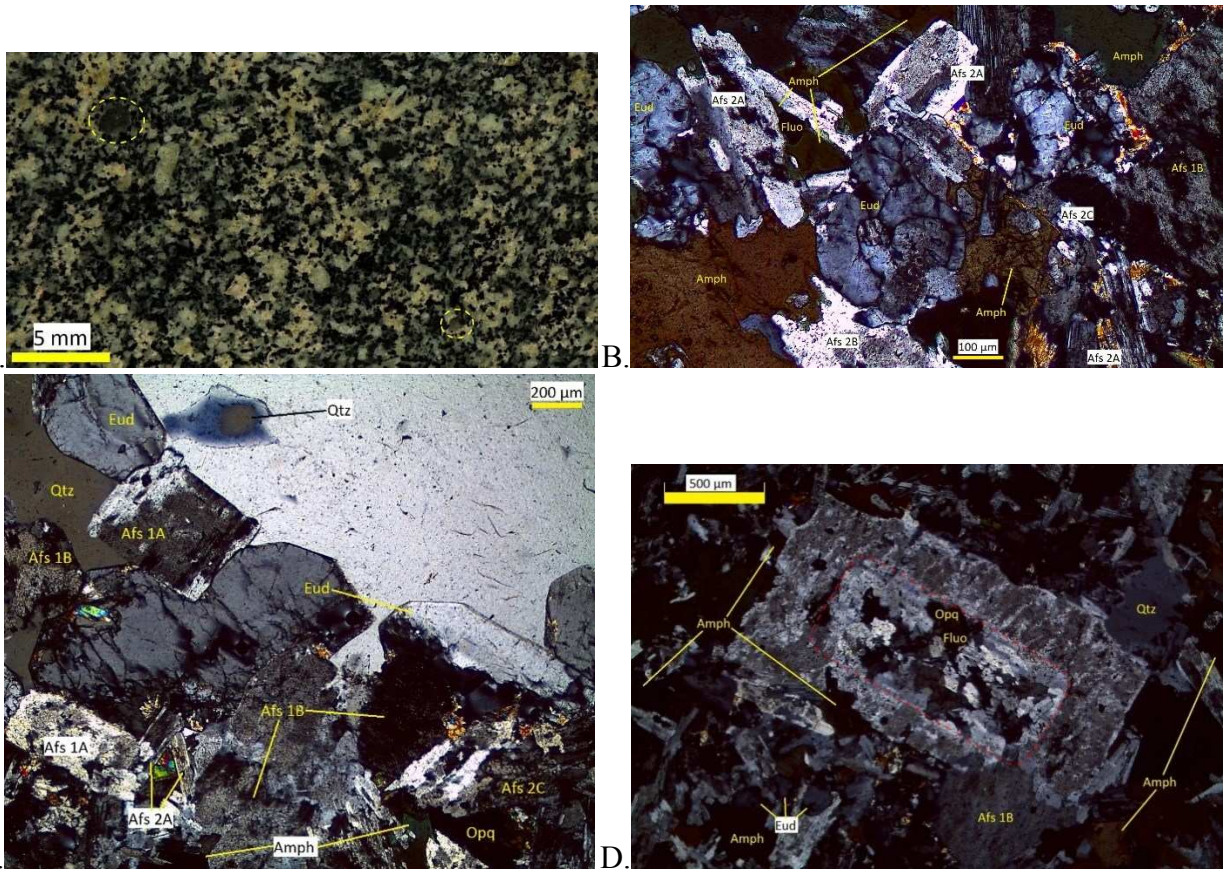


Figure 4.16. Images of PEASQ in hand sample and thin section. A. Billet sample showing macroscopic Qtz megacrysts (outlined within yellow dashed line) and overall porphyritic texture. B. Photomicrograph of typical textures in PEASQ. Sub-poikilitic anhedral Eud, cumulus-adcumulus sub-poikilitic Amph (weak Aeg alteration) partially replacing Afs, bimodal grain size in Afs, and minor Fluo. Note overall fine grain size and cryptic cumulus texture. XPL. C. Photomicrograph of cumulus Eud, atypically large and well-formed for PEASQ (and slightly white altered), bounding a quartz megacryst. Afs A-B are atypically coarse for lithology. XPL. D. Lithic inclusion (outlined in red dashes) with Afs mantle with texture reminiscent of Afs B. Core is composed of anhedral grains of feldspars with minor Fluo and opaques. Groundmass is composed of fine Afs A-B, cumulus-adcumulus, sub-poikilitic Amph, fine-gr. subhedral EUd, and minor Fluo. XPL.

4.3.3 Type III peralkaline rocks: porphyritic aenigmatite-amphibole syenite (PAAS)

Type III rocks are distinguishable from Type II rocks by finer grain size, a distinctly more melanocratic color in hand sample, the presence of aenigmatite, and eudialyte that only occurs in irregular feldspar-rich pods or lenses (Fig. 4.17). They are the only peralkaline rocks that do not contain groundmass eudialyte. PAAS are made up of a groundmass of fine cumulus alkali feldspar Afs A-B; 0.1-0.75 mm; 45-50%), anhedral cumulus-adcumulus amphibole (30-35%), anhedral intercumulus fluorite (1-4%), the coarse alkali feldspar phenocrysts with the clear mantling and perthitic texture (Afs D; 1-3 mm; 1-5%), and sub-poikilitic grains of aenigmatite (2-15%). Groundmass alkali feldspars display varying degrees of contact interdigitation with amphibole but largely retain a subhedral form (Fig. 4.17D). These prismatic cumulus alkali feldspar grains, which may be preferentially oriented, constitute the strongest evidence for a cumulus origin to this lithology. Aenigmatite, the diagnostic mineral of PAAS, occurs as irregularly distributed sub-poikilitic grains that partially to fully enclose grains of alkali feldspar and fluorite. Amphibole very rarely occurs as inclusions in aenigmatite, although aenigmatite grains are commonly in contact with amphibole. Discrete zones rich in alkali feldspar ± oikocrystic quartz (Fig. 4.17A-B) contain the only eudialyte present in PAAS as oikocrysts enveloping groundmass minerals amphibole, alkali feldspar, fluorite, and aenigmatite (see Fig. 4.4D). These zones do not have sharp contacts, and their envelopment of typical PAAS groundmass minerals indicates that this oikocrystic eudialyte may represent a late replacement or overgrowth texture.

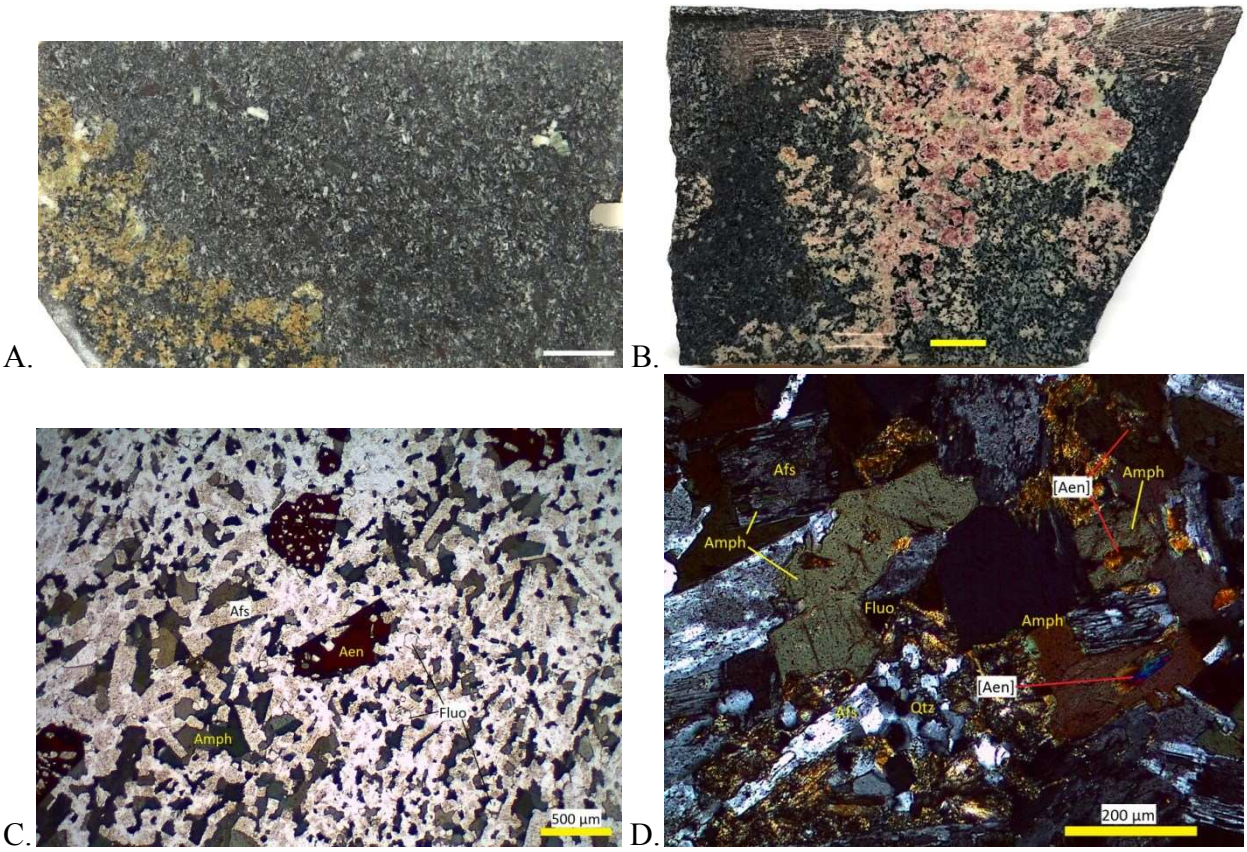


Figure 4.17. Images of porphyritic aenigmatite-amphibole syenite (PAAS) and zones of Eud-Afs±Qtz. A. Thin section billet containing typical PAAS and the edge of an Eud-Afs zone with moderate brown alteration. Black, subhedral, prismatic grains are poikilitic aenigmatite grains. Scale bar is 5 mm. B. Irregular Eud-Afs-Qtz zone comprising coarse, largely unaltered eudialyte oikocrysts rimmed by pale green alkali feldspar, cross-cutting PAAS. Note coarsening of PAAS adjacent to eudialyte-feldspar lens. Scale bar is 1 cm. C. Photomicrograph of typical PAAS groundmass of dominantly anhedral cumulus-adcumulus amphibole, cumulus alkali feldspar, and anhedral fluorite, with poikilitic aenigmatite. PPL. D. Photomicrograph of altered aenigmatite ([Aen]) possibly replaced by Amph, Afs, and very fine-gr. Qtz aggregates with adjacent Fluo. Note fragments of altered Aen within Amph grains. XPL.

4.3.4 Type IV peralkaline rocks: peralkaline pegmatites (PP)

Peralkaline pegmatites are made up of the same primary minerals comprising the main peralkaline cumulate suite (Afs, Amph, Qtz, Eud, Fluo), occurring with atypically coarse grain sizes. The secondary minerals commonly found in PP occurrences include zirconosilicates (either gittinsite or armstrongite), sulfides (sphalerite and galena), other unknown eudialyte alteration products (see Fig. 4.7), and aegirine replacing amphibole. They also feature

characteristic pegmatite mineral textures such as comb structures, show strong secondary alteration, and cross-cut the three main peralkaline rock types. While many of these occurrences contain crystals greater than 2.5 cm in size, the lithologic classification PP was extended to occurrences that do not reach this grain size threshold. These occurrences were grouped as pegmatites because they share the other notable characteristics mentioned above and are atypically coarse-grained (at minimum, roughly 50% of grains are greater than 0.75 cm). These occurrences are classified as peralkaline because all occurrences contain the same primary mineralogy as peralkaline rocks of Types I-III, as well as three whole-rock geochemistry samples that give peralkalinity index values greater than 1. The geochemistry samples represent the upper 1.5 m and lower 1.5 m of the thickest *sensu stricto* pegmatite observed (prismatic amphibole grains <7.5 cm), as well as one 10 cm-thick band with comb-structure amphibole grains up to 1.5 cm, strong aegirinization and eudialyte pseudomorphism, and several vol.% secondary sulfides and other opaques.

PP zones comprise bands that are typically less than 25 cm thick, but, as mentioned above, the greatest thickness observed is 3 meters. They are commonly observed in mixed units and were observed cross-cutting PEAS inclusions, ESC IV bands, PAAS inclusions, PEASQ, and, in a single instance, cross-cutting the middle EASC layer in the quartz megacryst-bearing layered cumulate sequence. Some general trends were identified in PP band texture and/or architecture. In drill core, the down-hole portion of many bands features lithic inclusions of the adjacent host rock and finer grain size. The up-hole portion tends to show the coarsest grains, with prismatic minerals (dominantly amphibole and its replacement products) oriented perpendicular to contacts in comb textures.

4.3.5 Fine-grained mafic intrusions (FGI)

Several bodies of fine-grained, magnetite-rich mafic rock cross-cut the Pajarita Mountain peralkaline pluton. FGI bodies (Fig. 4.18; p. 54) are composed of a fine groundmass of subhedral prismatic plagioclase (37-45%, 0.15-0.35mm), anhedral to subhedral biotite (12%, 0.05-0.2mm), anhedral to subhedral opaque grains dominated by magnetite and pyrite with minor galena (12-15% opaques, 0.05-0.15mm), anhedral orthopyroxene (12%, 0.05-0.15mm), dominantly interstitial fluorite (<0.35mm, 3-5%), and a second population of subhedral plagioclase grains (5%, 0.3-1.5mm). Roughly 80% of these coarse plagioclase grains are altered to carbonate, and interstitial carbonate also comprises 11-14% of the rock.

Only float of this lithology was observed during mapping for this study, and large areas mapped as gabbro by Molycorp geologists are almost entirely devoid of outcrop. These bodies were mapped according to magnetic highs given in ground magnetic surveys conducted by Molycorp. This unit was only observed in-situ in drill core in the North Area.

4.3.6 Basement xenoliths (BX)

Basement xenoliths (Fig. 4.19; p. 56) were observed at several stratigraphic intervals and within at least three lithologies of peralkaline rock Types I and II. Basement xenoliths are so characterized due to reaction textures at their contacts to their peralkaline host lithologies, and mineralogical and textural distinctness from the peralkaline syenitic rocks. One petrographic sample of a basement xenolith was studied. grain size is very fine and alteration intense. The groundmass is composed of plagioclase and pyroxenes with oikocrysts of orthopyroxene and clinopyroxene and blebs of opaque minerals with apparent iron oxide haloes. The overall texture is orbicular, with typically sub-rounded enclaves of fine-grained minerals within envelopes composed of plagioclase and pyroxenes of slightly coarser grain size and prismatic form

radiating outward from the core. When alteration is intense, abundant pyrite, sphalerite, galena, fluorite and several very fine-grained unknown phases are observed in vein and replacement textures. Large xenoliths (<5.9 m thick in core) are present in PEASQ and QM EASC (Fig. 4.19A). Significantly smaller xenoliths (5-75 cm thick in core) are hosted within both PEAS inclusions and ESC bands hosting PEAS inclusions in both North and South Areas (Fig. 4.19E).

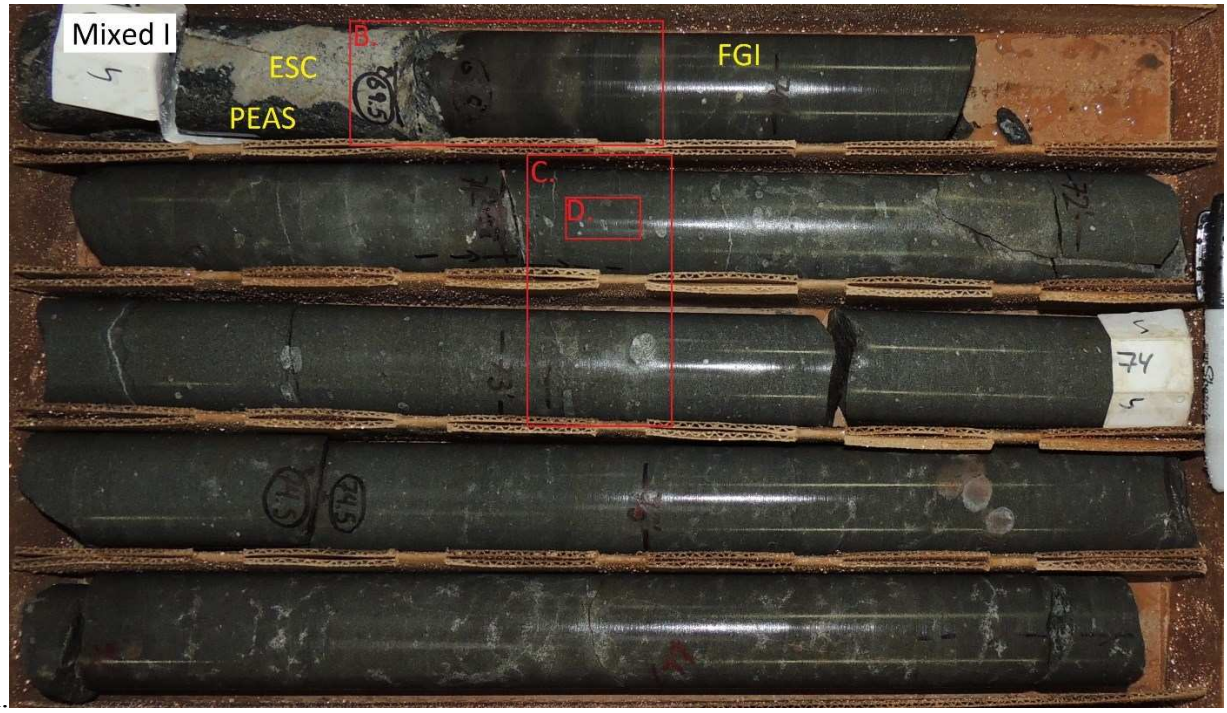
4.3.7 Permian sedimentary rocks (PS)

Permian sedimentary rocks (Fig. 4.20; p. 58) immediately adjacent to the Pajarita Mountain crystalline rocks consist largely of fossiliferous, dolomitic limestone containing chert lenses, iron oxide concretions, calcite veins, and detrital fragments. Many samples contain millimeter-scale blebs of black hydrocarbon. Mudrocks, sandstones and gypsum reported in the Lower Permian Yeso and San Andres formations in the immediate vicinity of Pajarita Mountain (Moore et al., 1988) were not observed. One outcrop sample of rock fragment-rich dolomitic limestone was collected to investigate the possibility of input of Pajarita Mountain peralkaline rock fragments into the adjacent shallow sea sediments during the Permian. This sample is from a South Area limestone outcrop meters from its contact to peralkaline rocks.

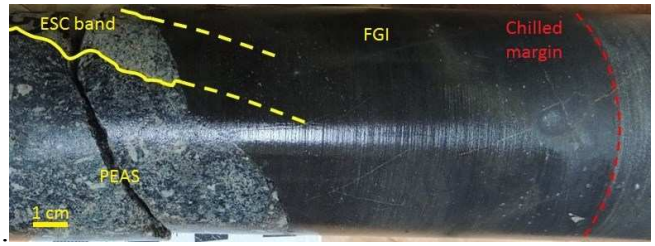
Some rock fragments within the oolitic, locally iron oxide-cemented, fossiliferous carbonate rock contain quartz megacrysts and heavily altered amphibole, alkali feldspar and eudialyte, indicating detrital fragments from the Pajarita Mountain peralkaline rocks. Other rock fragments have no obvious in-situ equivalent in the peralkaline rocks studied, although multiple stages of weathering (Permian shallow sea and modern subaerial) may obscure original textures and mineralogy. Sub-horizontal dips and peralkaline rock fragments in these sedimentary rocks suggest that the peralkaline complex was at a bathymetric high during Permian shallow sea deposition of these carbonate-dominant rocks.

Figure 4.18. Images of one 4.4 m thick FGI dike cross-cutting PEAS inclusions and their ESC IV host (North Area). A. A 2.8 m core interval showing upper contact and upper 2.7 m of the FGI dike and locations of images B-D. Box labeled "D" represents the rough location of the thin section displayed in D and E. B. Upper contact of FGI to host unit Mixed I, showing FGI cross-cutting both PEAS inclusion and ESC, as well as chilled margin. Light-colored enclaves in FGI are fragments of peralkaline host rock. C. Typical macroscopic texture of unit FGI showing peralkaline lithic inclusions, including QM EASC. Pale-colored areas appear to be intensely reacted lithic inclusions. D. Lithic inclusion of QM EASC in FGI groundmass, showing preserved quartz megacrysts, calcite (possibly replacement of eudialyte), and prismatic Afs A. Diamond-shaped grains appear to be biotite mantles around Afs. XPL. E. Typical groundmass of FGI sample. Note coarser plagioclase phenocrysts in upper right and association of opaques with biotite. PPL.

A.


Mixed I
ESC
PEAS
B.
FGI
C.
D.
74

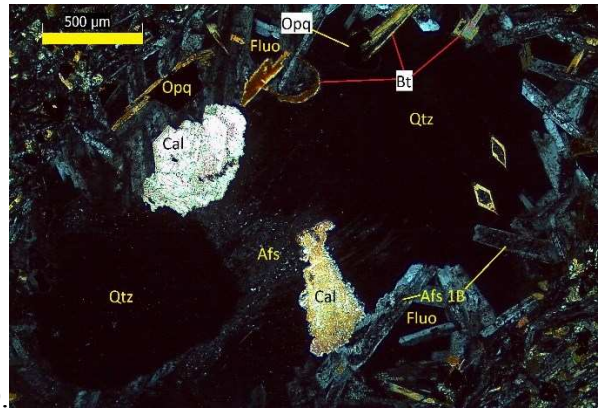
B.


ESC band
FGI
Chilled margin
PEAS
1 cm

C.


1 cm
QM EASC

D.


500 µm
Opq
Fluo
Opq
Bt
Qtz
Cal
Afs
Qtz
Cal
Afs 1B
Fluo

E.

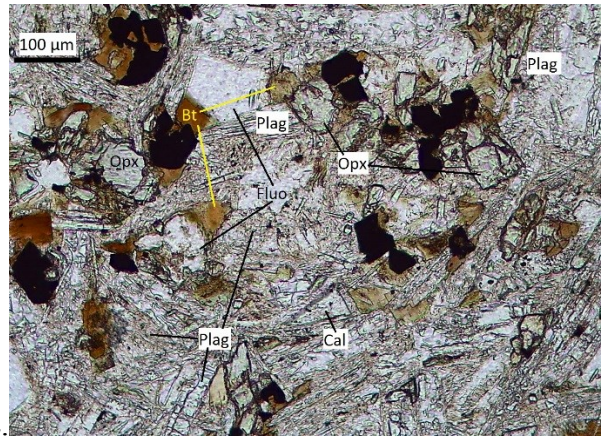
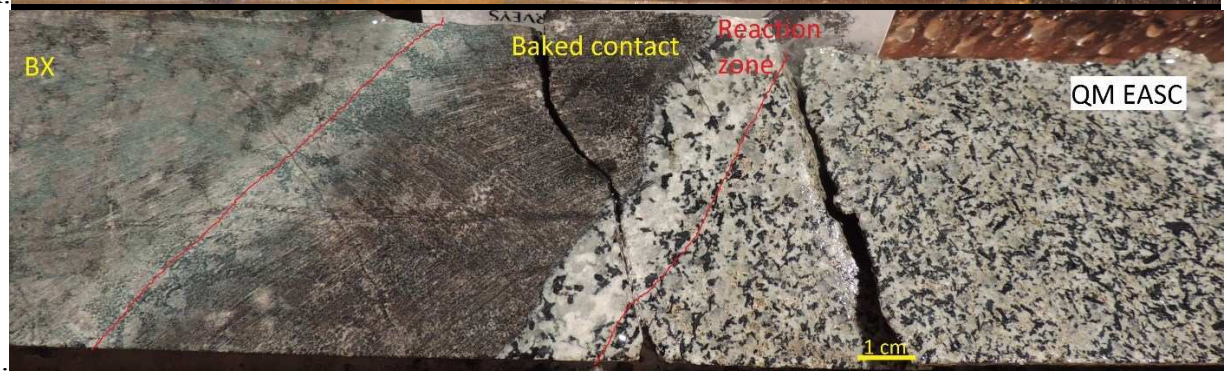

100 µm
Plag
Bt
Plag
Qpx
Opx
Fluo
Plag
Cal

Figure 4.19. Images of basement xenoliths in peralkaline rocks. A. 5.9 m-thick xenolith bounded above by QM EASC and below by PEASQ. Note alteration manifesting as intense veining and variations in color and texture. Locations of images C. and D. indicated by labeled boxes. B. Lower contact of 3.7 m-thick basement xenolith hosted in QM EASC, showing contact of xenolith and 1.25 cm thick reaction zone in QM EASC. Reaction zone is Qtz-rich, Amph-poor and slightly coarser grained than the adjacent QM EASC. C. BX showing multiple types of alteration including green (outlined in green dashes) and black veinlet selvages, and less altered xenolith material in center of image. D. Photomicrograph of least altered portion of thin section. Red lines delineate cores and mantles of orbicular texture. XPL. E. Basement xenolith (75 cm long) in ESC (South Area). Discontinuous reaction zones around xenolith traced in blue dashes and reaction ("baked") contact zones in xenolith traced in red dashes. Reaction zones consist of coarser than usual cumulus Eud and abundant intercumulus Amph.

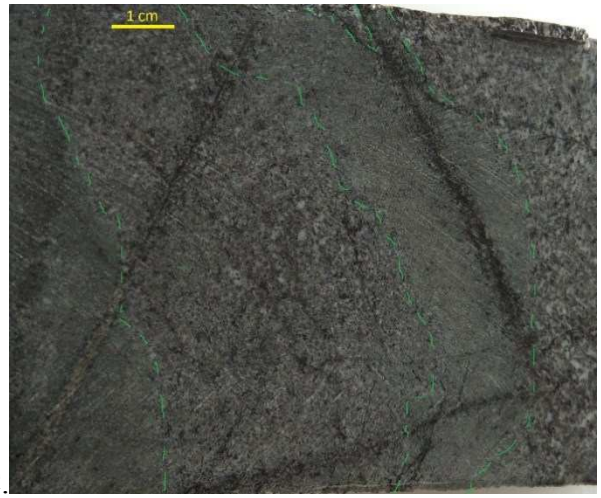
A.


PEASQ
QM
EASC

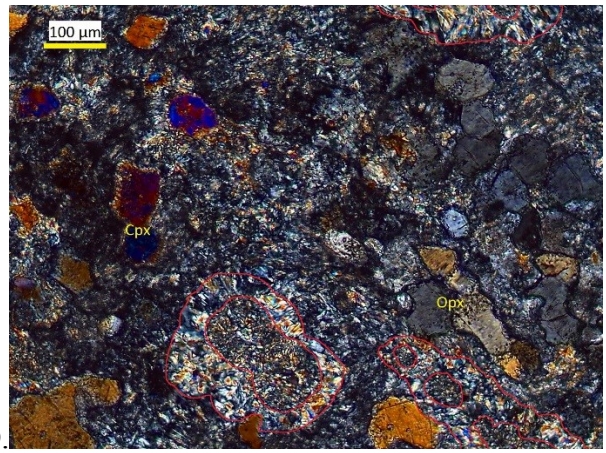
B.


BX
Baked contact
Reaction
zone
QM EASC
1 cm

C.


1 cm

D.


100 µm
Cpx
Opx

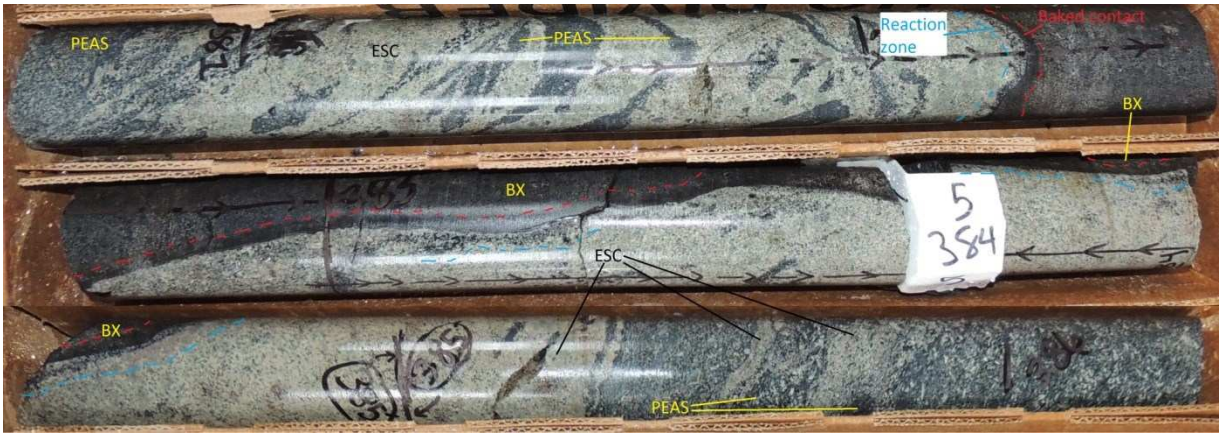
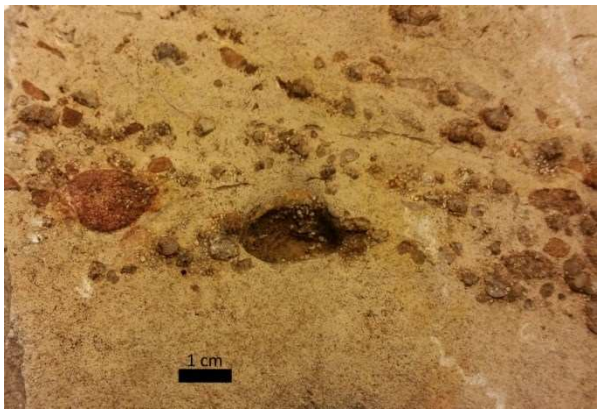
E. 

Figure 4.19. (cont.).

A. 

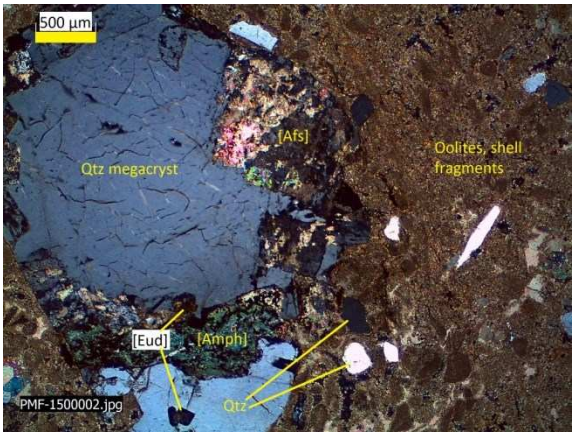
B. 

Figure 4.20. Images of Permian dolomitic limestone comprising the western half of the summit of Pajarita Mountain peralkaline rocks. A. Hand sample from which thin section in B. was cut. B. Photomicrograph of a fragment of QM EASC in oolitic, fossiliferous, dolomitic limestone. Quartz megacryst contains heavily altered eudialyte, alkali feldspar and amphibole with shapes and relict textures seen in in-situ QM EASC. XPL.

4.4 Whole-rock geochemistry

Cumulate rocks represent a combination of early-crystallizing cumulus grains and late intercumulus material that may not share a direct genetic link. Due to crystal separation and accumulation, whole-rock geochemical data do not represent the composition of melts, but may give an idea of the overall changes in modal mineralogy of these rocks. In particular, whole-rock data can be used to understand the distribution of the REE and Zr in the deposit. Representative

whole rock major and trace elements of the different lithologies from the second, targeted study are listed in Table 4.3.

Based on the full dataset from the targeted study (only partially represented in Table 4.2), TREO concentrations in Type I peralkaline syenitic rocks vary between 0.15 and 3.80 wt.%, and ZrO_2 concentrations between 0.23 and 7.47 wt.%, with the highest concentrations observed in ESC in the North Area. Concentrations in Type II peralkaline syenitic rocks are smaller, varying between 0.14 wt. % and 0.59 wt. % TREO and 0.20 and 1.13 wt. % ZrO_2. Type III rocks have the least significant TREO and ZrO_2, ranging between 0.10 and 0.20 wt. % TREO, and 0.09 and 0.22 wt. % ZrO_2. Only one targeted analysis of Type IV rocks (peralkaline pegmatites) was conducted, and it shows enrichment (0.78 wt. % TREO and 4.06% ZrO_2), but with a much greater ratio of ZrO_2 to TREO. The ratio of heavy rare earth oxides (HREO) to TREO are again highest for Type I, ranging from 0.34 to 0.49, while Type II ranges from 0.33 to 0.41 and Type III from 0.27 to 0.34. This ratio increases with increasing TREO concentration, with the greatest value (0.49) corresponding to the most highly mineralized sample of North Area ESC.

Table 4.3. Representative whole-rock major and trace element analyses of Pajarita Mountain peralkaline lithologies (see Table 4.2 for acronyms) and estimated modal mineralogy of samples.

Rock Type	Type I												Type II			Type III
Occurrence / location	Layers, QM Member, S. Area				Band, Mixed I, S. Area	Band, Mixed I, N. Area	Layer, NBR Member, N. Area	Layers, HG Member, N. Area		Layers, HMEC Member, N. Area			Roof layer, ULZ, S. Area	Inclusion, Mixed I, S. Area	Inclusion, Mixed I, N. Area	Inclusion, Mixed II, S. Area
Sample name	PM5-257.25 GC	PM5-297.83 GC	PM5-311.75 GC	PM5-367.42 GC	PM1-384.92 GC	PM3-91.18 GC	PM3-255 GC	PM3-330.75 GC	PM3-343.92 GC	PM3-418.92 GC	PM3-435 GC	PM3-445 GC	PM5-92.18 GC	PM1-489.67 GC	PM3-56.13 GC	PM5-348.83 GC
Lithology	QM EASC	EASC MA	EASC HA	ESC	ESC band	ESC band	EASC MA	ESC HG	EASC CG	EASC HA	ESC	ESC	PEASQ	PEAS	PEAS	PAAS
Oxides [unless otherwise noted] (wt %)																
SiO2	68.46	62.01	61.5	61.28	63.75	64.73	62.34	53.29	61.04	58.46	64.5	66.49	65.21	61.85	61.29	58.96
Al2O3	7.04	8.16	7.08	10.61	13.93	11.63	8.9	3.76	10.18	6.69	11.3	13.12	11.02	12.13	10.88	10.87
Fe2O3(T)	9.34	15.1	18.13	6.23	4.38	4.78	14.46	10.17	12.23	21.9	9.15	3.58	9.66	9.78	10.72	15.51
FeO	7.1	10.7	12.2	3	1.8	3.4	10.4	2.9	6.3	14.6	6.7	3.2	5.9	7.3	7.3	11
Fe2O3	1.41	3.26	4.53	2.92	2.33	1.02	2.85	2.91	5.21	5.63	1.76	0.07	3.12	1.67	2.6	3.26
MnO	0.267	0.339	0.384	0.256	0.157	0.177	0.315	0.558	0.273	0.43	0.211	0.143	0.234	0.23	0.251	0.28
MgO	0.12	0.28	0.37	0.28	0.93	0.23	0.17	0.11	0.16	0.13	0.14	0.08	0.24	0.37	0.28	0.22
CaO	2.91	2.45	1.8	3.88	1.53	1.96	1.35	6.23	1.53	1.16	1.09	1.21	1.61	1.75	1.64	2.18
Na2O	4.78	6.37	6.45	6.66	7.02	6.59	6.93	9.1	7.59	7.29	6.78	7.32	6.14	6.91	7.05	6.55
K2O	3.2	3.74	3.38	4.55	4.61	4.54	4.44	1.94	4.58	3.57	4.55	4.96	4.41	4.7	4.92	4.17
TiO2	0.264	0.472	0.561	0.204	0.139	0.381	0.397	0.263	0.334	0.558	0.197	0.073	0.429	0.507	0.452	0.776
P2O5	< 0.01	< 0.01	< 0.01	0.16	0.01	0.05	0.02	0.02	0.07	0.01	< 0.01	< 0.01	0.05	0.09	0.1	0.08
LOI	1.52	0.94	0.42	1.99	1.6	1.39	0.63	4.61	1.57	0.12	0.59	0.94	0.5	0.62	0.53	0.39
Sum	97.1	98.69	98.7	95.77	97.85	96.09	98.77	89.32	98.84	98.69	97.78	97.56	98.84	98.11	97.29	98.73
F (element)	0.28	0.54	0.66	0.13	0.14	0.08	0.52	1.07	0.56	0.83	0.24	0.02	0.47	0.49	0.55	0.86
TREO	0.981	0.630	0.477	1.643	0.930	1.146	0.709	3.795	0.822	0.274	0.816	1.154	0.510	0.467	0.547	0.103
ZrO2	1.63	0.93	0.77	2.87	1.79	2.03	1.07	7.47	1.25	0.42	1.18	1.59	0.75	0.85	0.96	0.09
HREO:TREO	0.40	0.37	0.38	0.41	0.43	0.40	0.43	0.49	0.42	0.37	0.43	0.42	0.34	0.35	0.37	0.34
REE (ppm)																
La	1020	742	531	1750	927	1200	703	3160	840	306	797	1180	639	567	629	120
Ce	2330	1590	1200	3870	2140	2790	1600	7570	1900	693	1840	2630	1360	1220	1390	268
Pr	282	188	143	467	252	332	195	935	227	83.5	224	315	159	142	164	33.2
Nd	1100	715	541	1800	978	1260	762	3860	877	318	866	1240	598	539	633	134
Sm	273	171	130	435	246	302	190	1020	217	73.5	222	308	137	125	149	27
Eu	24.1	14.1	10.8	37.6	21.3	27.2	16.2	90.2	18.7	6.19	19.8	27.5	11.6	10.9	12.9	2.14
Gd	280	171	130	454	272	319	206	1190	240	72.9	245	344	134	128	155	25.4
Tb	53.2	31	23.9	84.7	51.3	60.4	40.7	246	46.1	12.9	48	66.2	23.5	22.8	28.2	4
Dy	359	205	155	577	351	402	275	1700	309	85.1	333	454	149	149	185	24.9
Ho	74.3	42.1	32.1	122	74.4	86.7	60.5	379	65.3	17.9	71.5	96.6	29.7	30.5	38.4	5.3
Er	221	124	95.7	360	219	260	181	1130	189	54.7	214	288	83.6	88.3	110	16.7
Tm	33.1	18.8	14.8	54.3	32.7	38.6	27.2	166	27.2	8.94	32.4	43.7	12.3	13	16.2	2.88
Yb	206	120	96.1	335	200	235	170	1010	167	63.8	201	264	75.8	81.1	98.6	22.5
Lu	29.4	17.3	14.2	46	28.6	33.1	24.3	136	23	9.99	26.8	35.2	10.9	11.7	13.5	3.87
Y	1959	1155	895	3402	2006	2283	1503	9184	1751	503	1709	2396	875	807	985	174
Zr/Y ratio	6.15	5.99	6.35	6.25	6.62	6.57	5.28	6.02	5.30	6.15	5.13	4.90	6.37	7.77	7.24	3.88
La/Lu ratio	34.69	42.89	37.39	38.04	32.41	36.25	28.93	23.24	36.52	30.63	29.74	33.52	58.62	48.46	46.59	31.01

Table 4.3. (cont.)

Rock Type	Type I												Type II			Type III
Occurrence / location	Layers, QM Member, S. Area				Band, Mixed I, S. Area	Band, Mixed I, N. Area	Layer, NBR Member, N. Area	Layers, HG Member, N. Area		Layers, HMEC Member, N. Area			Roof layer, ULZ, S. Area	Inclusion, Mixed I, S. Area	Inclusion, Mixed I, N. Area	Inclusion, Mixed II, S. Area
Sample name	PM5-257.25 GC	PM5-297.83 GC	PM5-311.75 GC	PM5-367.42 GC	PM1-384.92 GC	PM3-91.18 GC	PM3-255 GC	PM3-330.75 GC	PM3-343.92 GC	PM3-418.92 GC	PM3-435 GC	PM3-445 GC	PM5-92.18 GC	PM1-489.67 GC	PM3-56.13 GC	PM5-348.83 GC
Lithology	QM EASC	EASC MA	EASC HA	ESC	ESC band	ESC band	EASC MA	ESC HG	EASC CG	EASC HA	ESC	ESC	PEASQ	PEAS	PEAS	PAAS
Other trace elements (ppm)																
Zr	12050	6921	5679	21260	13280	15010	7929	55270	9273	3095	8767	11750	5574	6268	7135	675
Nb	310	244	230	656	561	739	372	2210	480	87	386	555	209	351	258	73
Ta	33.1	19.5	16.3	60.6	41.6	46.4	31.4	165	32.9	4.1	35.2	49.4	16.9	22.7	22.3	2.3
Hf	277	173	146	471	319	383	225	1330	242	69.6	259	349	128	153	155	21.9
U	21.9	21.9	12.7	14.4	36.6	15.5	12	16.8	22.4	5.9	9.1	10.5	15.5	13.4	15.6	1.3
Th	109	37	55.4	18.5	287	14.4	48.9	12.1	35.9	43.6	12.4	19	76.7	71.1	73	6.1
Zn	540	910	1070	330	420	530	870	790	460	900	530	270	760	660	710	540
Mo	14	3	8	4	3	3	24	42	4	9	18	13	14	13	8	13
Rb	439	462	388	492	531	516	492	186	484	304	489	560	522	491	493	335
Sr	137	59	47	194	119	94	41	277	65	23	44	78	93	70	62	43
Sn	69	80	64	117	92	142	52	200	64	32	43	65	63	62	60	8
W	8	7	7	16	11	12	11	51	8	2	15	23	8	5	5	< 1
Pb	38	34	23	93	36	50	244	367	35	60	110	249	230	165	105	42
Ba	157	173	140	393	439	605	118	502	148	65	130	222	180	416	311	154
Sc	< 1	2	3	1	< 1	< 1	< 1	2	< 1	< 1	< 1	< 1	2	3	2	2
Be	44	79	44	58	77	53	35	19	40	36	42	53	50	44	42	18
V	9	< 5	6	< 5	< 5	7	5	< 5	< 5	< 5	< 5	< 5	< 5	5	< 5	9
Cr	< 20	< 20	< 20	< 20	40	< 20	< 20	< 20	< 20	< 20	< 20	< 20	< 20	30	< 20	20
Co	1	2	2	< 1	2	< 1	1	< 1	< 1	< 1	< 1	< 1	2	2	1	2
Ni	< 20	< 20	< 20	< 20	< 20	< 20	< 20	< 20	< 20	< 20	< 20	< 20	< 20	< 20	< 20	< 20
Cu	< 10	< 10	< 10	< 10	< 10	< 10	< 10	10	< 10	< 10	< 10	< 10	< 10	< 10	< 10	10
Ga	57	58	50	82	87	77	61	66	53	43	69	78	50	52	50	50
Ge	4	4	4	6	3	5	4	12	4	4	3	3	3	3	4	4
As	17	23	11	32	15	11	9	30	9	< 5	11	8	8	10	6	< 5
Ag	no data	no data	no data	no data	no data	no data	no data	no data	no data	no data	no data	no data	no data	no data	no data	0.5
In	0.4	0.6	0.5	0.6	0.4	0.6	0.4	1.2	0.4	0.5	0.3	0.3	0.3	0.4	0.4	0.3
Sb	< 0.5	< 0.5	< 0.5	< 0.5	1.3	< 0.5	< 0.5	< 0.5	< 0.5	< 0.5	< 0.5	< 0.5	< 0.5	< 0.5	< 0.5	< 0.5
Cs	1.5	1	0.6	1.1	2.6	1.7	1	1.7	1.1	< 0.5	1	0.9	1.2	1.9	1.5	2.2
Bi	0.4	0.7	0.4	0.6	0.6	< 0.4	< 0.4	0.5	< 0.4	< 0.4	< 0.4	< 0.4	0.5	0.6	< 0.4	< 0.4
Tl	0.6	0.5	0.3	0.4	0.8	0.7	0.4	0.3	0.5	0.3	0.4	0.4	0.4	0.7	0.6	0.3
Modal abundances (%, by visual estimate)																
Data type	Thin section	Thin section	Hand sample	Thin section	Hand sample	Thin section	Thin section	Thin section	Hand sample	Hand sample	Hand sample	Thin section	Thin section	Hand sample	Thin section	Thin section
Afs	40	50	35	44	42	51	49	18	45	36	46	61	52	50	55	50
Amph	20	25	42	8	10	3	30	10	26	48	20	8	20	36	30	36
Qtz	25	15	13	25	32	25	7	22	15	9	18	12	18	4	2	--
Eud	15	10	10	23	16	20	14	50	14	7	16	18	10	10	10	--
Fluo	--	<1	--	--	--	1	--	--	--	--	--	1	<1	--	3	4
Aen	--	--	--	--	--	--	--	--	--	--	--	--	--	--	--	10

CHAPTER 5

INTERPRETATION OF LAYERED SEQUENCES

Based on petrographic observations, the peralkaline rocks were divided into four rock types. Cross-cutting relationships indicate that Type III rocks are oldest, followed by Type II, Type I, and Type IV. Correlating these rock types between the North and South Areas allows them to be grouped into three main layered zones.

5.1 Layered sequences and correlation of North and South Area

Layering in Type I cumulate rocks is subdivided into layers, layering units, and members, as defined in Irvine (1982). Layers represent the least complex subdivision, consisting of a single sheet-like cumulate body of a single lithology or textural and/or modal variant of a lithology. A layering unit consists of a single set of stacked layers, generally with gradational internal contacts. Members are distinct packages, greater than 10 m in thickness, comprising one or more layering units (per Irvine, 1982) and bounded above and below by abrupt contacts. A member may consist of a single large, distinctive layering unit with gradational internal contacts, a rhythmic sequence of similar layering units, or a combination thereof.

The quartz megacryst-bearing cumulate sequence (referenced in section 4.3) that proceeds, from bottom to top, ESC – EASC – QM EASC, is known as the "QM Member" in reference to its upper lithologic layer's cumulus quartz content (Fig. 5.1). Within this single layering unit, variations between each layer are significant enough to represent three different lithologies. Contacts between layers are observed to be either gradational or abrupt. Layering is

defined by modal mineralogy, texture, and phase variations; the contact from ESC up to EASC manifests in decreasing eudialyte, increasing amphibole, and increasing cumulus texture of amphibole, while the contact from EASC to QM EASC is seen in the appearance of cumulus quartz megacrysts and a subtler increase in eudialyte. In the South Area, the cumulus quartz phase contact typically takes the form of a gradational upward increase in the size and abundance of megacrystic quartz. However, this contact was observed to be sharp in one South Area drill hole as well as in its surface expression in the North Area. The increasing amphibole and decreasing eudialyte between ESC and EASC correlate to variations in TREO and ZrO_2 (Fig. 5.1). Modal changes within layers may be significant as well; note amphibole nearly doubling and the other cumulus minerals showing a complementary decrease in abundance within EASC. The scale of these variations may be as small as several centimeters.

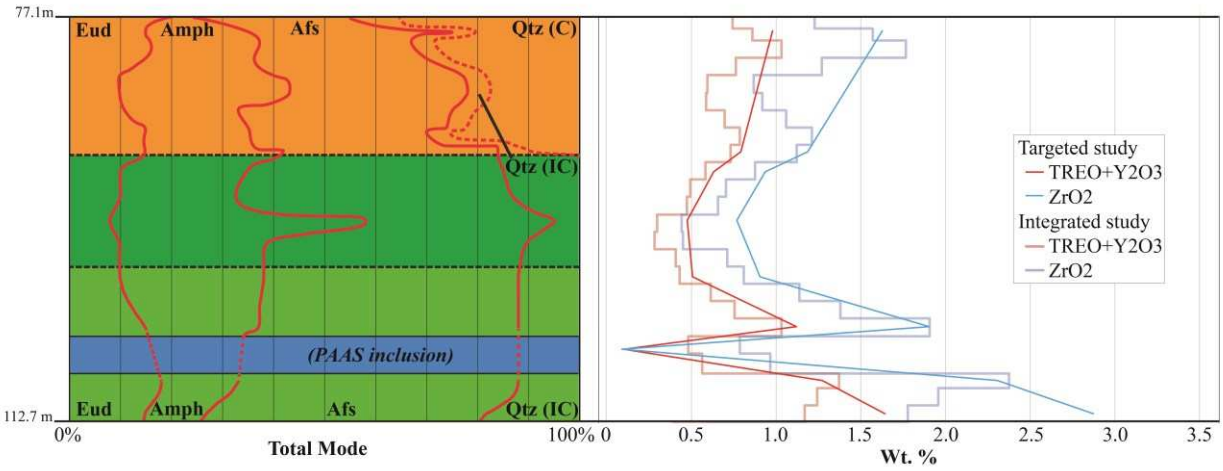


Figure 5.1. Schematic of QM Member from drill hole 05 in the South Area, including modal mineralogy and whole-rock TREO and ZrO_2 grades (wt.%). "Targeted study" data are from the second round of whole rock geochemistry sampling with <8 cm homogeneous samples representing a known lithology. "Integrated study" data are from continuous sampling on 1.5 meter intervals; many of these samples contain multiple lithologies. Depths indicated are from collar of drill hole and are included for scale (apparent thickness). Note appearance of cumulus ("C") quartz alongside intercumulus ("IC") quartz at EASC – QM EASC contact.

The QM Member is encountered in all three drill holes in the South Area, with an apparent thickness from 15 to 32.2 m and down-dip lateral continuity of at least 125 m in the South Area (Fig. 4.11A-B). Because of this consistent lateral continuity, and because some of the richer TREO and ZrO_2 grades in the pluton are found within the basal ESC, the QM Member is a central example of igneous layering as a major control on REE-Zr mineralization. The QM Member is also observed at surface in the North Area, an observation critical to the proposed correlation of the North and South Area sections, as shown in Figure 5.2 (p. 66).

The QM Member consistently occurs between the same units in the South Area. It occurs above a mixed unit known as Mixed II, which is characterized by abundant lithic inclusions of PAAS and in turn occurs above Mixed unit I (see Fig. 5.2; Table 5.1). In one drill hole (Fig. 5.1), the basal ESC layer is repeated, occurring in its typical position above the contact to Mixed II atop Mixed I, as well as above a fragment (or second lens) of Mixed II greater than 3.25 m thick. Consistently overlying the QM Member is an up to 60 m thick body of Type II PEASQ. Mixed unit QM EASC II, unique from Mixed I and II in containing bands of QM EASC, locally constitutes the upper contact of the QM Member; more often, though, it occurs as isolated lenses within the overlying PEASQ. Three occurrences of the upward sequence Mixed I – Mixed II – QM Member – PEASQ in the South Area led to the interpretation of a loose stratigraphy for the South Area section.

Interpretation of this sequence was expanded in order to posit that the igneous stratigraphy observed in the South Area correlates with that observed in the North Area roughly 1.5 km away. QM EASC and EASC are discretely present in the North Area with similar positions relative to Mixed I (see Fig. 4.11C-D). In the North Area, Mixed I consists primarily of PEAS lithic inclusions hosted within Type I ESC, a characteristic of Mixed I in the South

Area. While the North Area occurrence lacks the heterogeneity of some Mixed I zones observed in the South Area (i.e. bands of EASC, pegmatites, lenses of PEASQ, PAAS inclusions, basement xenoliths), there is sufficient similarity to warrant classification together. Thin sections of ESC IV from the upper portion of the North Area Mixed I occurrence and ESC I from the base of the QM Member in the South Area are similar enough in texture and cumulus mineralogy that these are interpreted to represent equivalent layers in the QM Member; the North Area QM Member simply contains an accumulation of PEAS inclusions at its base. Although Mixed II was not observed as a discrete interval in the North Area, PAAS lithic inclusions were found within EASC within tens of meters of the EASC – Mixed I/ESC contact. This degree of variability falls within reason for distal manifestations of the same stratigraphic interval roughly 1.5 km apart.

Table 5.1. Summary of characteristics of mixed units

Map Units (not listed in stratigraphic order)	Lithologies occurring as bands/ in-situ bodies	Lithologies occurring as lithic inclusions	Distribution
Mixed I	ESC, EASC, PEASQ, PP	PEAS; trace PAAS & BX	Below S. Area quartz megacryst-bearing layered unit, <104 m thickness observed. Below N. Area quartz megacryst-bearing layered unit and above other N. Area layered units, 68 m thickness observed. Is not laterally continuous in N. Area.
Mixed II	ESC; minor PP & EASC	Abundant PAAS (defines unit); trace PEAS	Below S. Area quartz megacryst-bearing layered unit and above Mixed I. 6-25 m thickness observed.
QM EASC II	QM EASC, EASC, PEASQ; minor PP & ESC	PEAS, PAAS	N. & S. Areas, outside of quartz megacryst-bearing layered units within adjacent PEASQ (S. Area) or EASC (N. Area). 2.1 - 12.2 m thickness observed.

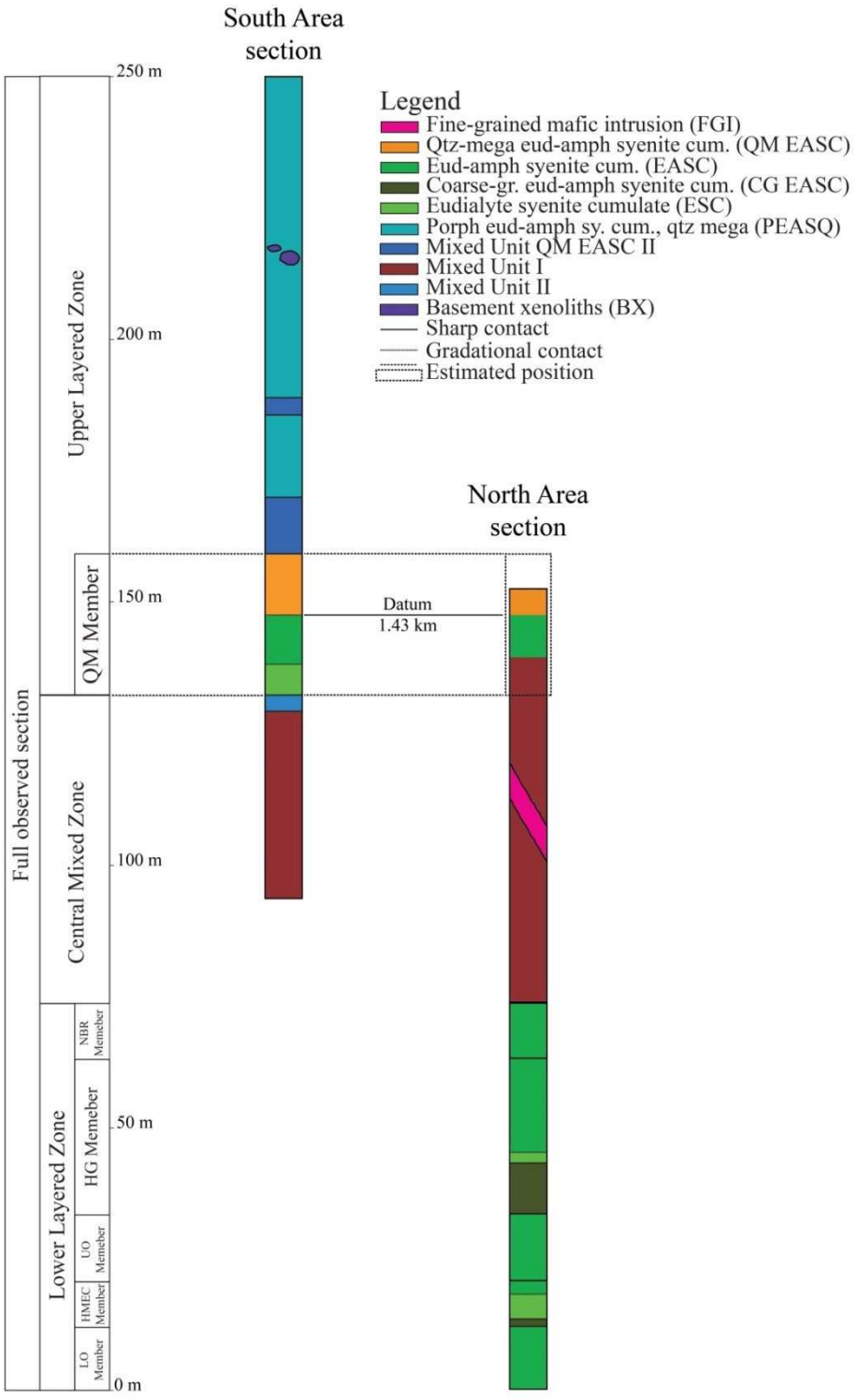


Figure 5.2. Lithological sections of layered syenite units and proposed correlation of North and South Area sections. The stratigraphy is subdivided into Lower Layered, Central Mixed, and Upper Layered Zones. The Lower Zone is comprised of Type I cumulates, the Central Mixed Zone contains rocks of Types I-IV, and the Upper Layered Zone mainly consists of Type II rocks with a sequence of Type I layered rocks at the base. Detailed definition of lithologies is given in Table 4.1 in Chapter 4. Mixed map units are described in Table 5.1.

Although the full, uninterrupted section was not observed in the North Area and variations abound, tight enough control on the location of the EASC – QM EASC contact was established to enable its use as a datum plane through which to combine the sections with measured confidence. Figure 5.2 shows the resulting combined section, adjusted to true thickness to account for the overall structural orientation of the sections in each area. The combined section, roughly 250 m in thickness, has been broken into an Upper Layered Zone, a Lower Layered Zone, and an intervening Central Mixed Zone.

The Upper Layered Zone consists of the QM Member and the overlying thick body of PEASQ, and the Central Mixed Zone consists of heterogeneous units Mixed I ± Mixed II. The Lower Layered Zone (LLZ) was observed in underlying contact with Mixed I in the only North Area drill core not disrupted by faulting. The LLZ consists of Type I medium- and coarse-grained peralkaline syenitic cumulates (ESC, EASC) displaying both rhythmic and irregular layering by modal mineralogy and texture. Individual layers vary in true thickness from less than 0.4 m to over 13 m, and were grouped into five layered members. These include: the Lower Oscillatory (LO) Member; the {High-Amph EASC} – {Moderate-Amph EASC} – ESC – {Coarse-grained EASC} (HMEC) Member; the Upper Oscillatory (UO) Member; the High Grade (HG) Member; and the Narrow Banded Rhythmic (NBR) Member (Fig. 5.3; p. 69).

The predominant pattern of layered units in the Lower Layered Zone is simpler than that described in the QM Member. Layering units (0.37 to 8.4 meters thick) consist of a basal layer of amphibole-poor, eudialyte-rich, medium-grained cumulate (low-amphibole EASC and/or ESC) that gradationally changes upward to a similar lithology rich in well-formed cumulus

amphibole (higher modal amphibole EASC). At their simplest, units from the Lower Layered Zone consist of just this two-layer sequence of EASC. A systematic rhythmic layering can be observed in the geochemical data for TREO and ZrO_2, which can be related to modal amounts of eudialyte in the succession (Fig. 5.3). The Narrow Banded Rhythmic Member exemplifies this basic pattern. The NBR Member is made up of six layering units (0.37 – 2.23 m thick) of EASC with consistent variations in amphibole and eudialyte content. Each layering unit consists of a basal layer with low to moderate amphibole (15-30%) that gradationally increases to moderate to high amphibole (30-50%) in the upper layer. Accompanying this gradational amphibole increase, in five of six layering units, eudialyte gradationally decreases from high or moderate (15-25%) at the base to moderate to poor (5-12%) at the top, with a corresponding decrease in TREO and ZrO_2. These variations in metal concentration are on too small a scale, however, to be reflected in Figure 5.3. The six stacked layering units have abrupt contacts with one another. Heterogeneity in the NBR Member occurs in one interval that contains several stacked PEAS lithic inclusions up to 0.73 m thick hosted within EASC occurring in intervals up to 0.23 m thick.

Lower Layered Zone layering also includes oscillatory layering, exemplified in the 17.9 m thick UO Member. In this member, one continuous 13.4 m thick EASC body with strong cumulus textures displays four gradational changes in which amphibole content (and inversely proportional eudialyte content, as described above) varies upward from moderately high (38%) to moderate (30%) to moderately low (22%) to moderate (32%) to high (46%) with no clear pattern. Below the abrupt basal contact of this layering unit, a second, 4.5 m thick layering unit shows a similarly unpredictable, gradational EASC layering sequence. Accordingly, no clear pattern of TREO and ZrO_2 concentration is visible.

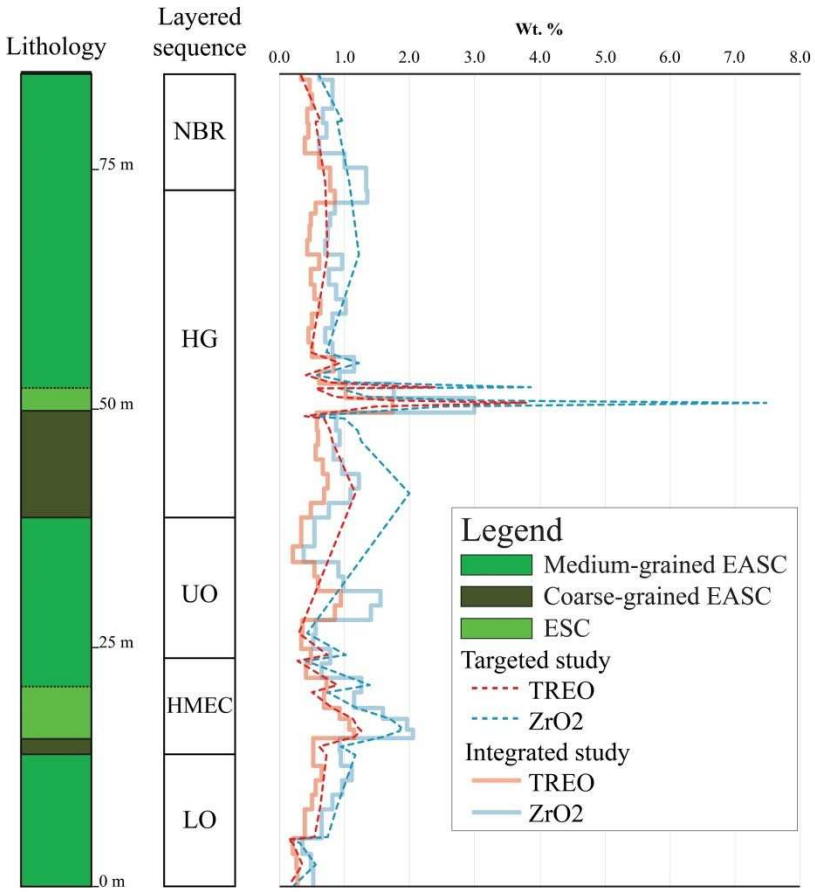


Figure 5.3. Lower Layered Zone stratigraphic column showing lithology of the layered units (ESC and EASC) and whole-rock TREO and ZrO_2 grades (wt.%) from integrated and targeted studies.

5.2 Igneous processes

Based on detailed petrographic observations, field relations, whole-rock geochemistry, and interpretation of layered sequences, this study presents evidence for three processes in the genesis of the Pajarita Mountain pluton having contributed to controls on REE-Zr mineralization. First, the observed peralkaline syenitic rocks formed through at least three main episodes of peralkaline magma emplacement. Second, these peralkaline magmas underwent separation and accumulation of cumulus minerals. Third, the pluton experienced interaction with variable melts as it evolved. Each of these processes appears to have played a role in the genesis of the pluton and to have had an impact on the distribution of REE and Zr mineralization.

Peralkaline syenitic rock types I, II and III are each interpreted to represent a distinct peralkaline magmatic pulse from a deeper magma chamber, with Type III being oldest and Type I being youngest. Cross-cutting relationships provide evidence for this succession, particularly given the presence of lithic inclusions of PEAS (Type II) and PAAS (Type III) within Type I cumulate lithologies. Contact relationships between Type II PEAS inclusions and a Type I ESC host vary between sharp and diffuse within the same stratigraphic zone (see Fig. 4.15C), suggesting varying degrees of solidification of PEAS at the time of ESC introduction. Inclusions vary in shape from angular to rounded, which may be a product of varying degrees of resorption or reaction of inclusions with the host and/or flow regime. Concentric zonation in inclusions (see Fig. 4.15B,D) also suggests varying degrees of reaction. Additionally, the stronger porphyritic texture and finer groundmass that characterize Type II and III peralkaline syenitic rocks relative to the more equigranular, medium-grained Type I rocks, suggest a different evolutionary cooling path. These relationships between inclusions and Type I host rocks are interpreted to set the intrusive stage of Type I rocks apart in time from the intrusive stages of Type II and III rocks.

Although both Type III and Type II rocks are porphyritic, Type III rocks are distinguished from Type II rocks by their lack of groundmass eudialyte, the presence of aenigmatite, and the unique population of perthitic and distinctly mantled alkali feldspar phenocrysts (Afs D). Although PAAS are also peralkaline, these significant mineralogical differences and the resulting much lower TREO and ZrO_2 contents of Type III rocks suggest a different, less evolved parental melt to those that produced type I and II rocks. Hence, even if cross-cutting relationships between Type II and Type III rocks are more ambiguous, Type III peralkaline syenitic rocks can be interpreted as the oldest of the three rock types. Type IV

peralkaline pegmatites were observed cross-cutting rocks of types I-III and, as such, represent the final peralkaline melts to intrude the Pajarita Mountain complex. Type I rocks contain the highest known concentrations of TREO and ZrO_2 in the pluton, and the more evolved character of this melt may plausibly be the cause of this trend. The progressive increase in mineralization grades from oldest to youngest melt generations indicates that fractionation in the parental magma chamber was important for the primary enrichment of incompatible elements in the melt, including the REE and Zr.

There is textural, structural and geochemical evidence for separation and accumulation of early cumulus crystals during the formation of the Pajarita Mountain peralkaline syenitic rocks, which had an impact on the distribution of REE and Zr mineralization. Microtextural evidence takes the form of well-formed cumulus crystals with notably less in the way of accommodative contacts (which would suggest simultaneous growth) than would be expected from non-cumulate plutonic rocks. These cumulus textures are present in Types I-III, but they increase in clarity through time, from Type III to Type I; this progressive variation in crystallinity further supports the concept of each type having a distinct history and emplacement timing.

The several types of layering described in section 5.1, which show clear differences in cumulus mineralogy, mode and texture within laterally continuous (QM Member) and repetitive layering (LLZ members) units, are robust indicators of accumulation during fractional crystallization of cumulus crystals. Concentration of eudialyte correlates with REE and Zr enrichment (see Fig. 5.1; Table 4.3), which is also reflective of the importance of fractional crystallization for the distribution of mineralization with the different layered zones. There is a general trend of eudialyte being concentrated at the base of layering units (see Fig. 5.1), with the highest grades of combined TREO and ZrO_2 over 11 wt.%. Well-formed crystals concentrated

in specific layers suggest that eudialyte was an early-crystallizing phase that separated early from its parent melt.

Evidence for interaction of the cumulus pile with multiple melt infiltration events is reflected in the mantled mineral textures observed throughout the pluton. Mantled feldspars like the albite-mantled alkali feldspar grains (Afs A, C, D) with ragged cores suggestive of partial resorption, are a classical textural indicator of magma mixing, with further evidence shown by these grains' occurrence alongside amphibole characterized by increasing Na content from cumulus core to adcumulus overgrowth. Existing alkali feldspar and amphibole grains would evidently have been put out of equilibrium by injection of new melt, resulting in reaction mantles and adcumulus overgrowths reflective of more Na-rich composition. These textures and chemical variations can be interpreted to represent magma mixing most likely associated to recharge from a larger magma body and/or migration of intercumulus melt within the cumulus pile. The formation of eudialyte, typically an early-crystallizing phase in this system, as oikocrysts enclosing groundmass minerals also suggests magma recharge and introduction of a more evolved, REE-Zr-enriched melt.

The diverse range of replacement textures observed among alkali feldspar, amphibole, and quartz that are both cumulus and post-cumulus in texture (see section 4.2) is suggestive of more local changes in the intercumulus liquid. In addition, the presence of cumulus quartz rimmed by intercumulus amphibole in QM EASC constitutes a reversal of the expected crystallization sequence in which intercumulus quartz crystallizes last. This texture indicates the possible introduction of a less fractionated liquid still crystallizing amphibole at this evolutionary stage of the layered sequence. Additional textures of amphibole replacement by quartz and, in some instances, feldspar (Fig. 4.9) indicates compositional changes of the residual intercumulus

liquid during crystallization. The causative mechanism requires a more detailed study of the chemistry and zoning of these minerals within the different rock types. However, mineral textures and bulk rock geochemistry clearly yield evidence for fractional crystallization and injection of melts with variable composition in the Pajarita Mountain pluton, with possible variations of pressure-temperature-composition (P-T-x) conditions through time.

CHAPTER 6

CONCLUSIONS

This study provides evidence that the Pajarita Mountain intrusion is a layered intrusion that is composed of peralkaline syenitic cumulate rocks. Rare earth element and zirconium mineralization is controlled by the distribution of magmatic eudialyte group minerals. Layering is defined by variations in phase, texture, and/or mode, and contacts between layers may be abrupt or gradational. Some members feature rhythmic repetition of specific layered sequences.

This study's observations present clear evidence for several magmatic processes that are responsible for the genesis of the Pajarita Mountain pluton and involved in controlling REE and Zr mineralization. Firstly, the pluton was formed through emplacement of multiple pulses of peralkaline magma. Secondly, these peralkaline magmas underwent separation and accumulation of cumulus minerals. Thirdly, the pluton experienced interaction with variable melt compositions as it evolved.

The observed peralkaline syenitic rocks formed through three main episodes of peralkaline magma emplacement corresponding to rock types I-III and emplacement of minor pegmatites (Type IV). Cross-cutting relationships indicate the ages of the rock types relative to one another, with Type III being oldest, followed by Type II, Type I, and Type IV. Correlation of the North and South Area sections enables one to distinguish three layered zones corresponding to the Lower Layered, Central Mixed, and Upper Layered Zones. The Lower Zone is comprised of Type I cumulates, the Central Mixed Zone contains rocks of Types I-IV, and the Upper Layered Zone consists of a basal sequence of Type I layered rocks overlain by Type II rocks.

The distinct timing of rock types I-III is also shown in variations in overall rock texture (porphyritic vs. equigranular), mineralogy (presence or absence of groundmass eudialyte and aenigmatite), the character of alkali feldspar phenocrysts, and whole-rock geochemistry, most notably the TREO and ZrO_2 grades. Type I rocks, the youngest non-pegmatite peralkaline syenitic rocks, contain the highest concentrations of eudialyte and TREO and ZrO_2 in the pluton, as well as the most prominent examples of layering and cumulate mineral textures. The highest grades are found within eudialyte syenite cumulate occurrences at the base of layered units in the Lower Layered Zone, in bands that cross-cut the Central Mixed Zone, and at the base of the QM Member of the Upper Layered Zone. These instances of modal and textural layering, as well as the cumulate textures they display, provide evidence for early crystal separation and accumulation during the genesis of the Pajarita Mountain pluton.

Many textures observed in the Pajarita Mountain peralkaline syenitic rocks are interpreted as being caused by interaction of the cumulus pile with variable intercumulus liquids. Interpretation of these textures provides evidence for several processes that may have caused this heterogeneity. Alkali feldspar mantling and adcumulus amphibole textures are interpreted as produced by magma mixing with more Na-rich younger melt. Cumulus quartz rimmed by intercumulus amphibole suggests mixing via magma recharge as coarse quartz was likely crystallizing last from a highly fractionated melt. The apparent restart of crystallization of earlier-fractionating phases such as amphibole could be produced by introduction of a less-fractionated melt of similar origin. Magma recharge may have implications for REE-Zr mineralization as well. Textural interpretation suggests that eudialyte is typically an early-crystallizing cumulus phase, so the appearance of post-cumulus, sub-poikilitic to oikocrystic eudialyte in some peralkaline syenitic cumulates may indicate the onset of crystallization of a

new batch of enriched melt injected into an existing cumulus framework. Finally, the wide variety of replacement and/or reaction textures between amphibole, alkali feldspar, and quartz are interpreted as products of localized, relatively minor changes in intercumulus melt creating disequilibrium within the cumulus pile.

REFERENCES

Adams, D. C. and Keller, G. R., 1994, Possible extension of the Midcontinent Rift in west Texas and eastern New Mexico: Canadian Journal of Earth Science, v. 31, p. 709-720.

Arzamestsev, A., Yakovenchuk, V., Pakhomovsky, Y. and Ivanyuk, G., 2008, The Khibina and Lovozero alkaline massifs: Geology and unique mineralization, Excursion Guide, 33rd International Geological Congress, Excursion No. 47, August 2, 2008, 58 p.

Bauer, P. W. and Pollock, T. R., 1993, Compilation of Precambrian Isotopic Ages in New Mexico: New Mexico Bureau of Mines and Mineral Resources Open-File Report 389, 128 p.

Beland, C., 2014, The Magmatic-Hydrothermal Transition in Peralkaline Rhyolite at Terceira, Azores: MSc. thesis, University of Toronto.

Borst, A. M., Friis, H., Andersen, T., Nielsen, T. F. D., Waight, T. E., and Smit, M. A., 2016, Zirconosilicates in the kakortokites of the Ilímaussaq complex, South Greenland: Implications for fluid evolution and high-field-strength and rare-earth element mineralization in agpaitic systems: Mineralogical Magazine, v. 80(1), p. 5-30.

Borst, A., Waight, T., Smit, M., Friis, H., and Nielsen, T., 2014, Alteration of eudialyte and implications for the REE, Zr and Nb resources of the layered kakortokites in the Ilímaussaq intrusion, south west Greenland: ERES2014: European Rare Earth Resources Conference, 1st, Milos, Greece, 2014, Proceedings, p. 325-332.

Brown, W. L. and Parsons, Ian, 1989, Alkali feldspars: ordering rates, phase transformations and behaviour diagrams for igneous rocks: Mineralogical Magazine, v. 53, p. 25-42.

Chakhmouradian, Anton R. and Wall, Frances, 2012, Rare Earth Elements: Minerals, Mines, Magnets (and More): Elements, v. 8, number 5, p. 333-340.

Deer, W. A., Howie, R. A., and Zussman, J., 1992, The Rock-Forming Minerals, 2nd Edition: Essex, Pearson Education Limited, 696 p.

Dostal, J., 2016, Rare metal deposits associated with alkaline/peralkaline igneous rocks: Reviews in Economic Geology, v. 18, p. 33-54.

Foord, E. E. and Moore, S. L., 1991, Geology of the Bent Dome, Otero County, New Mexico: New Mexico Geological Society Guidebook, 42nd Field Conference: Sierra Blanca, Sacramento, Capitan Ranges, p. 171-174.

Frost, R. B., Barnes, C. G., Collins, W. J., Arculus, R. J., Ellis, D. J., and Frost, C. D., 2001, A Geochemical Classification for Granitic Rocks: Journal of Petrology, v. 24, number 11, p. 2033-2048.

Gysi, A. P. and Williams-Jones, A. E., 2013, Hydrothermal mobilization of pegmatite-hosted REE and Zr at Strange Lake, Canada: A reaction path model: Geochimica et Cosmochimica Acta, v. 122, p. 324-352.

Gysi, A. P., Williams-Jones, A. E., and Collins, P., 2016, Lithogeochemical vectors for hydrothermal processes in the Strange Lake peralkaline granitic REE-Zr-Nb deposit: Economic Geology, v. 111, p. 1241-1276.

Irvine, T. N., 1982, Terminology for Layered Intrusions: Journal of Petrology, v. 23(2), p. 127-162.

Jacobson, H. S., 1986, Pajarito Mountain Prospect, Mescalero Apache Indian Reservation, Otero County, New Mexico: Unocal Molycorp internal report, v. I & II.

Kelley, V. C., 1968, Geology of the Alkaline Precambrian Rocks at Pajarito Mountain, Otero County, New Mexico: Geological Society of America Bulletin, v. 79, number 11, p. 1565-1572.

Kottlowski, F. E., 1985, Shoreline Facies of the Yeso Formation in the Northern Pedernal Hills: New Mexico Geological Society Guidebook, 36th Field Conf, Santa Rosa, p. 167-169.

Lindhuber, J. J., Marks, M. A. W., Bons, P> D., Wenzel, T., and Markl, G., 2015, Crystal mat-formation as an igneous layering-forming process: Textural and geochemical evidence from the 'lower layered' nepheline syenite sequence of the Ilímaussaq complex, South Greenland: Lithos, v. 224-225, p. 295-309.

Linnen, R., and Keppler, H., 2002, Melt composition control of Zr/Hf fractionation in magmatic processes: Geochimica et Cosmochimica Acta, v. 66, p. 3292-3301.

Lloyd, E. Russell, 1949, "Pre-San Andres Stratigraphy and Oil Producing Zones in Southeastern New Mexico," New Mexico Bureau of Mines and Mineral Resources Bulletin 29.

Marks, M. A. W., Hettmann, K., Shilling, S., Frost, B. R. and Markl, G., 2011, The Mineralogical Diversity of Alkaline Igneous Rocks: Critical Factors for the Transition from Miaskitic to Agpaitic Phase Assemblages: Journal of Petrology, v. 52, number 3, p. 439-455.

Martin, R. F. and De Vito, C., 2005, The patterns of enrichment in felsic pegmatites ultimately depend on tectonic setting: The Canadian Mineralogist, v. 43, p. 2027-2048.

McDonald, R., 2012, Evolution of peralkaline silicic complexes: Lessons from the extrusive rocks: Lithos, v. 152, p. 11-22.

Möller V., and Williams-Jones, A.E., 2016, Petrogenesis of the Nechalacho Layered Suite, Canada: Magmatic evolution of a REE-Nb-rich Nepheline Syenite Intrusion. J. Petrol. V. 57, p. 229-276.

Moore, S. L., Foord, E. E., Meyer, G. A., and Smith, G. A., 1985, Mineral Resources of the Mescalero Apache Indian Reservation, Otero County, New Mexico: Administrative Report, United States Geological Survey for the United States Bureau of Indian Affairs, 78 p.

Moore, S. L., Foord, E. E., and Meyer, G. A., 1988, Geologic map of a part of the Mescalero Apache Indian Reservation: Report, United States Geological Survey for the U.S. Bureau of Indian Affairs, 42 p.

Moore, S. L., Thompson, T. L. and Foord, E. E., 1991, Structure and igneous rocks of the Ruidoso region, New Mexico: New Mexico Geological Society Guidebook, 42nd Field Conference: Sierra Blanca, Sacramento, Capitan Ranges, p. 137-145.

Perlewitz, P., 1986, Analysis of the Pajarito Mountain prospect on the Mescalero Apache Indian Reservation located in Otero County, New Mexico: United State Bureau of Mines for United States Bureau of Indian Affairs, technical report, 13 p.

Pfaff, K., Krumrei, T., Marks, M., Wenzel., T, Rudolf, T., and Markl, G., 2008, Chemical and physical evolution of the 'lower layered sequence' from the nepheline syenitic Ilímaussaq intrusion, South Greenland: Implications for the origin of magmatic layering in peralkaline felsic liquids: Lithos, v. 106, p. 280-296.

Schilling, J., Marks, M. A. W., Wenzel, T., Vennemann, T., Horvath, L., Tarassoff, P., Jacob, D. E. and Markl, G., 2011, The Magmatic to Hydrothermal Evolution of the Intrusive Mont Saint-Hilaire Complex: Insights into the Late-stage Evolution of Peralkaline Rocks: Journal of Petrology, v. 25, p. 2147-2185.

Schonenberger, J., Marks, M., Wagner, T., and Markl, G., 2006, Fluid-rock interaction in autoliths of agpaitic nepheline syenites in the Ilímaussaq intrusion, South Greenland: Lithos, v. 91, p. 331-351.

Segerstrom, K. and Brauch, E. F., 1976, Status of Mineral Resource Information for the Mescalero Indian Reservation, New Mexico: United States Geological Survey and United States Bureau of Mines for the United States Bureau of Indian Affairs, Administrative Report BIA-16, 33 p.

Sheard, E. R., Williams-Jones, A. E., Heiligmann, M., Pederson, C., and Trueman, D. L., 2012, Controls on the Concentration of Zirconium, Niobium, and the Rare Earth Elements in the Thor Lake Rare Metal Deposit, Northwest Territories, Canada: Economic Geology, v. 107, p. 81-104.

Sherer, R. L., 1990, Pajarito yttrium-ziconium deposit, Otero County, New Mexico: New Mexico Geology, v. 12, p. 21.

Sorensen, H., 1997, The agpaitic rocks – an overview: Mineralogical Magazine, v. 61, p. 485-498.

Tabet, D. E., 1991, Market analysis for the Pajarito Mountain lanthanide project, Mescalero Apache Indian Reservation, New Mexico: Pentastar Support Services, Inc. for the United State Bureau of Indian Affairs, Branch of Energy and Mineral Resource Assistance, administrative report BIA/Pentastar 16, 18 p.

Thompson, M. L., 1942, "Pennsylvanian System in New Mexico," New Mexico Bureau of Mines and Mineral Resouces, Bulletin 17.

Woodward, L. A., 1991, Tectono-metallogenic maps of mining districts in the Lincoln County porphyry belt, New Mexico: New Mexico Geological Society Guidebook, 42nd Field Conference: Sierra Blanca, Sacramento, Capitan Ranges, p. 283-290.

APPENDIX A

MINERAL CHEMISTRY

Alkali feldspar

Alkali feldspar grains of the two groundmass textural populations, Afs A and Afs B, were imaged via BSE and analyzed via EDS. BSE imaging and EDS analyses were conducted on medium-grained Afs A and B groundmass grains from Type I peralkaline syenitic rocks, as well as fine-grained Afs A and B groundmass grains from Type II and III peralkaline syenitic rocks.

Figure A.1 displays BSE images of Afs A and B crystals, all of which were shown in photomicrographs under cross-polarized light in Figure 4.1. Major element chemistry of compositional zones observed in these grains was tested via EDS. The locations of the spot analyses taken for a fine-grained Afs A grain (Fig. A.1B) and a medium-grained Afs B (Fig. A.1C) are shown as labeled yellow crosses and the results of those analyses are given in Table X and Table Y. In both cases, to the limitations of the EDS method, analyses gave end-member compositions for K-feldspar and albite with no Ca detected in any analysis. Minor Fe detected in albite in spot analysis 7750 may be the result of contamination from amphibole or iron oxide dustings observed on some Afs grains.

EDS analyses of Afs A and B grains from peralkaline syenitic rocks of Type I (two EASC samples, two ESC samples, two QM EASC samples), Type II (one PEASC sample) and Type III (one PAAS sample) gave similar results. Sampling included grain mantles and both regular, sub-parallel lamellae erratic zones from all three rock types. No Ca was detected in any Afs analysis and the vast majority of analyses showed end-member albite and K-feldspar only. What minor Na is detected from a handful of K-dominant analyses is readily attributable to

contamination from adjacent zones, given the statistical robustness of these results, but it may be real.

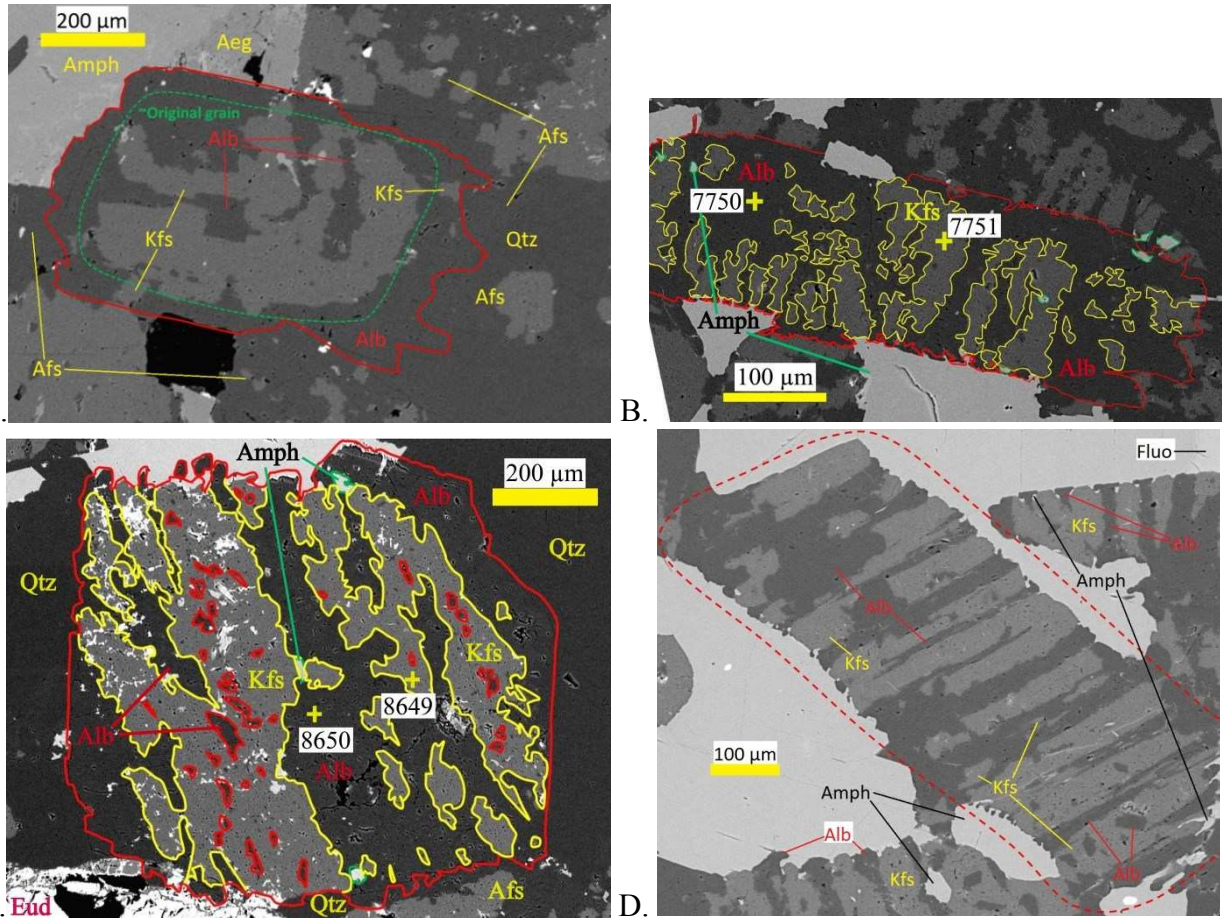


Figure A.1. BSE images of Afs grains sampled by EDS spot analyses. A. Medium-grained Afs A groundmass grains from QM EASC (same grain shown in Fig. 4.1A). Compositions determined by EDS. B. Fine-grained Afs A groundmass grain from PAAS (same grain shown in Fig. 4.1B) showing spot locations for EDS data in Table A.1. C. Medium-grained Afs B groundmass grain from QM EASC (same grain shown in Fig. 4.1C) showing spot locations (yellow crosses) for EDS data in Table A.2. D. Fine-grained Afs B groundmass grain from PAAS (same grain shown in Fig. 4.1D). Compositions determined by EDS.

Table A.1. Data from EDS spot analyses on Afs A grain shown in Figs. A.1B and 4.1B. Data are given in weight % element.

Spot	O	Na	Al	Si	K	Fe	Total
7750	44.1	9.7	12.1	29.0		0.9	95.8
7751	38.0		9.8	24.7	14.1		86.6

Table A.2. Data from EDS spot analyses on Afs B grain shown in Figs. A.1C and 4.1C. Data are given in weight % element.

Spot	O	Na	Al	Si	K	Total
8649	38.0		9.9	24.6	14.5	87.0
8650	39.1	8.1	10.7	26.0		83.9

Amphibole

Amphibole grains from Type I, II and III peralkaline syenitic rocks were imaged and analyzed in an effort to investigate variations in major element chemistry between cumulus cores and adcumulus rims. Fig. A.2 and the accompanying EDS results in Table A.2 illustrate patterns of increasing Na and decreasing Ca moving from core to contact zone to rim in the subhedral cumulus-adcumulus amphibole grain seen in Fig. 4.2A.

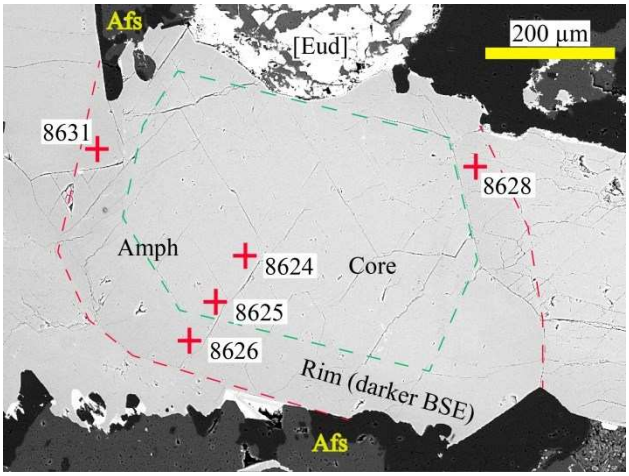


Figure A.2. BSE image of cumulus Amph grain with adcumulus overgrowth from QM EASC (same grain shown in Fig. 4.2A, rotated roughly 100 degrees counterclockwise) showing spot locations (red crosses) for EDS data in Table A.3. Green dashed line delineates approximate cumulus grain boundary as seen in photomicrograph; red dashed line delineates approximate outermost extent of darker BSE adcumulus rim.

Table A.3. Data from EDS spot analyses on Amph grain shown in Figs. A.3 and 4.2A. Data are given in weight % element.

Spot	Description	O	Na	Mg	Al	Si	K	Ca	Ti	Mn	Fe	Total
8624	Core, lighter BSE	34.5	6.9	0.3	0.4	19.6	1.3	1.5	0.7	0.5	28.5	94.2
8625	Core-rim contact	36.0	7.4	0.2	0.3	20.4	1.4	1.2	0.7	0.5	28.8	96.8
8626	Rim, darker BSE	35.0	7.4	0.2	0.3	19.8	1.8	0.4	0.7	0.4	28.7	94.7
8628	Rim, darker BSE	35.3	7.4	0.2	0.4	20.3	1.7	0.4	0.7	0.5	29.0	95.9
8631	Rim, darker BSE	34.5	7.6	0.2		19.7	1.6	0.5	0.8	0.4	27.8	93.0

Aenigmatite

Aenigmatite was identified in PAAS samples via EDS on two grains. Results are given in Table A.4. BSE response from aenigmatite is shown in Figure A.3.

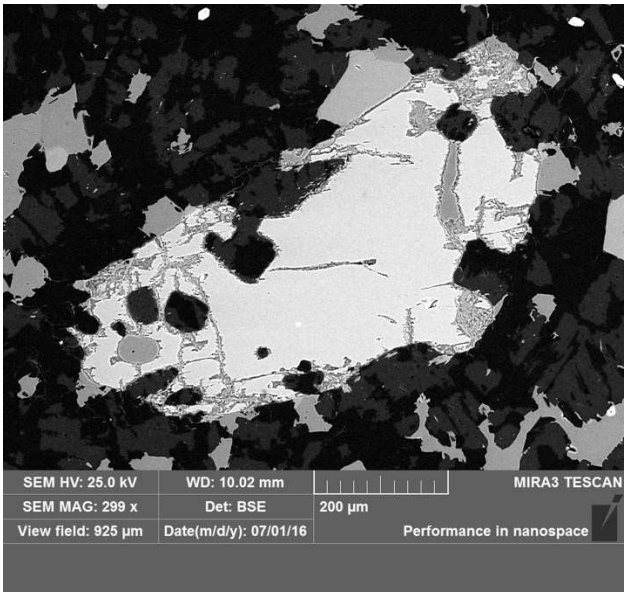


Figure A.3. BSE image of aenigmatite in PAAS.

Table A.4. Data from EDS spot analyses on two Aen grains. Data are given in weight % element.

Spot	O	Na	Si	Ti	Mn	Fe	Total
7743	32.6	5.2	15.3	6.2	0.6	33.3	93.2
7744	33.0	5.1	15.6	6.1	0.6	35.1	95.4